

TORQUE CONTROL OF A
PERMANENT MAGNET BRUSHLESS DC MACHINE
FOR A HYBRID ELECTRIC VEHICLE

A Thesis

Presented to

The Graduate Faculty of the University of Akron

In Partial Fulfillment
of the Requirements for the Degree
Master of Science

Christophe X. Salgues

August, 2008

TORQUE CONTROL OF A
PERMANENT MAGNET BRUSHLESS DC MACHINE
FOR A HYBRID ELECTRIC VEHICLE

Christophe X. Salgues

Thesis

Approved:

Accepted:

Advisor
Dr. Iqbal Husain

Dean of the College
Dr. George K. Haritos

Committee Member
Dr. Robert Veillette

Dean of the Graduate School
Dr. George R. Newkome

Committee Member
Dr. Joan Carletta

Department Chair
Dr. Alexis De Abreu-Garcia

Date

ABSTRACT

This thesis describes the development of the torque control algorithm for a Permanent Magnet Brushless DC (PM-BLDC) machine used as a starter/generator in a hybrid electric vehicle. A comparison of the different methodologies and concepts known for a starter/generator application is presented. It is followed by a presentation of the PM-BLDC machine drive including the structure of the controller. The Proportional-Integral controller technique has been chosen for current or torque control for its ease of implementation in a DSP. The feasibility of using the PM-BLDC machine drive for a starter/generator application was first studied through simulation. The transition from the simulation to the application itself was not seamless; the biggest challenges were dealing with noise and assumptions made within the model. On the other hand, the experiments proved that the concept is suitable for the starter/generator application. The fault tolerance and robustness of the starter/generator in the vehicle need to be investigated.

ACKNOWLEDGEMENTS

First, I would like my advisor, Dr Iqbal Husain, who gave me this opportunity to study in the United States and deepen my knowledge on motor drives. Thus, he introduced me to hybrid technology through the Challenge X project, which is the field I decided to get specialized in.

Also, I would like to thank my committee members who, throughout the project, offered me their help and expertise to achieve the goal of this thesis.

Finally, I would like to thank my fellow students with whom I worked and who helped me, the first of them being Ludovic Chretien. Also, the whole Challenge X team for their enthusiasm in this project: I learned a lot working with them.

TABLE OF CONTENTS

	Page
LIST OF TABLES	ix
LIST OF FIGURES	x
CHAPTER	
I. INTRODUCTION	1
1.1 Thesis Motivation	3
1.2 Thesis Organization	4
II. PM-BLDC MACHINES AND STARTER/GENERATORS	6
2.1 Machines used for Starter/Generators.....	6
2.2 Permanent Magnet Brushless-DC (PM-BLDC) Machines.....	9
2.3 Review of PM-BLDC Machine Control.....	11
2.3.1 PI controller	12
2.3.2 Hysteresis control.....	14
2.3.3 Constant voltage/frequency control.....	15
2.3.4 Robust control with sliding observer	16
2.4 Electric Machine and ICE Coupling.....	18
2.5 Conclusions.....	19
III. PM BLDC MACHINE OPERATION AND SIMULATION RESULTS	20

3.1 Theory of PM-BLDC Machines	20
3.2 Current PI Controller Gains	25
3.3 Simulations	28
3.3.1 Controller lock	31
3.3.2 PM-BLDC machine block	33
3.3.3 Inverter and source blocks	34
3.4 Simulation Results	34
3.5 Conclusion	42
IV. PM-BLDC MACHINE DRIVE IMPLEMENTATION	44
4.1 Hardware Components.....	44
4.1.1 Electric machine.....	44
4.1.2 Power inverter	45
4.1.3 Electronic boards	46
4.1.3.1 Power board	47
4.1.3.2 Instrumentation board	49
4.2 DSP Programming	51
4.2.1 Control software.....	51
4.2.1.1 Global architecture.....	51
4.2.1.2 Interrupt architecture.....	55
4.2.2 CAN protocol and code	62
4.2.2.1 Presentation of the CAN protocol and the DSP CAN module	62
4.2.2.2 Messages' format	63
4.2.3. Fault management.....	64

4.2.3.1 Instrumentation board errors.....	65
4.2.3.2 Power supply board.....	66
4.2.3.3 Motor.....	66
4.2.3.4 Inverter.....	67
4.2.3.5 DSP.....	69
4.2.3.6 CAN bus communication.....	70
V. EXPERIMENTAL RESULTS.....	71
5.1 Proceedings of the Experiments.....	71
5.1.1 Low power testing with a DC machine dynamometer.....	71
5.1.2 Testing with the Diesel engine.....	74
5.2 Results at Low Power.....	77
5.2.1 Motoring test.....	77
5.2.2 Generating tests.....	80
5.3 Medium Power Tests with Diesel Engine.....	81
5.4 Full Power Testing with Diesel Engine.....	83
5.4.1 Startup.....	83
5.4.2 Generation testing.....	84
5.4.2.1 Moderate ICE speed tests.....	84
5.4.2.2 Higher speeds and protection.....	88
5.5 Changes in the Simulation.....	94
5.6 Summary.....	98
VI. SUMMARY AND CONCLUSIONS.....	99
6.1 Summary.....	99

6.2 Contributions.....	100
6.3 Suggestions for Future Work.....	101
6.3.1 Improvements in simulation	101
6.3.2 Design of a feed-forward compensator.....	102
6.3.3 Additional experiments.....	103
6.3.4 Noise immunity and controller ruggedness	103
6.3.5 Single-current sensor control.....	104
6.3.6. Current overshoot control	104
REFERENCES	105
APPENDICES	107
APPENDIX A: PM-BLDC MACHINE SYSTEM SIMULATION BLOCKS.....	108
APPENDIX B: ELECTRONIC BOARD CIRCUITS.....	117
APPENDIX C: PICTURES OF THE ACTUAL HARDWARE.....	121
APPENDIX D: CAN MESSAGES DESCRIPTION	123
APPENDIX E: FAULTS DESCRIPTION	124

LIST OF TABLES

Table	Page
3-1: Generating mode simulation results summary	42
4-1: Position detection	57
5-1: Summary of generation testing.....	94

LIST OF FIGURES

Figure	Page
2-1: Construction of a PM-BLDC Machine.....	9
2-2: AC machine.....	10
2-3: PM-BLDC MACHINE drive architecture.....	11
2-4: System continuous model.....	13
2-5: Hysteresis control principle.....	14
2-6: PM drive architecture with speed control of [4] and [5].....	15
2-7: C- Dump converter.....	16
3-1: PM-BLDC machine composed back-EMF and current waveforms' shapes.....	21
3-2: PM-BLDC machine phase model.....	24
3-3: Actual motor composed back-EMF shape.....	29
3-4: Simulation's system block representation.....	30
3-5: 6-switch inverter.....	31
3-6: Simulation's current controller's block.....	33
3-7: E_a , E_b and E_c at 4290rpm.....	35
3-8: E_a and I_a at 4290rpm/7524W.....	36
3-9: T and T_{ref} at 4290rpm/7524W.....	36
3-10: E_a and I_a at 4290rpm/16840W.....	37

3-11: T and T_{ref} at 4290rpm/16840W	38
3-12: E_a and I_a at 5720rpm/20900W	39
3-13: T and T_{ref} at 5720rpm/20900W	39
3-14: E_a and I_a at 8580rpm/15300W	41
3-15: T and T_{ref} at 8580rpm/15300W	41
4-1: Relay driver circuitry.....	48
4-2: Digital signals level adaptation	49
4-3: Flow-chart diagram of the DSP operations	52
4-4: PWM generation.....	55
4-5: Flow-chart of the DSP program	56
5-1: DC machine dyno test setup	72
5-2: Test setup with Diesel Engine	75
5-3: E_{ab} and I_a at 1083rpm/712W.....	77
5-4: E_{ab} and I_a at 743rpm/1466W.....	78
5-5: E_{ab} and I_a at 236rpm/155W.....	80
5-6: E_{ab} and I_a at 1162rpm/2281W.....	81
5-7: E_{ab} and I_a at 4290rpm/7524W.....	82
5-8: I_a at 4290rpm/16840W	85
5-9: I_a at 4290rpm/11450W	86
5-10: I_a at 5720rpm/15050W	87
5-11: I_a at 4290rpm/16800W	89
5-12: I_a at 4862rpm/19030W	90
5-13: I_a at 5720rpm/20900W	91

5-14: I_a at 8580rpm/7600W	92
5-15: I_a at 8580rpm/15300W	93
5-16: E_a and I_a at 4290rpm/16846W, ICE speed = 1500 RPM, phase current command = 150A.....	95
5-17: T and T_{ref} at 4290rpm/16846W	96
5-18: E_a and I_a at 8580rpm/15274W, ICE speed = 3000RPM, phase current command = 68A.....	97
5-19 T and T_{ref} at 8580rpm/15274W	97
6-1: Feed-forward model	102
A1: Main simulation window	108
A2: “BLDC” block	109
A3: “Controller” block.....	110
A4: “Modulo $2*\pi$ ” block	111
A5: “Subsystem 1” block.....	112
A6: “Subsystem 1” block.....	113
A7: “In1 – Position indicator” block in “Controller” block.....	114
A8: “Subsystem” block.....	115
A9: “PI controller” block	116
B1: Power Supply board schematic	117
B2: Circuitry for information through Pull-up signals	118
B3: CAN communication hardware.....	119
B4: Current sensing circuitry	120
C1: Power Supply and Instrumentation Boards.....	121
C2: Inverter	122

C3: PM-BLDC Machine..... 122

CHAPTER I

INTRODUCTION

The increasing cost of gas at the pump, the desire for independence from foreign oil and the impact of the vehicles' pollution on the environment and on people's health have led automobile manufacturers to develop alternative technologies for commercial and personal transportation. Different solutions have been considered: new types of fuel (ethanol, Bio-diesel, hydrogen) and their accompanying new technologies (flex-fuel), electric cars (GM's EV1), hybrid cars (Toyota Prius and Camry, Honda Civic and Accord, Ford Escape, etc.) and the latest trend the "plug-in" hybrids (on-road replenishment of the batteries as well as "at home," plugged into the power grid).

In an effort to develop the hybrid cars of the near future, General Motors and the U.S. Department of Energy have launched a 3-year competition named Challenge X, wherein 17 universities, including the University of Akron, compete in developing hybrid concept-cars using a stock model of a Chevrolet Equinox. The University of Akron decided to develop a hybrid electric vehicle based on a series/parallel architecture. In series operation, the internal combustion engine (ICE) is decoupled from the wheels and is used solely to recharge a set of batteries or to provide energy to an electric motor used to drive the car. In parallel operation, the electric motor and the combustion engine combine their effort to move the car, hence acting in "parallel." By combining both

technologies, the University of Akron's architecture allowed for two additional specific modes of operation: split-parallel, where the combustion engine provides motion to the front axle and power to the electric motor acting on the rear axle, and peak-parallel, where the starter/generator coupled to the combustion engine also acts as a motor, hence increasing the torque capability of the vehicle.

Hybrid electric vehicles employ a wide variety of electric machines. The types of electric machines used depend on their utility in the vehicle as well as on manufacturing considerations. The number of electric machines present in the vehicle also depends on the type of hybrid vehicle architecture implemented. For the competition, the University of Akron had chosen to use two electric motors for its series-parallel operation. One is used for the propulsion, while the other one is used as a starter/generator, belt-coupled to the combustion engine.

Starter/generator machines play two roles in a car: they provide cranking torque to start the internal combustion engine and also serve the purpose of recharging the battery and providing electrical power to all the electrical accessories operating while the car is being used. In the University of Akron's configuration, the battery being recharged is a high-voltage battery that provides energy to the electric motor used for propulsion. Also, the starter/generator acts as a power-assist device to the internal combustion engine in Akron's configuration.

For power density considerations, a Permanent Magnet Brushless DC (PM-BLDC) electric machine was chosen for the starter/generator application. This choice necessitated the development of the controller by the University of Akron. The

development of the torque controller for the electric machine forms the basis of the research conducted and presented in this thesis.

The first part of the thesis will present a review of the starter/generator systems and of PM-BLDC machine control. In the second chapter, the control implemented and the simulation will be reviewed in detail. It will be followed by a presentation of the physical implementation of the system. Finally, the results obtained during experiments will be presented and analyzed, followed by conclusions drawn from the complete study of the system.

1.1 Thesis Motivation

Electric machines are one of the key elements of the electric and hybrid vehicles. The development of electric machines and controllers to improve the power density and efficiency is of high interest to the industry. The power density and weight/power ratio are indeed critical to the development of any vehicle; this is especially true for electric and hybrid vehicles, where energy savings is one of the goals. The reduction of energy loss by developing an efficient torque controller for a hybrid vehicle starter/generator prototype is the primary motivation for this research.

Starter/generator applications in hybrid vehicles have been mostly developed around induction machines and at low to medium power range (3 to 5kW) [2,3,10]. The generator coupled to the ICE in the hybrid vehicle developed at the University of Akron was required to deliver a maximum power of 20kW. This thesis' contribution is in developing a starter/generator for a higher power level with a PM-BLDC machine than is generally found in hybrid vehicles. It also demonstrates the feasibility of power

generation over a wide speed range. Also, a comprehensive fault detection scheme was developed that made the starter/generator particularly suitable to be used as a component of a complex hybrid vehicle system.

1.2 Thesis Organization

The thesis presents the development of the controller for a PM-BLDC based starter/generator for a hybrid electric vehicle. It is provided to familiarize the reader with starter/generator applications in hybrid vehicles. It will explain the different steps used to design and develop a suitable controller, the first of which is to model and simulate the system.

In the second chapter, different torque control methods for PM-BLDC machines described in various publications will be presented. Also, equivalent applications will be analyzed to present the common problems associated with PM-BLDC machine drives. Examples of starter/generator applications with emphasis on perturbation related issues will be presented. Comparative studies of the different electric machines used in starter/generator applications will be presented.

In the third chapter, the theory of the PM-BLDC machine operation and the controller developed for the application will be presented. The computer simulation of the PM-BLDC machine drive developed for analysis will be presented in detail. Furthermore, results and conclusions derived from the simulations will be presented.

In the fourth chapter, the hardware design is presented. Interface circuitry had to be developed to sense the currents needed to be controlled, as well as the motor's

position; the schematics and their explanations are presented in this chapter. The software developed for the controller is also presented with details.

In the fifth chapter, the experimental results are presented. Experiments were conducted on different setups to test at various power levels. This section explains in detail how the experiments were conducted and the results that were obtained. Analysis of the results is also presented.

In the last chapter, a summary of the work is presented, along with recommendations and suggestions for future research work, and for the next generation of this project.

CHAPTER II

PM-BLDC MACHINES AND STARTER/GENERATORS

A review of the existing literature on the subject was made to determine the appropriate control strategy to use for torque control in the PM-BLDC based starter/generator. Also, a comparative study of other starter/alternator ensembles was run to understand the behavior of an electric machine coupled to an internal combustion engine and the potential difficulties that could arise. This chapter also presents a comparison between the different motors available for the starter/generator application.

2.1 Machines used for Starter/Generators

Electric machines are classified according to the mechanism of establishing the rotating field in the stator and the rotor. Rotating stator fields in electrical machines are generated using electrical excitation. In addition, a field at the rotor must also be created, i.e. the rotor has to be magnetically oriented in order to make it spin. Different solutions exist to produce the rotor field:

- The rotor's field can be induced from the stator, because of the rotor's structure (as in the induction machine)
- The rotor can be electrically excited so that it would create a magnetic field with a constant orientation (as in the synchronous machine)

- The shape of the rotor can induce reluctance variations in the stator (as in the switched reluctance machine)
- The rotor can be permanently magnetized with permanent magnets (as in the PM machines).

The conventional induction and synchronous machines have certain disadvantages: in the case of synchronous machines, the need for an electric source to energize the rotor leads to a less efficient system. In addition, electrical losses will occur if mechanical connectors, such as rings and brushes, are used to provide the rotor with the DC-excitation. These elements will also suffer from mechanical aging, which makes them less reliable. As for induction machines, part of the current in the stator must serve to magnetize the rotor, and therefore does not contribute to the production of torque, which will reduce the efficiency. One criterion of good operation is the smoothness of the rotation of the rotor; the switched reluctance motor is prone to high torque ripple, which makes it a bad candidate for applications that require smooth operation. The motors with permanent magnets are the most efficient because they don't require an external field excitation. In this category of motors, two main motors emerge: the Permanent Magnet Synchronous Machine (PMSM) and the Permanent Magnet Brushless Direct Current machine (PM-BLDC). PMSMs have sinusoidal back-EMF, while PM-BLDC machines have trapezoidal back-EMF.

Any one of the machines mentioned can be used for the starter/generator application [3]. The researchers in [3] selected an induction machine for a three-phase 4kW starter/generator for the ease of manufacture and cost. The induction motors have good efficiency and smooth torque, and have been widely studied and used, which gives

them an advantage. However, the rotor losses and the cooling of the rotor are a concern for the induction machine.

Switched reluctance machines are attractive because of their simple design, and fault-tolerance capability in the face of switch failures. However, their study and development are still in an early stage and their use in current industrial applications is still limited.

Finally, PM machines are attractive because these machines have the great advantage of having the highest efficiency. The cost is an impediment due to the use of expensive permanent magnets. The permanent magnets are also vulnerable at elevated temperatures.

In [2], another type of permanent magnet electric motor, known as double-stator electric machine, is used to develop a starter/generator application. The interest of this research was to develop a motor drive that would be compact, have a high starting torque and a wide speed range when operated as a generator. The general idea is to have, from the center of the motor to the outside, first a stator, then the rotor, and finally the second stator. The rotor is made of permanent magnets, while the stators have windings. A finite element analysis was conducted and prototypes were built; they showed improvements over the level and the shape of the voltage generated by this special kind of motor. The best improvements were made possible by adjusting the pitch displacement of the two stators. The latter factor was also considered in order to obtain attractive values of average torque and torque ripple.

The electric machine chosen for the Akron hybrid vehicle starter/generator is a PM-BLDC machine. The selection was based on both the availability of a 20kW PM-

BLDC machine and the technical advantage of this machine for the intended application. The review of PM Brushless Machines and their control will be presented next.

2.2 Permanent Magnet Brushless-DC (PM-BLDC) Machines

Permanent Magnet Brushless-DC machines are widely used in the industry for their ease of control and their high power density. Their drawbacks are the high price (due to the rare-earth magnets) and relatively high torque ripple, compared to a sinusoidal machine.

The PM-BLDC machine is made of two main parts: one with windings, another one with permanent magnets. The magnets, generally positioned on the rotor, provide a constant magnetic field. The stator, which holds the windings, is constituted of several phases (most commonly three). Figure 2-1 shows a machine with four poles (four magnets), and a crude example of three phases at the stator, with two windings per phase.

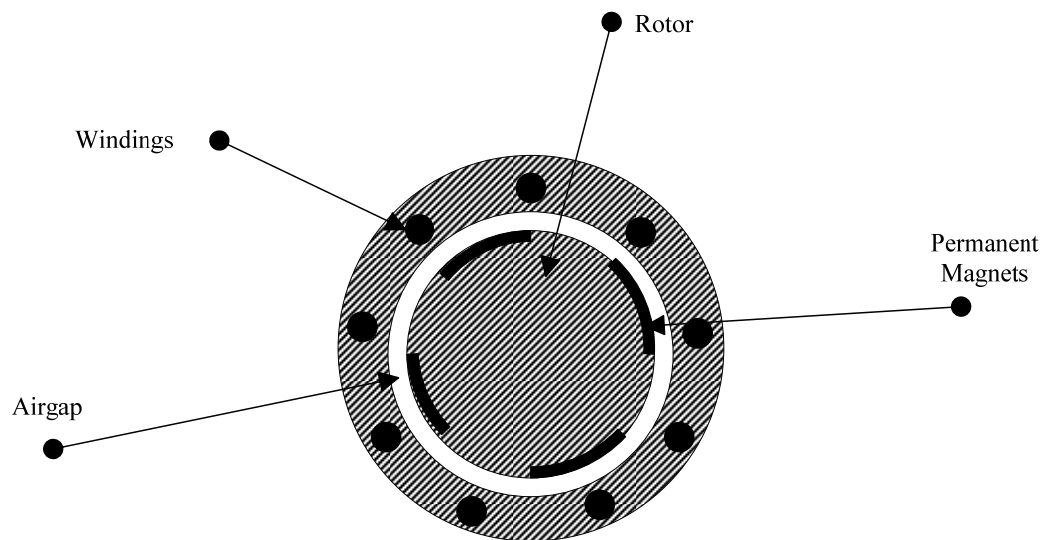


Figure 2-1: Construction of a PM-BLDC machine

Let us consider a three-phase machine with four poles, as shown in Figure 2-2 (much like Figure 2-1). The stator phases are fed with three 120° electrically shifted sinusoidal

voltages, each of which induces a field. The phase shifted fields combine through vector addition to result in the stator field.

Let the stator field be identified by an arrow in Figure 2-2(a). The pole thus represented is defined as a north pole. It will attract the closest south pole of the rotor, whose magnetic field will align with the stator field, as can be seen in Figure 2-2(a). As phase voltages vary sinusoidally, the stator field will rotate, because of space phase shifts of the 3-phase stator windings. Since the rotor and the stator fluxes are synchronized, the rotor will rotate at the same speed as illustrated in Figure 2-2 (b) and (c). This is a simplified example since losses are not taken into account.

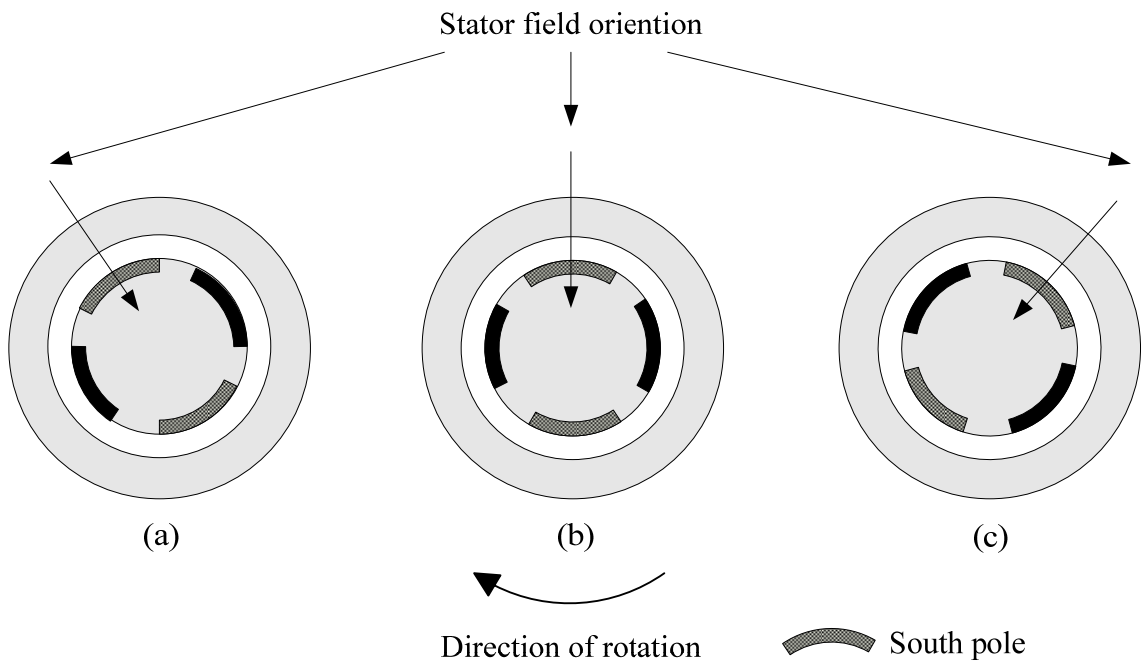


Figure 2-2: AC machine

The characteristic shape of the back-EMF of the PM-BLDC machine is trapezoidal. This is in contrast with the PMSM, which has a sinusoidal back-EMF. The windings are wound in a different fashion to obtain such a result. The control of a PM-

BLDC machine is based on using only the flat portion of the back-EMF in combination with rectangular shaped currents to produce torque ([1]).

Figure 2-3 represents a PM-BLDC machine drive. The controller generates the signals to command the power switches in the inverter in order to deliver the proper currents to the phases. The rotor position and the phase current is used to control the torque and, depending on the application, the speed of the PM-BLDC machine.

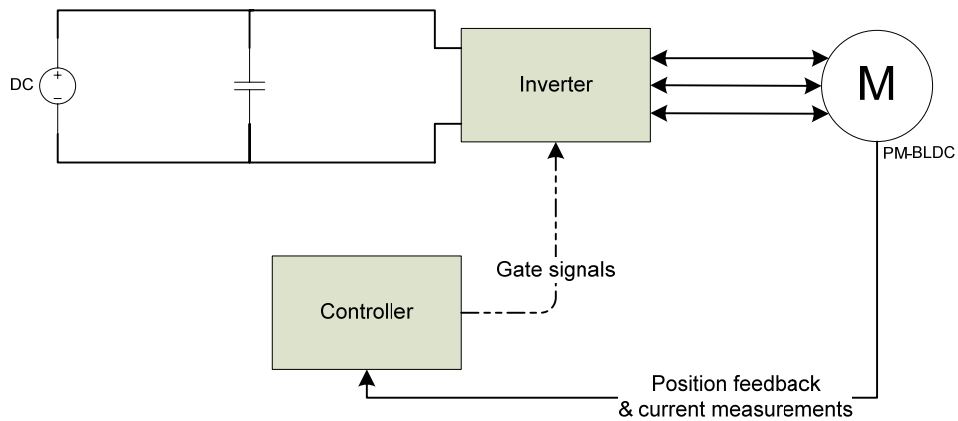


Figure 2-3: PM-BLDC machine drive architecture

PM-BLDC machines are widely used in hard-drive servos at small power levels and are also used for hybrid vehicle applications [4], [5], [6], [7] at higher power levels. There are many other applications of PM-BLDC machines, ranging in power levels from fractional kiloWatts to multiple kiloWatts.

2.3 Review of PM-BLDC machine control

The variables of an electric machine that can be controlled are speed, torque, and phase currents. The regulation can be made open-loop, where no feedback is used, or closed-loop, where feedback is used. A two-stage controller consisting of an inner loop

and an outer loop has been designed for the closed loop drive system. The driver system controller will be presented in this part of the chapter.

In electric machines the torque is controlled in the inner loop and the speed is controlled in the outer loop. The torque in PM machines is controlled by regulating the current. The common approaches for current control in a PM-BLDC machine are the PI controller and the hysteresis controller. These two controllers along with a couple of other PM control methods are described below.

The control strategies to be presented are the ones that can be or have been used to control PM-BLDC machines, some of them in starter/generator applications. Furthermore, a discussion on the methods of coupling an electric motor and internal combustion engine will be presented.

2.3.1 PI controller

An efficient and quite robust way to control the torque, i.e. the current, in a motor is to use a Proportional-Integral (PI) controller. The continuous time equation of the PI controller is

$$C(p) = K \left(1 + \frac{1}{T_i \times p} \right) \quad (2.1)$$

where K is the proportional gain and $\frac{K}{T_i}$ is the integral gain, and p is the Laplace complex variable. The closed-loop system can be represented as in Figure 2-4. The purpose of the controller in this closed-loop system is to minimize the error between the reference and the feedback. In addition to this tracking ability, it is also used to improve

the system's dynamic response and behavior. One way to understand the PI controller behavior is to break down its action between the proportional and integral terms.

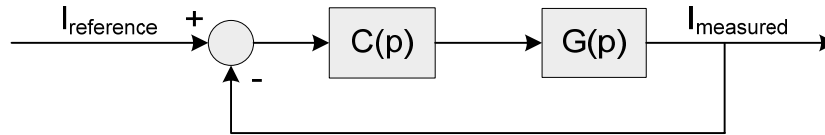


Figure 2-4: System continuous model

The action of the proportional part of the controller can be summarized as giving an immediate response to a difference between the reference and the feedback. A large proportional gain will make the controller more sensitive and hence make the system potentially more unstable; the system would likely be oscillating because a small variation in the difference would result in a larger than needed action of the controller. It would hence overshoot and react by overcompensating in the other direction. On the other hand, if the system is stable, it will ensure a fast response with a small steady-state error. As the system converges towards the reference, the action of the proportional term will reduce, unless perturbations in the system appear.

The integral term, conversely, uses past as well as present values of the error. Because past and present errors are integrated, a steady-state error will result in an increasing compensating action of the controller. This, in turn, will make the difference between the reference and the measured value to converge towards zero.

It must be understood that, with a pure proportional controller, the system would always need a non-zero error in order to generate a non-zero command. The addition of the integral term keeps the last updated command even though the system output has

reached the reference. Thus, the necessary command is produced when there is a zero error.

2.3.2 Hysteresis control

The hysteresis control is also referred to as bang-bang control. Indeed, hysteresis control consists of defining a band around the desired value of current. Then, in case of an inverter, depending on the position of the rotor, switches will be closed until the current has reached the upper limit of the predefined band. Then, the switches would be turned off until the current reaches the lower limit of the band.

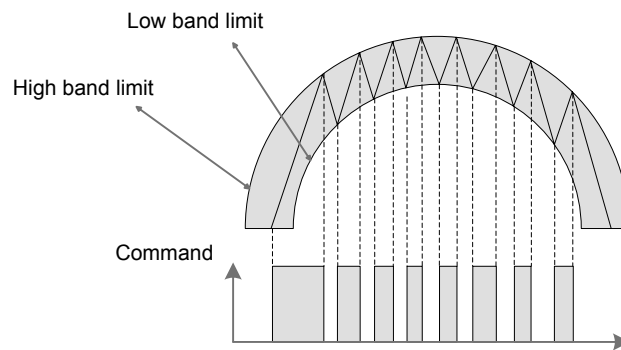


Figure 2-5: Hysteresis control principle

With the hysteresis control, the frequency of the command signals is not constant as shown in Figure 2-5. This is in contrast with PWM control signals, which operate at fixed frequency. When hysteresis control is implemented by analog means, the current ripple can easily be contained within the defined band, since the current reference will be virtually constant during the period of the command signal. However, if the hysteresis control is implemented digitally, the current becomes more prone to overshoots because the command signals are turned on and off with a fixed periodicity; hence, the command

could still be on even though the current has exceeded the range leading to an overshoot. Current undershoots can be explained with the same logic, but they are of less concern because they will not have any consequences unlike large overshoots.

2.3.3 Constant voltage/frequency control

The current controller in [4] addresses the issue of torque control, i.e. current control, by implementing a constant voltage over frequency control. The pulses injected to the inverter's power switches have a fixed duty cycle, but their frequency varies to compensate for the variations in the speed. Hence, to facilitate torque smoothness, a constant ratio of voltage to frequency is implemented. This provides a voltage command to the inner-loop controller that ultimately controls the torque (current). The controller will hence act on the DC voltage provided to the inverter by controlling the turn on and off of a thyristor based AC/DC converter that provides the DC voltage to the motor's inverter. In [4], this torque control scheme is implemented in the inner loop of a speed control system for a PM-BLDC machine, as shown in Figure 2-6.

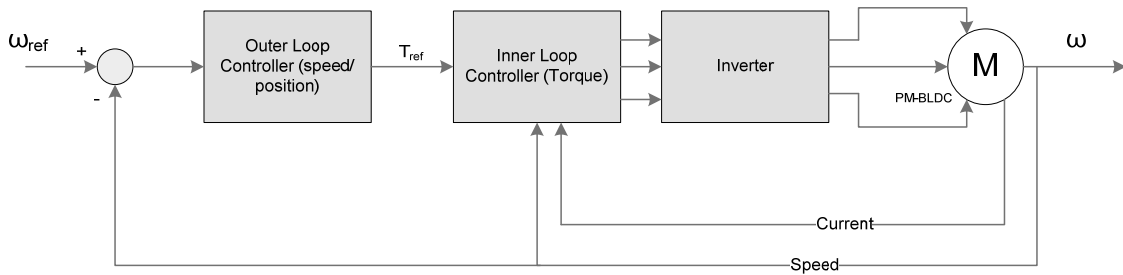


Figure 2-6: PM drive architecture with speed control of [4] and [5]

The inverter used in [4] is a C-dump converter, as depicted in Figure 2-7; this converter is lower cost than conventional inverters because it uses fewer power switches

for a given number of phases. However, it needs access to the neutral point of the motor, which is rarely available. Each phase needs only one switch in order to control the current flow; when the switch is turned off, energy flows from the phase to a capacitor that will need to get discharged through another arm of the inverter after several cycles.

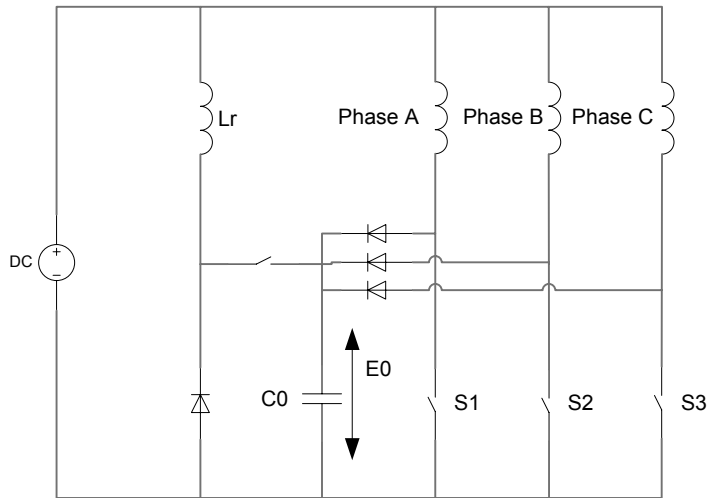


Figure 2-7: C- Dump converter

The experimental results in [4] show good control over the phase currents, but the shape of the phase voltage waveform displays big spikes, such as the ones found in the current phase waveform during the off period.

2.3.4 Robust control with sliding observer

In [5], the authors applied a robust control methodology by developing a sliding observer (also called a Variable Structure Strategy, or VSS) for a five-phase PM-BLDC machine. Based on a torque reference provided by an outer-loop controller following a speed reference, an inner-loop torque controller was developed. The drive system is the same as that shown in Figure 2-6 . The control algorithm ensures that the instantaneous

electro-magnetic torque follows the reference torque as closely as possible. This torque tracking is achieved with minimum current, which increases the efficiency of the system.

To simplify the control, a model of the motor in the DQ-axis coordinates is developed. By adding constraints, the controller achieves electro-magnetic torque T_e control using the torque-current relationship

$$T_e = \frac{5}{2} \times \frac{P}{2} \times \lambda_m \times i_Q \quad (2.2)$$

where P is the number of pairs of poles, λ_m is the flux linkage and i_Q is the current on the Q axis.

The selection of the switching surfaces s_D and s_Q of the sliding mode are defined as

$$\begin{aligned} s_D &= i_{D_{ref}} - i_D \\ s_Q &= T_{ref} - T_e \end{aligned} \quad (2.3)$$

The control functions are

$$\begin{aligned} v_D(x,t) &= V_D \times \text{sgn}(s_D) \\ v_Q(x,t) &= V_Q \times \text{sgn}(s_Q) \end{aligned} \quad (2.4)$$

with v_D and v_Q being the D and Q axes voltages, respectively.

The inequalities for the VSS conditions to hold true are:

$$\begin{aligned} V_D &> R \times i_D - \omega \times (L_{QQ} \times i_Q + L_{QD} \times i_D) + \frac{\partial [L_{DQ} \times i_Q + \lambda_m]}{\partial t} \\ V_Q &> R \times i_Q + \omega \times (L_{DD} \times i_D + L_{DQ} \times i_Q) + \frac{\partial [L_{QD} \times i_D]}{\partial t} \end{aligned} \quad (2.5)$$

where i_D and i_Q are the currents on the D and Q axis, L_{QD} and L_{DQ} the mutual inductances between the D and Q axes, L_{DD} and L_{QQ} are the phase inductances and ω is the electrical speed.

The controller developed in [5] proved to attain a fast transient response in simulation and a torque ripple of about 12%. Experimental results correlate the fast transient response capability observed in the simulation. However, the torque appears to have noise not present in the simulation, probably due to the switching noise induced by the inverter and by the sensor measuring the torque.

The achieved torque ripple is attractive with five phases, but this is a “natural” tendency when increasing the number of poles. The drawbacks are increased mechanical and winding complexity.

2.4 Electric Machine and ICE Coupling

The 4-kW induction machine based starter/generator described in [3] used a belt-drive instead of a chain or a gear drive for its simplicity of mounting in an existing vehicle. The belt coupling also enabled a larger machine to be installed in the vicinity of the existing alternator. Other advantages are that a belt-drive can be easily adapted for different configurations, and also that there is no need for lubrication. In comparison, it is difficult to design a gear-drive to operate at high speeds; doing so would require the development of dual-stage gears that require transmission modifications, or the use of costly higher grade materials and manufacturing processes. The disadvantages with a chain drive are a non-negligible acoustic noise and an additional level of maintenance that increase cost to the final customer.

The researchers of [3] found the belt solution to meet the system requirements. It also underlined among other issues the need to carefully model mechanical transients and electrical behavior. These came into play while testing the application.

2.5 Conclusions

Several ways to control the torque of a PM-BLDC machine have been developed and tested over the past decade as has been seen in this chapter. Likewise, with the development of hybrid technologies, several designs for starter/generator applications have been attempted.

The torque control of a PM-BLDC machine using a PI controller is the primary objective of this research. The development of the torque controller and its implementation in a digital signal processor are the main tasks accomplished for the thesis work. The description of the machine model and the simulation of the system are presented in the next chapter.

CHAPTER III

PM BLDC MACHINE OPERATION AND SIMULATION RESULTS

The principles of operation of the PM-BLDC machine and the PI controller used for current regulation are presented in this chapter. The simulation model developed to analyze the machine, the inverter and its controller and the results obtained are then presented and discussed.

3.1 Theory of PM-BLDC Machines

The PM machines have permanent magnets in the rotor, while the stator carries the windings. Depending on the winding arrangement the two PM machine types are the permanent magnet synchronous machine (PMSM) and the permanent magnet brushless DC (PM-BLDC) machine. When their rotors are spun by another motor, a difference of potential appears between two phases, which is called back-electro-motive force (back-EMF), in accordance with Faraday's law. Because of their different windings' configurations, the back-EMFs have different shapes for the two machines: in the case of the PMSM, the shape is sinusoidal; for the PM-BLDC machine, it is trapezoidal. Figure 3-1 shows the back-EMFs of the PM-BLDC machine:

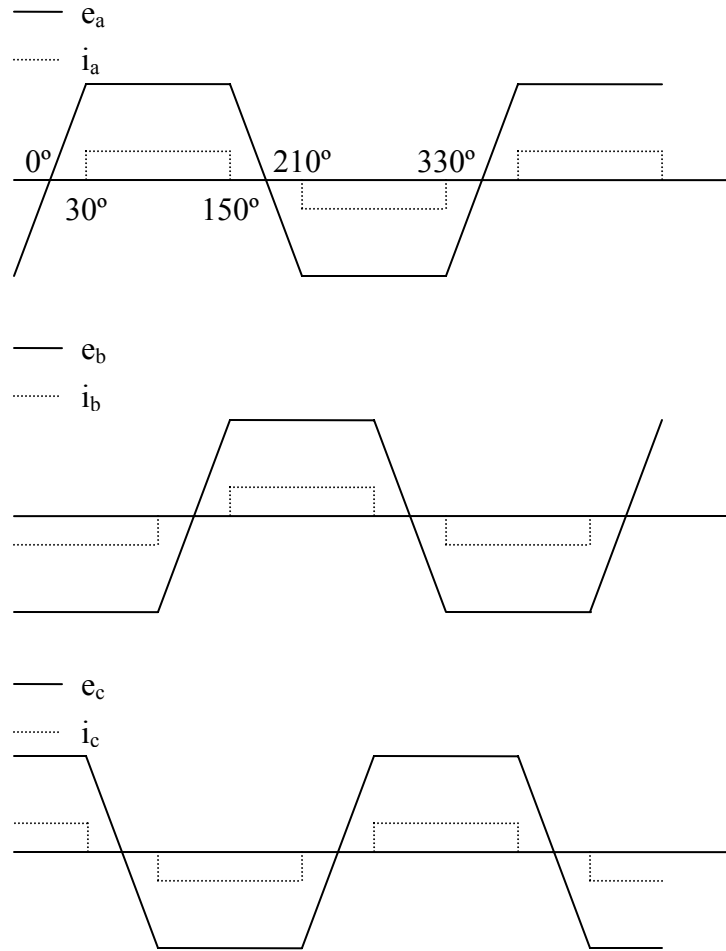


Figure 3-1: PM-BLDC machine composed back-EMF and current waveforms' shapes

Figure 3-1 also shows the shapes of the ideal currents would need to produce no torque ripple. However, due to non-instantaneous rise and fall times of the currents, the current waveforms are not exactly rectangular in practice.

The electrical model for the three-phase PM-BLDC machine can be written as

$$\begin{bmatrix} v_a \\ v_b \\ v_c \end{bmatrix} = \begin{bmatrix} R & 0 & 0 \\ 0 & R & 0 \\ 0 & 0 & R \end{bmatrix} \begin{bmatrix} i_a \\ i_b \\ i_c \end{bmatrix} + p \begin{bmatrix} L_a & L_{ba} & L_{ca} \\ L_{ab} & L_b & L_{cb} \\ L_{ac} & L_{bc} & L_c \end{bmatrix} \begin{bmatrix} i_a \\ i_b \\ i_c \end{bmatrix} + \begin{bmatrix} e_a \\ e_b \\ e_c \end{bmatrix} \quad (3.1)$$

where

- v_a, v_b and v_c are the phase voltages referenced to the neutral point of the machine
- i_a, i_b and i_c are the phase currents
- $e_a, e_b,$ and e_c are the phase back-EMFs referenced to the neutral of the machine
- R is the phase resistance
- $L_{a,b,c}$ are the phase inductances and $L_{ba}, L_{ca}, L_{ab}, L_{cb}, L_{ac}, L_{bc}$ are the mutual inductances between the phases

In the model, it has been assumed that phase inductances are independent of rotor position and that the system is perfectly balanced (mechanical construction assumed perfect), i.e.,

$$\begin{aligned} L_a &= L_b = L_c = L \\ L_{ab} &= L_{ca} = L_{cb} = M \end{aligned} \quad (3.2)$$

This leads to the simplified equation

$$\begin{bmatrix} v_a \\ v_b \\ v_c \end{bmatrix} = \begin{bmatrix} R & 0 & 0 \\ 0 & R & 0 \\ 0 & 0 & R \end{bmatrix} \begin{bmatrix} i_a \\ i_b \\ i_c \end{bmatrix} + \begin{bmatrix} L & M & M \\ M & L & M \\ M & M & L \end{bmatrix} p \begin{bmatrix} i_a \\ i_b \\ i_c \end{bmatrix} + \begin{bmatrix} e_a \\ e_b \\ e_c \end{bmatrix} \quad (3.3)$$

For a three-phase system with a neutral connection

$$i_a + i_b + i_c = 0 \quad (3.4)$$

Hence,

$$Mi_b + Mi_c = -Mi_a \quad (3.5)$$

Therefore,

$$\begin{bmatrix} v_a \\ v_b \\ v_c \end{bmatrix} = \begin{bmatrix} R & 0 & 0 \\ 0 & R & 0 \\ 0 & 0 & R \end{bmatrix} \begin{bmatrix} i_a \\ i_b \\ i_c \end{bmatrix} + \begin{bmatrix} L-M & 0 & 0 \\ 0 & L-M & 0 \\ 0 & 0 & L-M \end{bmatrix} p \begin{bmatrix} i_a \\ i_b \\ i_c \end{bmatrix} + \begin{bmatrix} e_a \\ e_b \\ e_c \end{bmatrix} \quad (3.6)$$

In a motor where the back-EMFs vary in a sinusoidal fashion, a transformation from the a,b,c representation to the d,q representation can be made in order to make the motor control easier. But applying this transformation to the PM-BLDC motor would make the equations even more complicated due to the need to decompose the back-EMFs into sinusoidal elements, using Fourier series. Hence D-Q transformation is not used in PM-BLDC machines.

The electro-magnetic torque completely balances the mechanical torque in steady state when mechanical losses are neglected. Hence, the electro-magnetic torque T_e equation of a PM-BLDC machine is given by

$$T_e = \frac{e_a i_a + e_b i_b + e_c i_c}{\omega_r} \quad (3.7)$$

The equation of motion is

$$p\omega_r = \frac{T_e - T_L - B\omega_r}{J} \quad (3.8)$$

where J is the moment of inertia, B the damping coefficient, ω_r the rotor speed and T_L the load torque. The equivalent circuit of one phase of the motor is given in Figure 3-2.

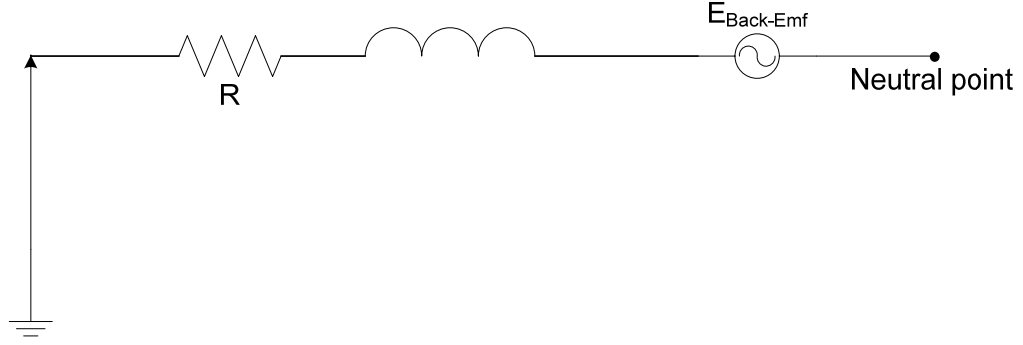


Figure 3-2: PM-BLDC machine phase model

The voltage equation per phase is

$$V_{phase} = R \times i_{phase} + (L - M) \times \frac{di_{phase}(t)}{dt} + e_{phase}(t) \quad (3.9)$$

At any point in time, two phases are conducting, as can be seen in Figure 3-2. For example, if the upper switch of phase A and the lower switch of phase B are commutating, we have

$$V_{DC} = v_a - v_b = R \times i_a - R \times i_b + p \times (L - M) i_a - p \times (L - M) i_b + e_a - e_b \quad (3.10)$$

Since the same current flows in phase A and phase B,

$$i_b = -i_a \quad (3.11)$$

Also, e_a and e_b having the same amplitude E but different signs (Figure 3-1) at the given instant, which gives

$$e_a - e_b = 2E \quad (3.12)$$

In the starter/generator application, the electrical dynamics are much faster than the mechanical ones. In the study of the torque controller, this leads to making the assumption that E , whose values is solely dependent on the value of the speed, is a

parameter that could be considered constant during the period when the current controller reaches a steady state.

By defining the machine input variable as

$$V' = V_{DC} - 2E \quad (3.13)$$

we get the machine transfer function

$$G(p) \equiv \frac{I}{V'} = \frac{1}{2R + 2Lp} \quad (3.14)$$

The above linearized model will be used to develop the PI current controller.

3.2 Current PI Controller Gains

The theory and architecture of the PI controller are presented in Section 2.3.1. From (3.14), the input to the PI controller is a current measurement and the output is a voltage command. Writing the equation of the closed-loop system (Figure 2-4) leads to

$$\begin{aligned} \frac{I_{measured}}{I_{reference}} &= \frac{C(p)G(p)}{1 + C(p)G(p)} \\ &= \frac{K(1 + T_i \times p)}{K(1 + T_i \times p) + T_i \times p(R' + L \times p)} \end{aligned} \quad (3.15)$$

In order to cancel the pole of the machine transfer function, the integral control parameter

is chosen as $T_i = \frac{L}{R}$. Hence, (3.15) becomes

$$\begin{aligned}
\frac{I_{measured}}{I_{reference}} &= \frac{K(1+T_i \times p)}{K(1+T_i \times p) + R'T_i \times p(1+T_i \times p)} \\
&= \frac{K}{K + L' \times p} \\
&= \frac{1}{1 + \frac{L'}{K} \times p}
\end{aligned} \tag{3.16}$$

with $R' = 2R$, $L' = 2L$

Discretizing the controller equation, we have

$$\begin{aligned}
C(z) &= K_p + K_{iz} \frac{1}{z-1} \\
\text{with } K_p &= K \\
K_{iz} &= \frac{K}{T_i} \times \text{sampling time}
\end{aligned} \tag{3.17}$$

In order to determine the gains of the controller, close attention had to be paid to the speed and torque variations of the generator. In the application developed by the University of Akron, the electric machine is coupled to the ICE, which introduces significant torque ripples.

The speed variations of the ICE, governed by equation (3.8), are much slower than the current and torque variations of the generator. The speed time constant is on the order of 100ms, whereas the electrical time constant of the generator is on the order of 8ms. Therefore, the speed is assumed to be constant during each sampling interval of the current control loop, and is taken into account in the estimation of the machine back-EMF used in equation (3.13).

The most critical restriction will be for the generator to reach a given current in one phase much faster than the phase conduction period. The worst case in that situation is at the highest speed at which the generator is supposed to be controlled.

In the final application, the ICE and the generator are coupled through a belt. The coupling ratio between the ICE and the generator is determined by the diameters of the pulleys in the mechanical belt coupling system. This coupling ratio was determined such that both machines would be used at their most efficient points during the generation. The coupling ratio was calculated to be 2.86:1. Following the specifications of the PM-BLDC machine (given by the manufacturer) and tests done on the ICE, the optimal operating speeds were respectively around 4500 RPM and 1600 RPM. Following the specifications of the PM-BLDC machine, its highest speed should be 10000 RPM. At this speed, a phase is active for 1 ms. A settling time of 0.5 ms was chosen for the current control loop. From the equation (3. 16), the time constant of the current control loop is $t_r = \frac{L'}{K}$.

At 3 times that value, the system has reached 95% of the reference value. Hence, the gain K can be calculated from

$$0.5\text{ms} = \frac{3L'}{K} \quad (3.18)$$

which leads to having $K = 1.92$.

The choice of the switching frequency was guided by the limitations of the hardware: inverter's switches, computation time in the DSP (Digital Signal Processor). Ideally, the higher the frequency, the lower will be the ripple in current; this results in a smoother torque. Also, above 20 kHz, the switching frequency starts being inaudible,

which hence lowers the sonic pollution. For practical purposes, a frequency of 20 kHz was chosen. Hence, according to (3.17), K_{iz} has the value

$$K_{iz} = \frac{1.92}{8 \times 10^{-3}} \times 50 \times 10^{-6} = 0.012 \quad (3.19)$$

3.3 Simulations

In order to verify the behavior of the motor with the controller, a simulation program of the PM-BLDC machine drive system was developed. The suitable software to use is Matlab with its sub-program Simulink.

The SimPowerSystems library was utilized to represent the inverter and the motor. Hence, a physical model of the power electronics and that of each phase of the motor is used. The back-EMF in each phase of the machine at any given rotor angle was represented using a look-up table. The back-EMF was assumed to be of the perfect trapezoidal shape of the back-EMF. This is not exactly true as can be seen in Figure 3-3, which shows the captured view of the phase-to-phase voltage of the motor driven by a DC motor at a given constant speed. The controller block in the simulation model was implemented using Simulink blocks.

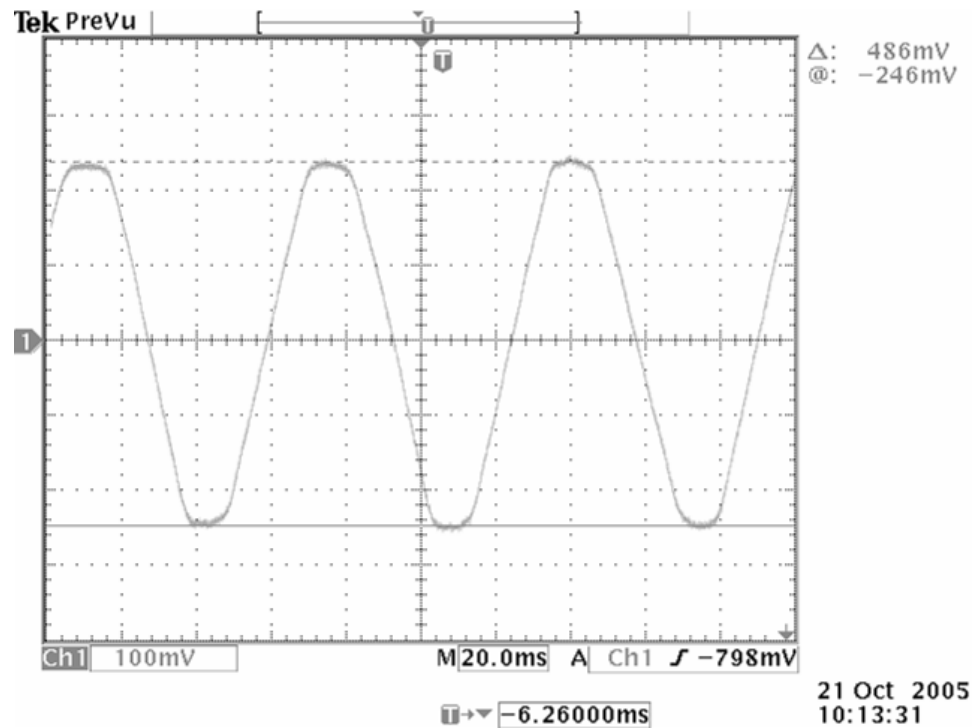


Figure 3-3: Actual motor composed back-EMF shape

The simulation should involve a more rigorous model of the diesel engine coupled to the PM-BLDC machine. However, the simulation was simplified by assuming ideal behavior of the ICE by keeping a constant speed and matching the braking torque applied by the PM-BLDC machine on the shaft in the generating mode. Indeed, this assumption can be formulated because of the inertia and time response of the diesel engine compared to that of the electric machine. Representing the motoring mode would require the modeling of a drive cycle of the car, where forces applied to the wheels would be known, hence to the transmission and the engine, which is beyond the scope of the material presented.

The block diagram of the system, shown in Figure 3-4, gives a visual representation of the components used in simulation. The system comprises four major

parts: the power source, the inverter, the PM-BLDC machine coupled to the ICE and finally the controller. The actual Simulink blocks can be found in Appendix A.

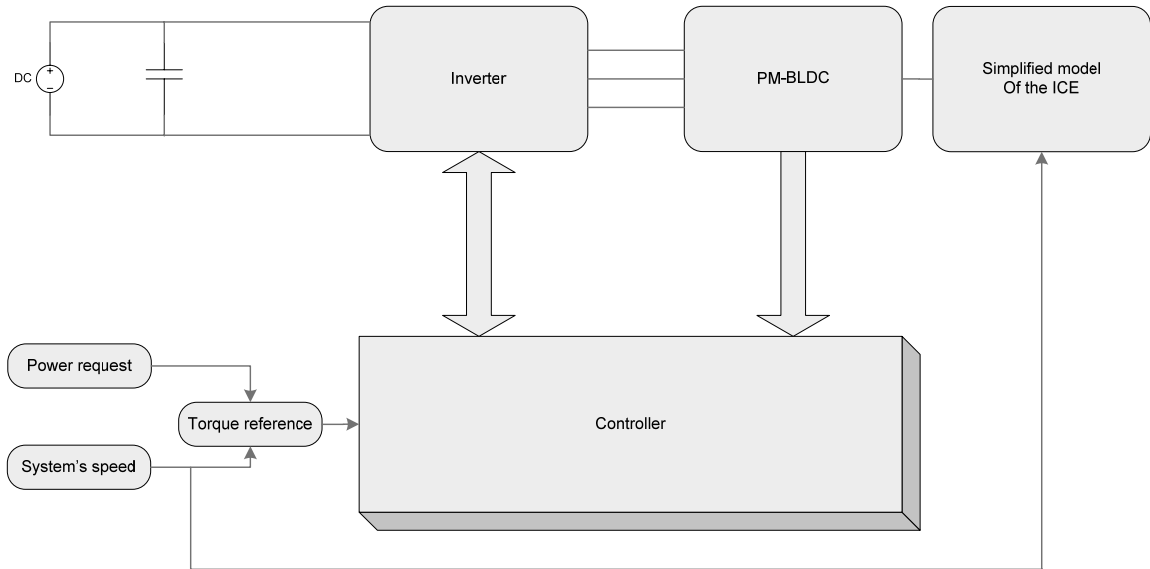


Figure 3-4: Simulation's system block representation

3.3.1 Controller block

A detailed view of the controller block is found in Figure 3-5.

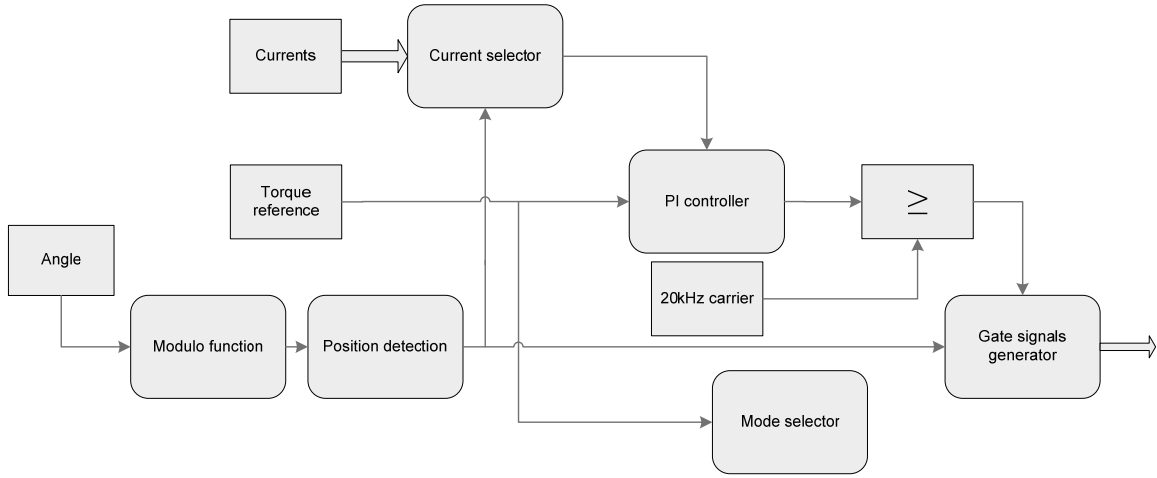


Figure 3-5: Simulation's current controller's block

The controller to be used in the final implementation is a Digital Signal Processor (DSP). The determination of the rotor's position as well as the generation of gate signals for power switches were implemented in simulation with the same accuracy as they would be in the final DSP program. The detailed contents of Figure 3-5 can be found in the figures of Appendix A. Figure 3-5 is the representation of Figure A3.

The rotor position calculations are described in Figures A4, A7 and A8. First, to ease the determination of the position, the latter is evaluated in Figure A2 from the relation $\omega = \frac{d\theta}{dt}$ and then modulated between 0 and 2π in Figure A4. Then, as seen in Figure A8, a number between 1 and 6 is assigned for each of the six intervals of position spaced by $\frac{2\pi}{6}$, starting at $\frac{\pi}{6}$; this represents the six different states the position Hall-effect sensors of the actual PM-BLDC machine can be in.

This information and the mode the system is in, motoring or generating, is what is needed by the subsystem shown in Figures A5 and A6 to determine which switches are to be used at a given point in time.

As for the PI controller, simple gain and discrete transfer function blocks were used, as can be seen in Figure A9.

The topology of the inverter is shown in Figure 3-56. In order to achieve the necessary speed response, a “hard switching” scheme was chosen. The difference between “hard” and “soft” switching is that in the case of the soft-switching, only the top switches in the inverter would turn on and off (Figure 3-56), while the others are kept continuously on during one conduction period. In the case of hard-switching, both switches turn on and off. For soft switching, a voltage of zero will appear across the two conducting phases because of one diode being forward biased, leading to the equation

$$0 = 2 \times R \times i(t) + 2 \times e(t) + 2 \times \frac{Ldi}{dt} \quad (3.20)$$

In hard switching, a negative voltage is applied because of two diodes being forward biased, leading to the equation

$$-V_{dc} = 2 \times R \times i(t) + 2 \times e(t) + 2 \times \frac{Ldi}{dt} \quad (3.21)$$

The current decays faster in the second case, which is an advantage for high-speed operation. Hence, hard switching was chosen over soft switching.

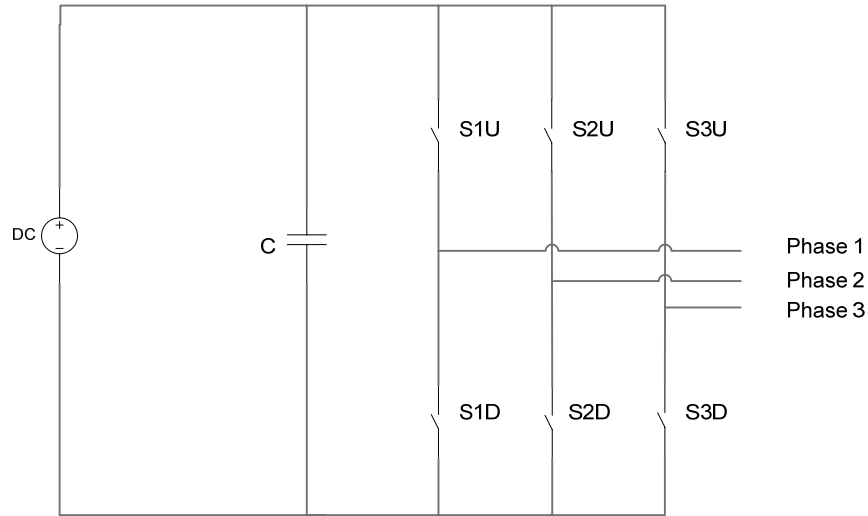


Figure 3-6: 6-switch inverter

3.3.2 PM-BLDC machine block

The electric motor phases were represented by their electrical equivalents as shown in Figure 3-2 by using the SimPowerSystems library. A detailed view can be found in Figure A2, in Appendix A. The back-EMFs were implemented by filling in look-up tables with a trapezoidal waveform that would represent the flux in the per-unit system and then scaled by speed. It is important to note here that the back-EMF waveforms have been idealized compared to the real ones; this will have an effect on the results of the simulations. Hence, differences with experimental tests should be expected. The resistances and inductances were implemented by using the RLC series branch blocks; only the elements' values need to be entered, no initial conditions are required. As stated earlier, the ICE was assumed to maintain a constant speed, and as such, no model was required to represent it.

3.3.3 Inverter and source blocks

The SimPowerSystems library contains blocks that were used to implement the inverter and the DC voltage source, as can be seen in Figure A1 of Appendix A. The inverter allows a choice of the type of switches to be included, and some key specifications such as snubbers or forward voltages. The type of power switches chosen was IGBT with diodes in parallel, to hence match the types used the final application; the other parameters were left untouched as the information on those were not available from the application's inverter specifications. The DC voltage source itself simply requires as an input the level of voltage desired.

3.4 Simulation Results

According to the strategy of the University of Akron's vehicle, the PM-BLDC machine is to be mostly used in the generator mode. Tests of this mode were run in simulation. Different speed and power levels were chosen according to the characteristics that the system would endure in the final application. Hence, tests at 1500, 2000 and 3000 rpm for the ICE were simulated: 1500 rpm is the speed at which the ICE is theoretically the most efficient and 3000 rpm is chosen to represent high-speed operation. Finally, 2000 rpm was chosen as an intermediate speed to verify the controller's operation. The limit of the power processed was defined by the specifications of the PM-BLDC machine, i.e. 20 kW. Different speeds and torques, and hence different powers, have been assumed in the simulations, with the controller gains tuned according to the controller study.

Figure 3-7, Figure 3-8 and Figure 3-9 show the back-EMFs, the phase current, and the torque of the PM-BLDC machine for the ICE speed of 1500 rpm (PM-BLDC machine speed of 4290 rpm) and a power request of 7524 W (10.1 HP). There is a current ripple of 20 A, which is reflected in the total torque, although the average values of torque and current follow the references. The error is close to zero and hence satisfactory since the current command was of 66 A and that the actual current appears to be around this value in Figure 3-8.

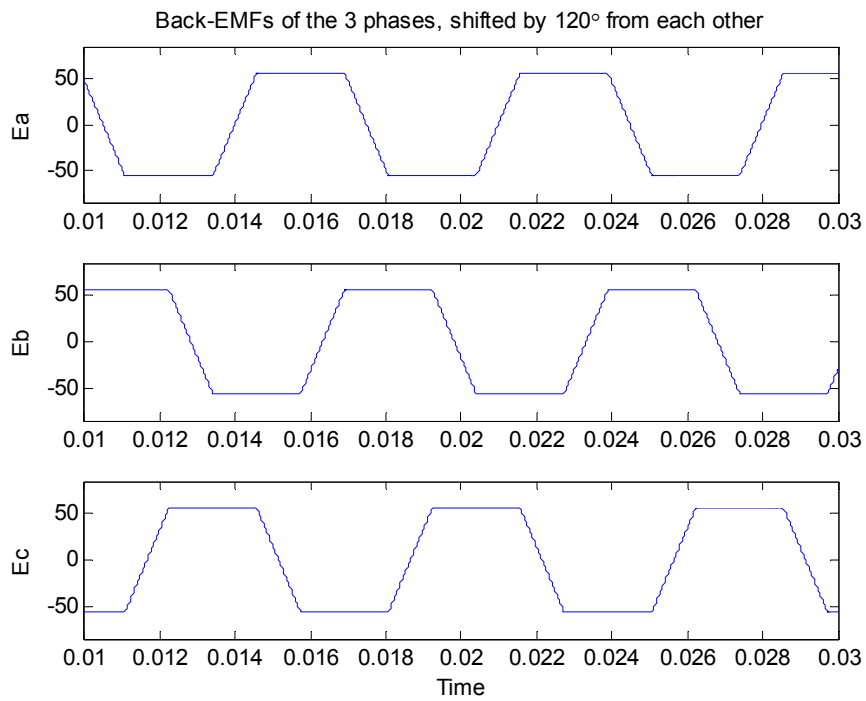


Figure 3-7: E_a , E_b and E_c at 4290 rpm

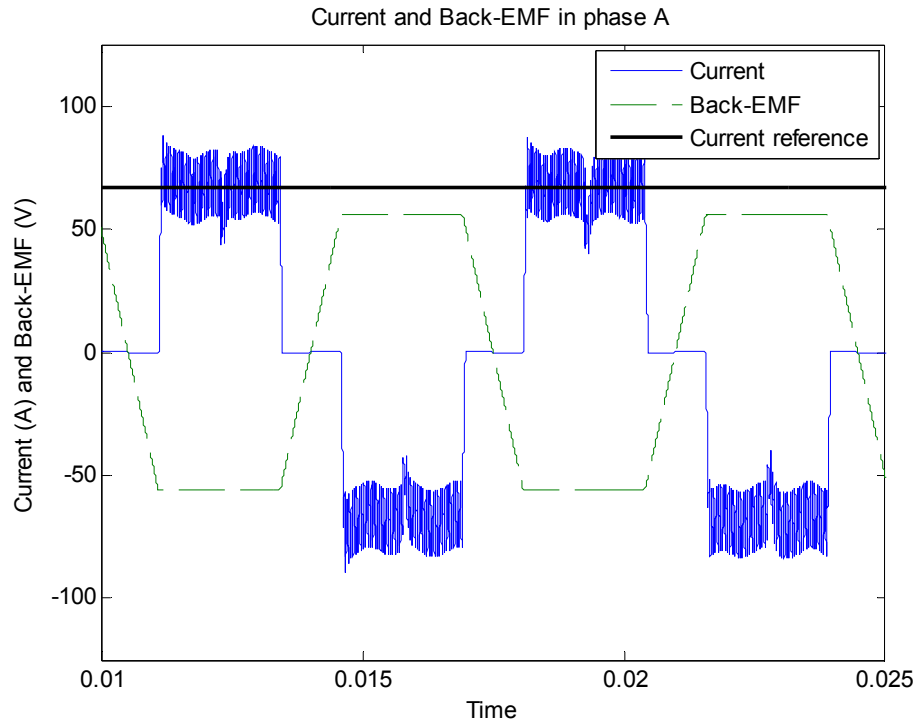


Figure 3-8: E_a and I_a at 4290 rpm, 7524 W

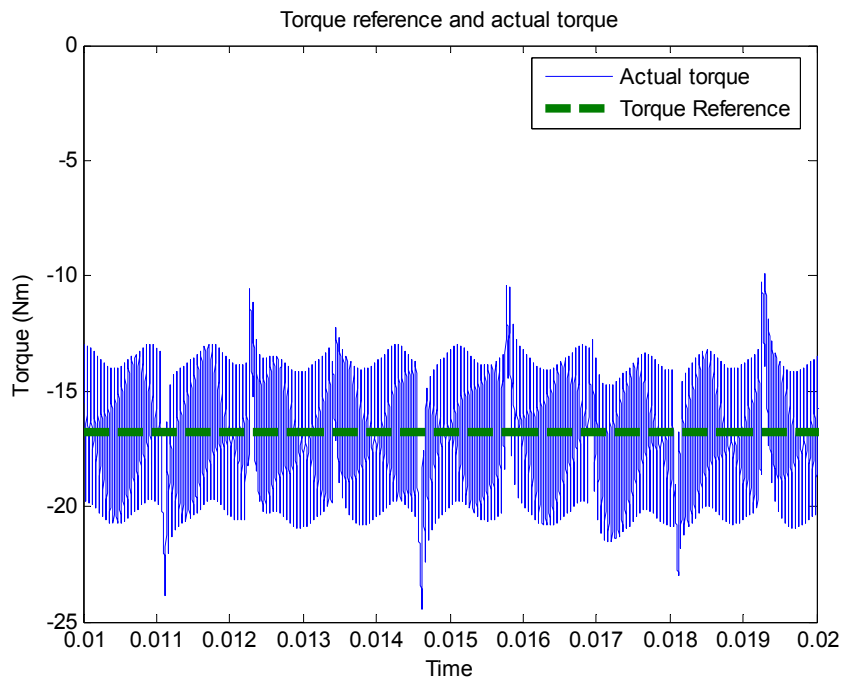


Figure 3-9: T and T_{ref} at 4290 rpm, 7524 W

Figure 3-10 and Figure 3-11 show the phase current and the back-EMF as well as the total torque for an ICE speed of 1500 rpm (PM-BLDC machine speed of 4290 rpm) and a power request of 16.84 kW (22.6 HP). As in Figure 3-8, a current ripple is observed. Though the reference has more than doubled, the ripple magnitude is still close to the ripple observed earlier; it is due to the switching frequency and the motor's parameters, which will be explained during the conclusions of the simulations.

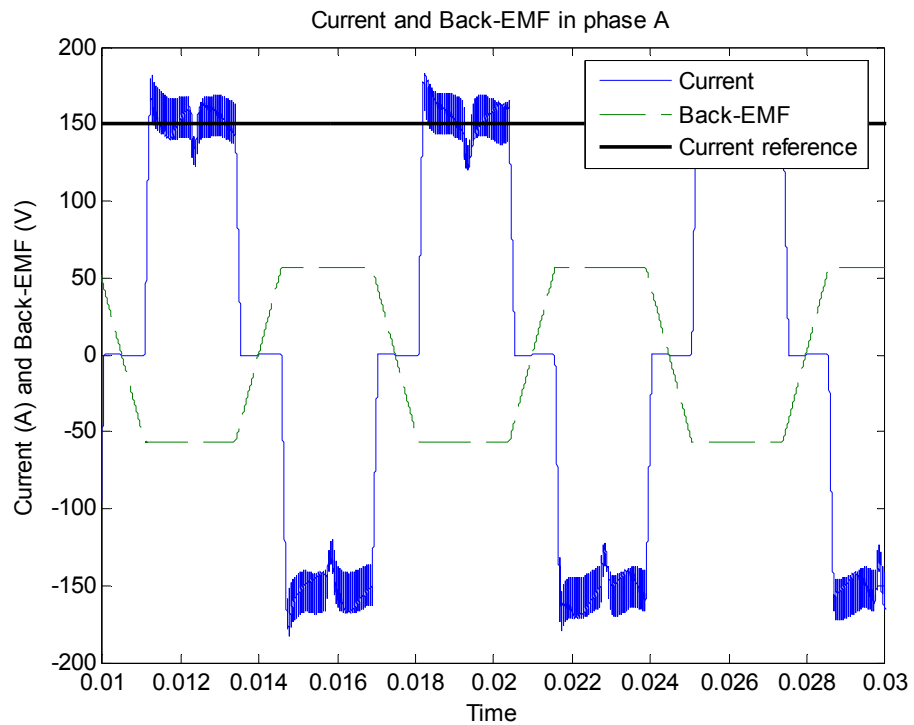


Figure 3-10: E_a and I_a at 4290 rpm, 16840 W

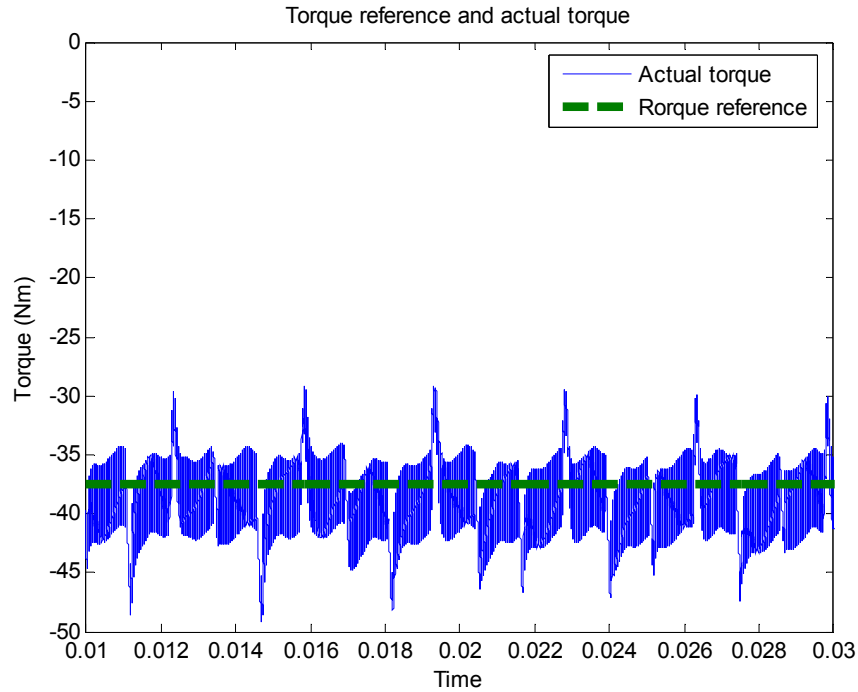


Figure 3-11: T and T_{ref} at 4290 rpm, 16840 W

Figure 3-12 and Figure 3-13 show the phase current and the phase back-EMF as well as the total torque for an ICE speed of 2000 rpm (PM-BLDC machine speed of 5720 rpm) and a power request of 20.9 kW (28.1 HP). Again, the ripple on the current and the torque remain similar to the previous cases, although the ripple is a slightly smaller.

The current magnitudes seen in Figure 3-10 and Figure 3-12 are similar, but the speed has increased by 33%. The controller is thus seen to control the current correctly over a range of speeds.

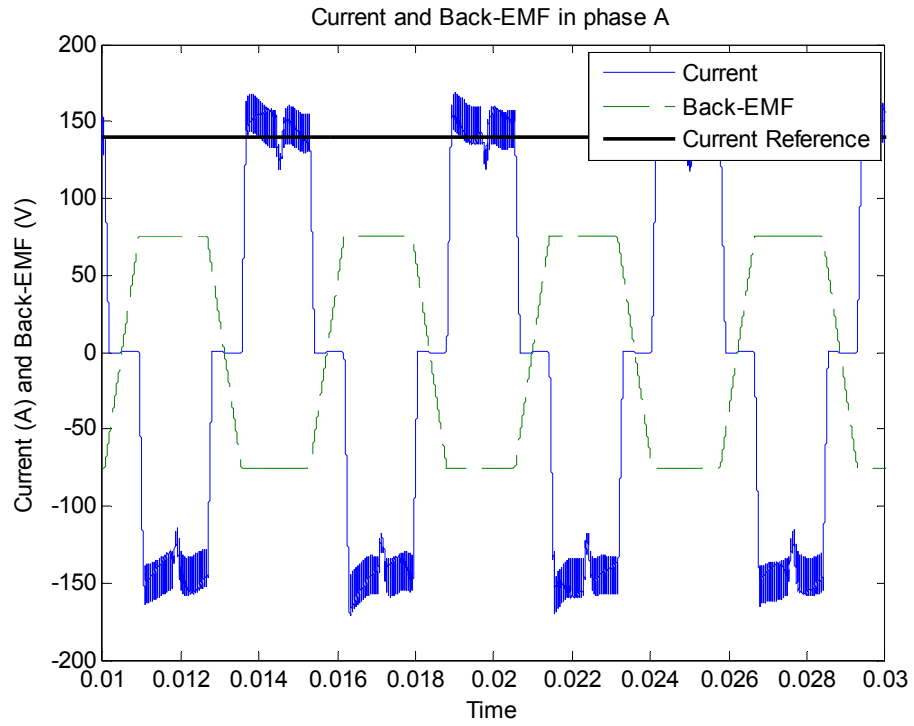


Figure 3-12: E_a and I_a at 5720 rpm, 20900 W

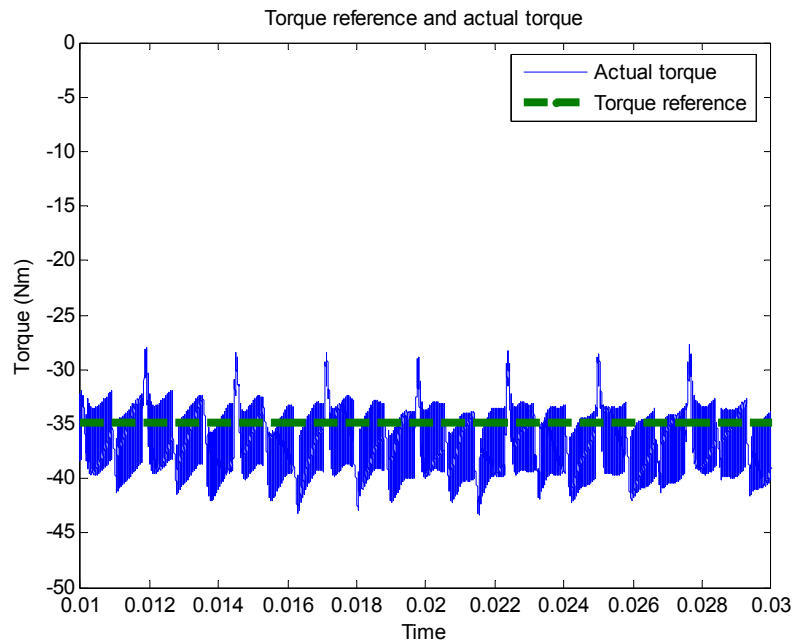


Figure 3-13: T and T_{ref} at 5720 rpm, 20900 W

Figure 3-14 and Figure 3-15 show the phase current and the back-EMF as well as the total torque for an ICE speed of 3000 rpm (PM-BLDC machine speed of 8580 rpm) and a power request of 15.3 kW (20.5 HP).

The current levels in Figure 3-8 and Figure 3-14 are the same but the speed has doubled. The shape of the current is slightly different from those in Figure 3-10 and Figure 3-12 for a similar current/torque reference: the current does not overshoot at the beginning of the phase conduction period. This is due to the fact that the back-EMF is higher, and consequently, the term $(L - M) \times \frac{di_{phase}(t)}{dt}$ from (3.9), will be smaller. Hence, the current will rise slower than at lower speeds and will tend to overshoot less. It also explains why the ripple is smaller.

Once again, the controller proves to achieve the performance similar to that observed for lower speed and power requirements.

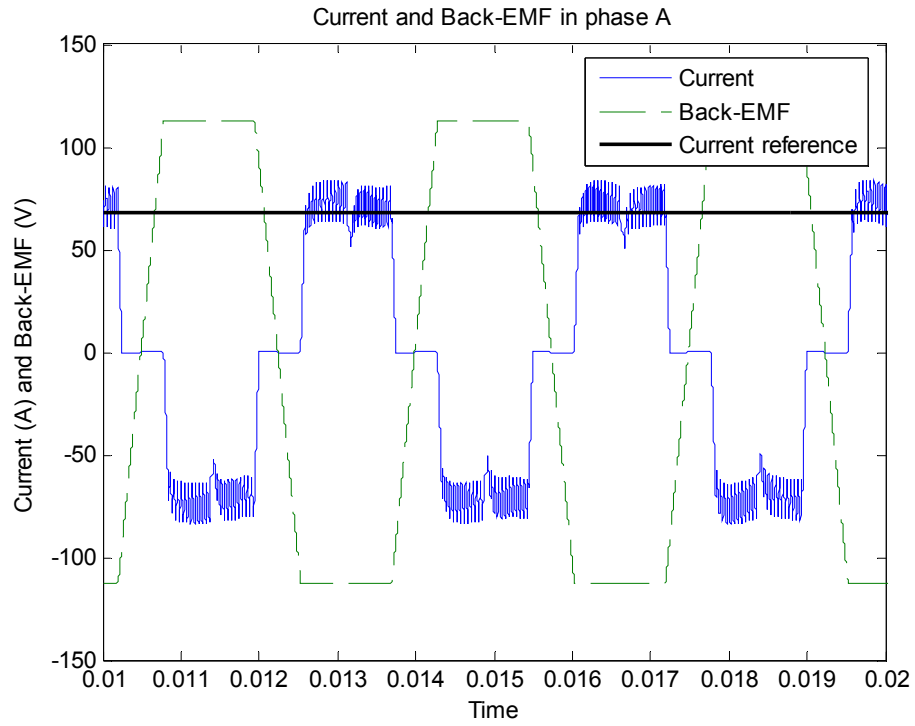


Figure 3-14: E_a and I_a at 8580 rpm, 15300 W

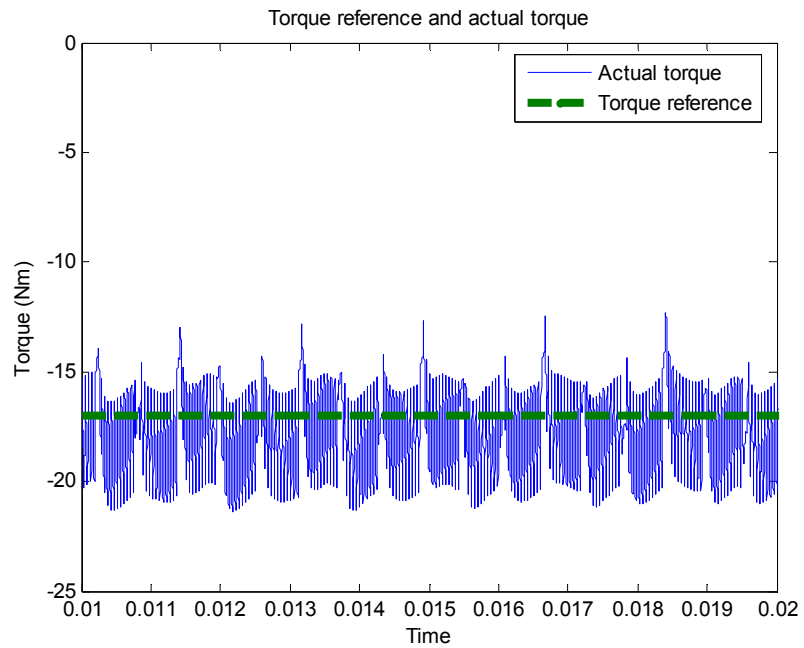


Figure 3-15: T and T_{ref} at 8580 rpm, 15300 W

The summary of simulation results for the 20 kW PM-BLDC machine at four operating points is given in Table 3-1.

Table 3-1 recapitulates the different tests points run during the simulations.

Table 3-1: Generating mode simulation results summary

Motor Speed (rpm)	Power (W)	Torque (N.m)	Phase current (A)
4290	7524	16.75	66.67
4290	16840	37.48	149.21
5720	20900	34.89	138.89
8580	15300	17.03	67.78

3.5 Conclusion

A current ripple is observed on each of the plots. The ripple depends slightly on the values of the referenced torque and speed, but is almost a constant, around 25-30A. This depends mainly on the switching frequency and the phase inductance of the machine.

A way to reduce this ripple would be to increase the switching frequency. If the example is taken of keeping the same duty ratio but with a higher frequency the average current level would remain the same, but the variations would be less.

The current and hence the torque have spikes that occur each time there is a change in the combination of the switches used. When the controller turns the switch off at the end of a phase conduction period of the inverter, there is still current flowing in the “turned off” phase at that time; the phase windings, because of their inductances, cannot have a discontinuity in their currents. But while this current decays and continues to flow in the “remaining phase,” the next phase turns on and hence starts to have current flowing

through it. This current and the one in the “remaining phase” add up and cause those spikes. To prevent such spikes, the controller would need to control the current in the “newly-turned on phase” so that the sum of the two currents described previously equals the desired current. This would imply to have a correction on the duty cycle applied to each switch and information on the current for each phase.

Those simulation results helped designing the controller for the torque control of the PM-BLDC machine and proved the choice of a PI controller to be appropriate. In the next chapter, the physical implementation of the system will be presented.

CHAPTER IV

PM-BLDC MACHINE DRIVE IMPLEMENTATION

After having verified through simulation that the concept of a torque controlled PM-BLDC machine coupled to an Internal Combustion Engine was viable, the hardware implementation of the controller and its integration with the power converter was initiated. The controller was implemented in a motor control digital signal processor (DSP). An electronic interface circuit to receive and process sensor feedback information from the machine and power converter and to send the pulse width modulated (PWM) gating signals to the power converter was developed. The details of the hardware implementation are presented in this chapter.

4.1 Hardware Components

The total system is composed of several subparts. Those parts will be presented in this subpart of Chapter IV.

4.1.1 Electric machine

The electric machine used in this project is a three-phase Permanent Magnet Brushless DC motor which was designed and built by Siemens. The machine is rated for

21kW continuous and 35.6 kW peak power operation. The rated torque is 20 Nm. The maximum rated torque is 60 Nm and the corner speed is 4500 RPM. The rated maximum speed is 10000 RPM. The back-EMF constant and the torque constant are respectively $0.125610551 \text{ V/rad.s}^{-1}$ and 0.251221101 Nm/A , respectively.

Hall-effect sensors for position feedback information are mounted on the motor. They need a 5V supply and the output R, S and T signals are provided through open-collector circuits. Those signals are 120 electrical degrees apart from each other. Each signal is in a high state for 180 electrical degrees and in a low state the rest of the time.

4.1.2 Power inverter

A power inverter made by Powerex was purchased for the PM-BLDC drive. This commercially built inverter is robust to survive the harsh environment inside the engine compartment of a vehicle. This inverter is rated for a bus voltage up to 600 V, currents up to 400 A and switching frequencies up to 20 kHz. It needs a power supply of 15 or 24 V; the 15 V input was chosen for the drive.

The above mentioned inverter has several features:

- shuts down if the supply voltage is too low (below 14.4 V)
- detects an over-current in either phase
- detects if the temperature of the heatsink, i.e., of the switches, is too high
- outputs several error messages: over-temperature, over-current in phase A, over-current in phase B, over-current in phase C; these are all digital outputs that need pull-up resistors in order to be used.

The inverter also has analog outputs:

- waveforms of the current in each phase
- waveform of the DC bus voltage
- temperature.

The phase current information was not suitable for this application because the resolution is too low, and additional current sensors were installed in the inverter. The voltage and temperature measurements are fed back to the DSP, but they are first scaled-down on the instrumentation board from 0-10 V to 0-3 V.

4.1.3 Electronic boards

Spectrum Digital has developed a board, called the eZ-DSP, that contains the TI TMS320F2812 DSP and additional circuitry to interface with it. This board was used as the controller board. In addition, two PCB boards were designed: one is referred to as the “power supply board” and the other one as the “instrumentation board.”

The power supply board provides power to the instrumentation board, the eZ-DSP board, and the inverter. Damage to the inverter that occurred during testing led to further modifications of the power supply board. Also, an area of the board was dedicated to driving the relays opening the motor’s phases. A MOSFET was used to drive the relays; it receives its gate command from the DSP through the instrumentation board.

The instrumentation board was designed to interface:

- the inverter error and measurement signals and the DSP
- the DSP’s PWM outputs and the inverter switch command pins
- the motor’s Hall effect position sensors and the DSP
- the phase currents and DC bus current sensors and the DSP

- the digital output of the DSP and the gate of the MOSFET driving the phase relays
- the CAN bus and the DSP

4.1.3.1 Power board

Following the power requirements of the instrumentation board, the eZ-DSP board and the inverter, several power supplies and voltage regulators were purchased. The schematic and the list of the devices used can be found in the Appendix B.

The MOSFET power device to drive the phase relays was installed on the power supply board. Its gate driver, however, is implemented on the instrumentation board. The circuit is described in Figure 4-1.

Appendix C contains several pictures of the final implementation of the inverter and of the controller.

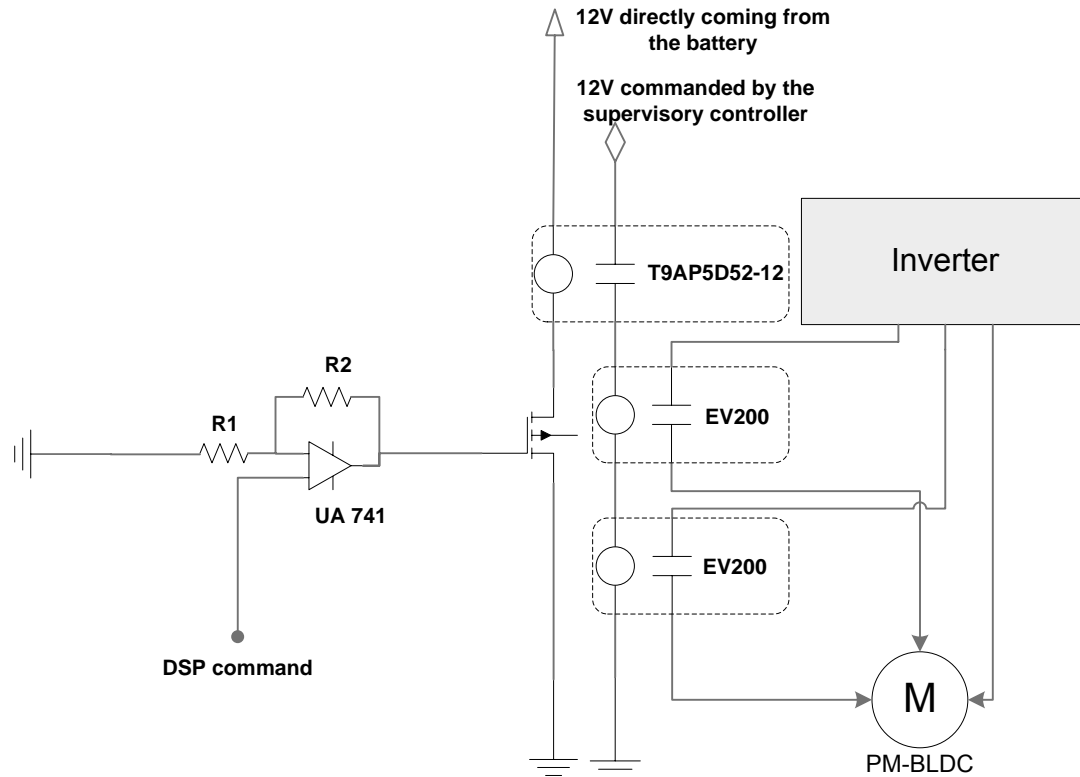


Figure 4-1: Relay driver circuitry

The T9AP5D52-12 relay is a normally closed contactor. The DSP can isolate the PM-BLDC machine through this relay in the event of a fault. However, the voltage driving the coils of the EV200 relays is commanded by the vehicle's supervisory controller. If a request comes from the DSP to open the phases or if there is a loss of communication with the DSP, then the supervisory controller can isolate the PM-BLDC machine.

The DSP controls the phase relays connected in series with the two phase coils of the PM-BLDC machine. The purpose of the relays is to isolate the machine from the inverter and DC bus in case of faults either in the machine or in the controller/inverter. In order to control both of the relays at the same time, a smaller relay controls the voltage applied to the coils of the phase relays. This relay needs 12 V and a current of 83 mA to

be engaged. Since the DSP digital pins cannot deliver such high power (they can deliver a maximum of 26.4 mW), an alternative was to use a MOSFET to control the path to the ground of the coil of the smaller relay. The MOSFET needs only a certain voltage at its gate and very small current to be turned on. The output voltage of the DSP digital pin had to be boosted through an op-amp (over 4.2 V for the chosen MOSFET). The circuit's schematic can be found in Figure 4-1.

4.1.3.2 Instrumentation board

Both the digital outputs of the inverter and the motor's Hall-effect position sensors' signals R, S and T require pull-up resistances. The advantage of the arrangement is that those signals can easily be scaled to the required level. In the case of the DSP, which is the final destination of those signals, this level is 3.3 V. The base of the circuitry designed on the board is described in Figure 4-2. The complete schematic for all the interfacing signals can be found in the appendix B.

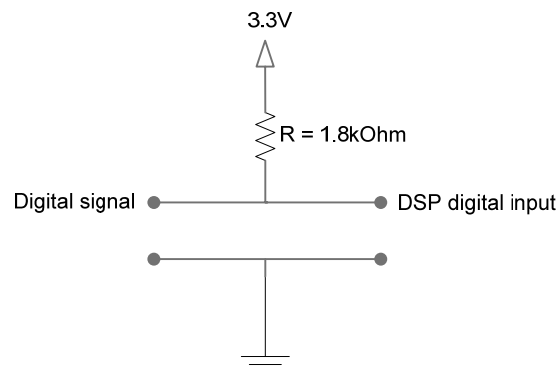


Figure 4-2: Digital signals level adaptation

In order for the DSP to access the CAN communication bus, a transceiver is needed. The transceiver MCP2551 from Microchip was chosen. The voltage level from

the TXD pin of the DSP to the transceiver matched, but the level delivered by the RXD pin of the transceiver was too high. The solution was to use a buffer with a supply voltage of 3.3 V that will maintain the high output signals at the same level. The circuitry implemented can be found in the appendix B.

The inverter measurements of the DC bus voltage and of the heatsink temperature are scaled between 0 and 10 V. In order to be measured by the Analog-to-Digital (A-to-D) converter of the DSP, the signals need to be further scaled down to 0-3 V. A simple voltage divider with a potentiometer for precision calibration was used.

The current sensor chosen for the application are the LA205-S manufactured by LEM. They measure both negative and positive currents, and output a current signal centered around 0 A. The output current signals must be converted to an equivalent voltage to be usable by the DSP; this is achieved using potentiometers. The datasheet recommends having a resistance value between 5 and 95 Ω when measuring currents up to 200 A and supplying +15 V and -15 V. In order to have an easy scaling process in the software, the potentiometer was set with a resistance value of 56 Ω . An offset of 1.5V has to be incorporated to capture the negative values of the currents since the A-to-D converter of the DSP can read only voltages between 0 and 3 V. The negative values are hence represented between 0 and 1.5 V, and the positive values are represented between 1.5 V and 3 V. The maximum current/torque reference that the software can work with is 150 A. In order to see the overshoots, it was decided to measure currents up to 200 A. The current measured hence varies between -5.6 V and 5.6 V (-200 A and 200 A). An offset of 1.5 V and a gain of 1/3.7 (1.5/5.6) were needed to be implemented to scale the signals between 0 to 3 V.

The circuitry designed to scale the current uses op-amps. The first stage is a voltage follower which offers protection against spikes to the rest of the circuitry. The second stage is an inverting summing amplifier. The design leads to have the current sensors “pointing” towards the inverter, not towards the motor, to read positive currents. Hence, positive currents are defined as currents flowing out of the inverter into the motor. A negative offset of -1.5 V was provided through a potentiometer and the -15 V supply. The final gain implemented to the voltage representing the current was $\frac{1}{4}$, instead of $\frac{1}{3}$. This was later compensated for in the DSP program.

The complete schematic of the circuitry can be found in appendix B.

4.2 DSP Programming

The simulation helped design the software architecture of the digital controller. This controller was later implemented in a digital processor, the DSP. This sub-section of the chapter presents the structure of the program, as well as an introduction to the CAN protocol used for the communication needs of the project.

4.2.1 Control software

In this part of chapter IV, the subparts of the software implemented in the DSP and their functions will be described.

4.2.1.1 Global architecture

The DSP tasks are to run the control algorithm and to communicate with the vehicle’s supervisory controller; it requires the command input from the supervisory

controller and sends back the subsystem (starter/generator) status to the supervisory controller. The flowchart in Figure 4-3 describes the operations within the DSP:

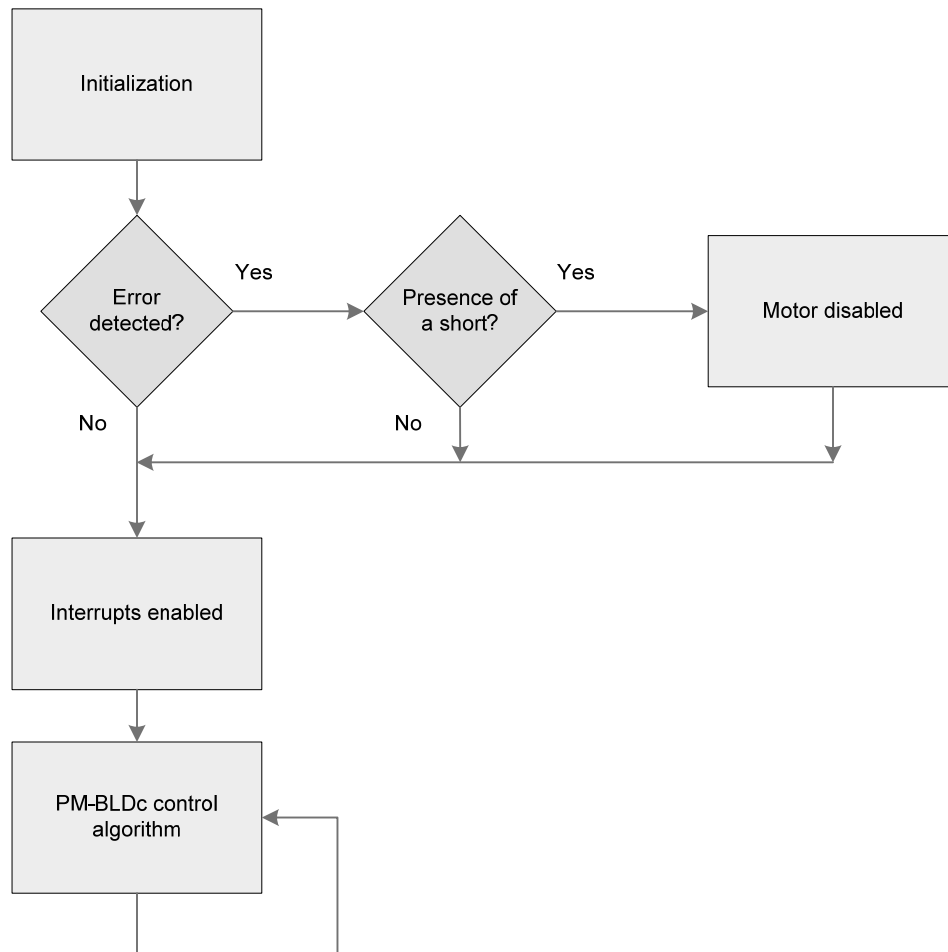


Figure 4-3: Flow-chart diagram of the DSP operations

During the initialization period, variables, constants and the peripherals of the DSP are initialized to known values and states. Then, as an early check, the DSP verifies that errors, such as shorts in the inverter, have not occurred. Existence of an error would prevent the starter/generator subsystem from being activated to deliver torque.

Once the control algorithm is started, instructions will be executed at periodic intervals of time. To run a program periodically, an option is to use one of the built-in

“general purpose timers” of the DSP that are part of the “Event Managers”. The Event Managers generate signals or information based on software or digital input signals (for example, generate interrupts on counter events or determine position from a position sensor). The timers have a counter, incrementing or decreasing in synchronization with a high-speed peripheral clock, which itself is a slower version of the CPU clock. The value of the counter is compared to either zero, the value of the period or to any other value stored in a specific register of the Event Timer. Depending on the mode chosen, any match between those values and the value of the counter can trigger an interrupt, trigger an A-to-D conversion, or toggle the state of digital output pins of the DSP.

PWM generation

When a match occurs between the Event Manager’s counter and a value set for comparison (such as zero, or a desired PWM period), some predefined digital pins can toggle from a high to a low state or vice-versa. This is useful in generating a PWM signal.

As mentioned in Section 3.2, a switching frequency of 20 kHz was chosen to have good control of the current and low switching noise. The timer’s counter runs along with the high speed peripheral clock that has been set to run at 37.5 MHz. The timer period has to be set based on this clock frequency to obtain a given PWM frequency. For the PWM frequency to be 20 kHz, the timer counter was to count up to 1875. In the final implementation the frequency is 22361 Hz (the timer counter was set to count up to 1677).

A-to-D conversions

The current measurements must be made accurately to ensure the best possible control. The measurements are to be captured at a periodic interval because of the command strategy chosen (PWM versus hysteresis). In order to have the most recent information of the phase currents, it is better to measure them when the device controlled is active. Hence, a phase current should be measured when the corresponding IGBT is ON.

One issue in capturing current measurements is that noise in the signal is worse when the IGBT switches turn ON or OFF. By using an up/down counter, A-to-D conversions can be started in the middle of the ON period of the switch. Hence, noise such as ringing due to the IGBT's closure can be expected to have receded when the measurement is taken. Figure 4-4 shows the timing for the measurement. The counter in the Event Manager is put in continuous up/down mode; the counter will be incremented (up) until the preset period value is reached, and then decremented (down) to zero. The A-to-D conversion is configured to start when the counter reaches its peak value. The start of an A-to-D command is sent at the same time when the interrupt generated by the Event Manager starts. The interrupt is a sub-routine where all the functions of the program are executed (as explained further in the thesis), including the current measurements. In order to have a stable measurement, at the beginning of the interrupt, the program polls a bit of the A-to-D converter register that shows the status of the converter; once this bit indicates the converter is not busy, the measurement is stable and accurate and hence logged for use by the control algorithm.

Figure 4-4 shows the logic chosen and the sequencing of events.

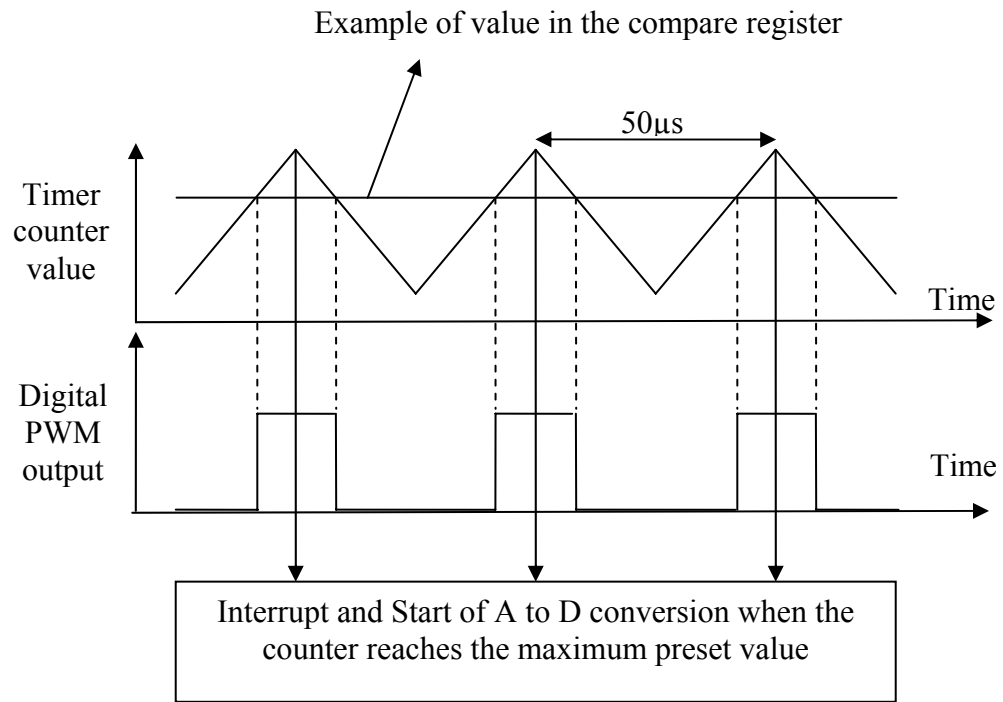


Figure 4-4: PWM generation and A-D conversions

4.2.1.2 Interrupt architecture

As seen above, the interrupt will occur at a frequency of roughly 22 kHz. The flow chart in Figure 4-5 shows the order of execution of the functions in the DSP software.

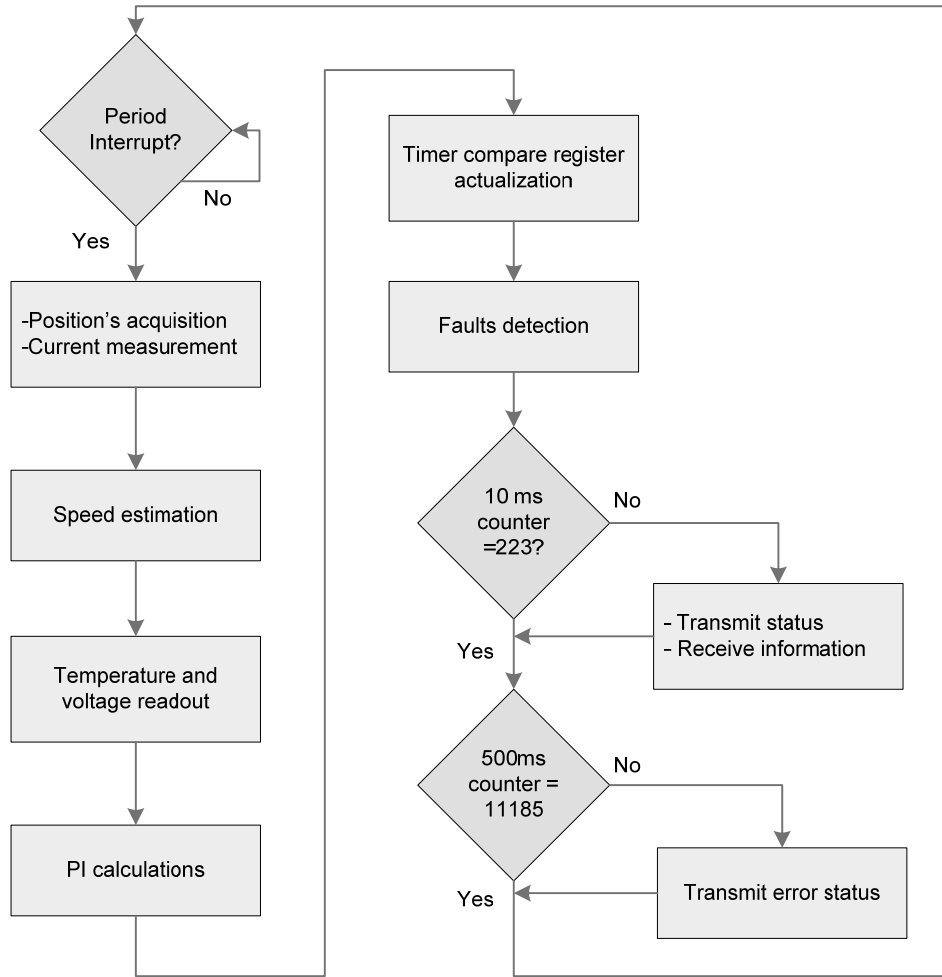


Figure 4-5: Flow-chart of the DSP software algorithm

Position Acquisition and Current Measurement

The position information is obtained from the Hall-effect sensors. The logic of the Hall-sensor output signals is binary; each output is a zero or a one depending on whether a north or a south pole is located in front of the corresponding sensor. Each sensor has a high and a low state, each lasting for 180 electrical degrees in one mechanical revolution of the rotor. The sensors are 120 degrees apart from each other. By combining the three

signals, a three-bit binary number can be associated with the position. The following Table 4-1 summarizes six position segments obtained from the Hall-sensor signals.

Table 4-1: Position detection

	sensor R	sensor S	sensor T	decimal value
30-90°	0	1	0	2
90-150°	1	1	0	6
150-210°	1	0	0	4
210-270°	1	0	1	5
270-330°	0	0	1	1
330-360°	0	1	1	3

The Hall-effect sensor outputs are tied to digital inputs of the DSP. Each time the program goes into the subroutine following the interrupt discussed earlier, any change in one of these digital inputs updates the position. The previous position information is saved so that it can be used for speed calculation, which will be described later.

Depending on the operating mode (motoring or generating) of the system, the switching configuration has to be changed. Hence, for the same rotor position, the switches used will not be the same. Also, the configuration changes according to the position, as seen in chapter III. Since there is a change of switching phase every 60 electrical degrees, a change in the decimal value representing the position indicates the need for a change in the switching pattern. In the program, two variables will indicate the states of the PWM outputs of the DSP: one encoded as a decimal value representing the position and the other describing the mode the machine is in (generating or motoring).

The A-to-D converters store the measured voltage in a 12 bit register, which in unsigned decimal has a maximum value of 4095. Due to the instrumentation board design, a value of 0 does not represent zero Amperes, but 1.5 Volts does. The ADC (A-to-D Converter) can sample a maximum voltage of 3 V; hence, zero current will be $4096/2=2048$. Subtracting this value to the value measured or subtracting the measured value from this value gives the absolute value of the current, which is needed to have a simpler control in the program. Since the gain on the board has been designed such that 3V represent 200 A and 0 V represent -200 A, an approximation in the program is made: an increment of 10 in the measured value represents 1 A. Only two current sensors were used, on phase A and phase B respectively, since current is always flowing in at least one of those phases at any time.

Speed Calculation

The speed is calculated from the information of change in position. The speed being the derivative of the position, the calculated speed will falsely be zero if the speed is determined while the number representing the position has not changed yet. The speed is calculated each time the position changes (every 60° electrical or 30° mechanical, which is $1/12^{\text{th}}$ of a mechanical turn). The program has to determine how much time has elapsed in between the 30° mechanical position change. A variable is used to track the time. It increments each time the program enters the interrupt. Knowing the time in between interrupts, and knowing that the motor has spun $1/12^{\text{th}}$ of a turn, the speed of the machine can be calculated. Since the maximum frequency at which the interrupt can

happen in the DSP is the PWM switching frequency (22361 Hz), the maximum speed that can be measured is $\frac{22361}{12} \times 60 = 111805$ rpm.

The precision on the speed is a function of the speed itself. At 10000 rpm, the above mentioned variable would read a value of 11.1805, which is not possible. It would be 11 or 12, i.e., 10164 rpm and 9317 rpm, respectively. Those speeds represent variations of 1.64 % and 6.82 % of the actual speed. For a lower speed such as 2000 rpm, the variable would be 55.90. It would be 55 or 56, i.e., 2032 rpm and 1996 rpm, respectively. Those speeds represent variations of 1.64 % and 0.17 % of the actual speed. It can then be seen that the precision on the speed measurement is greater at low speed than at high speed. Indeed, at high speed, the same step in the counter represents a much larger difference in speed than at lower speed. The supervisory controller required the speed of the ICE, which is belt-coupled to the PM-BLDC machine. The coupling ratio between the PM-BLDC machine and ICE of 2.86 makes the ICE speed less sensitive to the error due to fixed point calculations in the DSP.

Temperature and voltage readout

The inverter outputs a measurement of the temperature next to the IGBTs. This measurement is on a scale of 0-10 V. A voltage divider on the instrumentation board scales the signal down to 3 V for the ADC to measure it. As previously mentioned, the ADCs store a value between 0 and 4095. The specifications of the project required that the temperature be coded in 8 bits of a CAN message. Hence, the 12-bit sampled ADC value is shifted by 4 bits before transmission.

The bus voltage is used in the program during the fault detection process. The inverter outputs the bus voltage with a certain gain that is not suitable for the ADC; a voltage divider is used on the instrumentation board to scale the inverter's output. The scaling is such that the maximum ADC output value of 4095 corresponds to 512 V. The program converts the ADC value back into engineering units.

PI calculations

The proportional and integral gains determined in section 3.2 are values that require a precision smaller than $1/10^{\text{th}}$. The TMS320F2812 can only code integers, not floating values; the native precision is hence just down to unity. In order to get a precision lower than 1, a method is to multiply all the variables by a common factor that is a power of 2. At the end of the calculation, it is more efficient to shift by a number of bits (hence dividing by a power of 2), to get rid of the common factor instead of using the divider operator. For PI calculations, shifting by 8 bits, i.e. dividing by 128 (2^7) gave enough precision (0.0078125 per increment of 1).

The implementation of the PI equations themselves was performed by discretizing the PI controller equation (2.1). This resulting expression is in (4.1) which is repeated here for convenience.

$$\begin{aligned} error_{current}(t) &= I_{ref} - I_{measured}(t) \\ duty_{cycle}(t) &= K_p \times error_{current}(t) - K_p \times error_{current}(t-1) \\ &\quad + K_i \times error_{current}(t-1) + duty_{cycle}(t-1) \end{aligned} \quad (4.1)$$

with K_p being the proportional gain, K_i the integral gain, $I_{measured}$ the current measured and $error_{current}$ the difference between the reference and the measured currents.

In order to avoid overflow in the variables, saturation was imposed on the duty cycle.

The output of the PI controller, as mentioned in 3.2, represents a voltage, but what is needed is a duty cycle in order to drive the PWM outputs. The relation between the two is a ratio: 100% corresponds to the maximum voltage available. Using the actual bus voltage to do the calculations would mean doing a division in each control period, which is not computationally time efficient. To avoid this, the voltage was assumed to be at the lowest the system would ever experience, which is 280 V. The duty cycle calculated by the PI controller is the value that the counter of the Event Managers' counters will be compared to. The output of the PI controller must be scaled according to the value of the time period, which is 1677, in order to generate a duty cycle count. This leads to multiplying the PI controller output by 1677 and dividing by 280. In the implemented control algorithm the PI controller output is simply multiplied by 6, which is roughly equivalent.

While doing tests at high power, big overshoots in current appeared when switching from one phase to another, as will be explained in Chapter V. Experimental tuning of the PI was expected and attempted, but it didn't solve the problem. Feedback limitation appeared then to be a good solution to avoid those overshoots. Feedback limitation on the duty cycle as well as on the error in current was implemented in the software. For that purpose, the old value of the duty cycle as well as the of the error would be divided by two. This limitation was not sufficient at higher levels of current command. The same solution method was applied once again on the gain to limit the overshoot.

4.2.2 CAN protocol and code

The starter/generator, being a subpart of the vehicle, needed to communicate with the vehicle's supervisory controller, and possibly other subsystems to receive a torque command and to send a feedback of the speed. The CAN communication protocol was the standard chosen by the University of Akron to provide means of communication between the subparts of the system, as it was also the system already in place in the stock vehicle. A presentation of the standard and the practical use of it are presented next.

4.2.2.1 Presentation of the CAN protocol and the DSP CAN module

The Controller Area Network (CAN) protocol was first introduced in 1986 by Bosch. This communication protocol operates with messages which have a defined and unique identifier. The identifier defines a level of priority on the bus; the lowest binary value among all the identifiers represents the highest priority on the bus. If two units are trying to access the bus at the same time, the one that has a message with the lowest identifier number would take over and the other units would need to wait in order to access the bus and communicate. This leads to having a very robust, very versatile communication system, since no changes need to be made to the other stations in order to add a unit to the bus.

Two different types of message identifiers exist: standard identifiers (11 bits long) and extended identifiers (29 bits long). In accordance with the rest of the sub-systems involved in the project, the standard identification has been chosen.

In the DSP, a built-in module of 32 mailboxes and functions handles the CAN communication. The programmer has only to configure the format of the messages (identifier and data length) and to implement functions to manage those messages.

4.2.2.2 Messages' format

For this particular application, it has been decided that three different messages would be sent to the DSP, and three messages would be sent by the DSP.

Messages sent to the DSP:

- A high priority message to open the DC-power bus and phases relays. Its identifier has the hexadecimal value of 0x240, is sent aperiodically, and has one byte of content.
- A command message sent every 10 ms, with the identifier's value of 0x340, and with four bytes of value.
- A status message, broadcasted every 500 ms, with an identifier's value of 0x4F0, and with eight bytes of value.

Messages sent by the DSP:

- A high priority message that tells the supervisory controller to immediately isolate the generator, if necessary, sent aperiodically, with the identifier's value of 0x148, and with one byte of data.
- An error message sent every 500 ms, with the identifier's value of 0x448, and containing two bytes of data.
- A status message sent every 10 ms, with the identifier's value of 0x440, and containing six bytes of data.

To send a message, a certain procedure has to be followed:

- Scaling data and loading the data field of the actual message in the appropriate mailbox
- Setting the transmission flag
- Resetting the acknowledge flag

To receive a message, the following needs to be done:

- Polling the Received-Message-Pending Register
- Resetting this register if one of the bits was at a high state
- Retrieving the value from the data bytes and scaling them

Appendix D shows a complete description of the messages.

4.2.3. Fault management

The program was designed so that it could detect errors of many different natures. The origins of these errors could be in any one or more of the following hardware subsystems:

- Instrumentation board
- Power supply board
- Motor
- Inverter
- DSP
- CAN bus

Faults are analyzed to isolate a subsystem. Some of these faults are detected directly from measurements. There are also many faults that cannot be sensed directly but are detected or suspected through signal analysis.

If the fault was critical enough to damage the system or to disrupt its normal functionality, then it would be considered critical and would lead to a local shutdown. The controller would turn-off the power switches, open the phase relays and hence the starter/generator system would be out of commission. It would also report to the supervisory controller via the CAN communication, which would then take action to further isolate the system.

Some faults are considered non-critical. It means they do not have a destructive impact on the system. The inverter will be rebooted to clear those faults.

The different faults detected are here presented. A table summarizing them as well as the actions taken accordingly can be found in Appendix E.

4.2.3.1 Instrumentation board errors

The instrument board or any one of its components could lose its power and stop functioning properly. The only possible way to identify such a fault is to detect an out of range value on each sensor. This takes care of loss of power but also of shorts in the phases.

If the connector from the board to the DSP gets shorted with the 3 V power supply, the DSP would detect it as an out-of-range fault. The same would happen if the pins were all shorted to ground. That fault raises two flags for position error and generator critical fault. The command for the generator will not be executed anymore. The DSP will resume operation once the connection is reestablished. Since a critical fault error has been sent, the supervisory controller will stop the operation with the starter/generator.

4.2.3.2 Power supply board

The DC/DC converters used as power supplies could malfunction, which would lead to either a non-symmetric readout of the currents (if only the positive or the negative supply voltage is to fail) or no readout at all. The second is already taken into account in the DSP, as will be seen later in this chapter. The first case would resemble having current in one phase when it is not supposed to happen. The approach to handle this situation is explained later in the chapter.

4.2.3.3 Motor

The motor comprises of the windings, the permanent magnets and the position Hall-effect sensors. The permanent magnets are supposed to be robustly mounted. The windings, which constitute the phases, can short between them or with the chassis. As for the hall-effect sensors, internal problems could lead either to erratic outputs, no output or all the outputs at a high-level.

Shorts between the phases where the current cannot be measured (i.e. somewhere between the phases relays and the motor itself) cannot be detected by the DSP through current measurements. This short would lead to an abrupt increase of temperature and most notably to an application of braking torque on the engine shaft. The cooling system will try to keep the temperature at an acceptable level. But the torque applied to the shaft will have more immediate adverse implication on the behavior of the engine and the vehicle. Presuming that the coupling system is still intact after such a sudden surge of braking torque, it will be hard to restart the engine with the stock starter (due to the

braking torque provided by the short between phases) assuming that the engine had stalled. The temperature rise on the coolant is the only way to detect such a fault.

4.2.3.4 Inverter

There are two types of protections implemented in the DSP for the Power Inverter:

- one reading the faults from the inverter
- one using phases A and B current measurements

Faults from the Inverter

The inverter outputs open-collector signals for the faults it detect. There are a total of four fault detecting signals: over-current in phase A, over-current in phase B, over-current in phase C and overtemperature. When one of those errors occurs, the inverter is in a “tripped” state. Those signals are connected to digital inputs of the DSP. These errors are polled at every PWM cycle, within the interrupt. When one of those errors occurs, a counter in the DSP program is incremented. When the counter reaches a preset value (five in the program), it raises a flag that is sent to the supervisory controller. That leads the supervisory controller to change its global strategy accordingly by either totally stopping operations with the generator or using it at lower power range.

DSP Interpretation of Currents Measurements

The currents sensed in phase A and phase B determine if an over-current fault occurred in the Power Inverter.

A batch of tests is run at two different periods of time: initially while the DC bus and phases relays are open before any power is processed, and during normal modes of operation. During its initialization, when the relays are open, the DSP software tests if the relays are really open and if there are no shorts in the phases. Three different tests are conducted to reach a conclusion:

- if a current is present in a phase when the phase is not supposed to be powered
- if a current is present anywhere when the current command is supposed to be zero
- if both sensors read saturated values at the same time.

For the first test, two similar versions are run sequentially for phase A and phase B. The software checks after a given time whether or not the current in the turned-off phase has depleted or not. Since most of the range is used and that noise is also on the ADC, it is impossible to correctly detect over-current values during normal operations that could indicate a short. The option adopted is to wait for the current to be depleted after the command has been set to zero. 5 ms is sufficient time for the current to reach zero based on experimentally measured turn-off-times.

The next test reads the current on the bus and in both phases while the current command is at zero. Likewise, the test is run 5 ms after the current command has been set to zero. It is also checked whether the voltage is quickly changing and approaching bus voltage value broadcasted over the CAN bus. A short in a phase would cause an over-current on the DC bus when the capacitors of the inverter are initially connected to the High-voltage DC-bus.

The last test checks whether or not the sensors are reading the same saturated value at the same time. This could mean that the sensors circuitry got damaged or the phases A and B upper or lower switches are shorted.

Those three tests all set a flag in message 0x448, informing the supervisory controller that a fault has occurred from which the system can't recover. The supervisory controller should immediately stop using the starter/generator and should open the relays that are part of that sub-system.

4.2.3.5 DSP

The problems that could happen to the DSP are primarily hardware problems: the power supply not working anymore, or ADC or digital inputs damaged by over-current or over-voltage.

If the power supply fails, the DSP stops functioning, and messages are no longer broadcast over the CAN network. This is a fault considered by the supervisory controller as 'time out'. If it doesn't receive any messages from a sub-system within a set period, it assumes that something is wrong with this subsystem and acts accordingly.

Digital pins that the DSP polls for errors or motor's position could get damaged and stay in a permanent state (high or low). If it is an error from the inverter that always stays on, it will be reported as a serious fault to the supervisory controller. If the position Hall-effect sensors are all at the same state, its numerical representation represents an abnormality and would trigger a local fault (inverter stopped). Also, the input of the ADC could stay in a high or low voltage state; this would be detected the next time the DSP makes a faults inspection, i.e., at the next interrupt.

A software problem could also happen in the DSP that could force it to be trapped in an infinite loop and never recover from it. The consequences can be of diverse nature, such as a constant behavior of the PWM pins (i.e. locked with a certain duty cycle). The supervisory controller can then detect this wrong behavior because the DSP will stop sending CAN message, which is a time-out error that would lead the supervisory controller to isolate the generator subsystem by opening the phase relays.

4.2.3.6 CAN bus communication

On the DSP side of the CAN module, the program checks that the periodic messages from the SCM are received with the expected period, plus a 50% safety margin. If messages are not received, the DSP switches to a safe mode by forcing the generator's current command to zero. The DSP recovers when it again begins receiving messages from the SCM.

In this chapter, the implementation of the PM-BLDC machine controller has been presented. This involved the development of torque controller algorithm and fault management structure for the PM-BLDC starter/generator. The software has been implemented on a TI DSP. The electronic circuitry for the interface between the controller and the inverter and between the controller and the machine had to be developed. In the next chapter, the tests for the starter/generator subsystem, including their results, will be presented and analyzed.

CHAPTER V

EXPERIMENTAL RESULTS

The controller was tested on different test setups to verify the controller operation. The interface circuits were tested independently before integrating those with the controller. In this chapter, different results obtained from various test setups will be presented and compared with the simulation results. Finally, a description of the communication tests will be presented.

5.1 Proceedings of the Experiments

The testing of the controller and its different components took place in phases. The goal was to go in steps in order to test the control algorithm first at low speed and power levels, and then at nominal operation points. The following subsections of this chapter present the different test-setups on which the motor controller was tested, as well as the scope of the tests done on each of them.

5.1.1 Low power testing with a DC machine dynamometer

In the first phase, the PM-BLDC machine and controller were tested with a 5-kW DC machine dynamometer. The complete setup, as shown in Figure 5-1, included the following:

- the motor/generator and its controller's setup
- a DC machine mechanically coupled to the PM-BLDC machine
- a string of 76 Maxwell ultra-capacitors connected in series to form the DC-bus similar to what will be in the car except at a lower voltage level
- a resistor bank to load the DC machine when used as a load
- an autotransformer to initially charge the ultra-capacitors

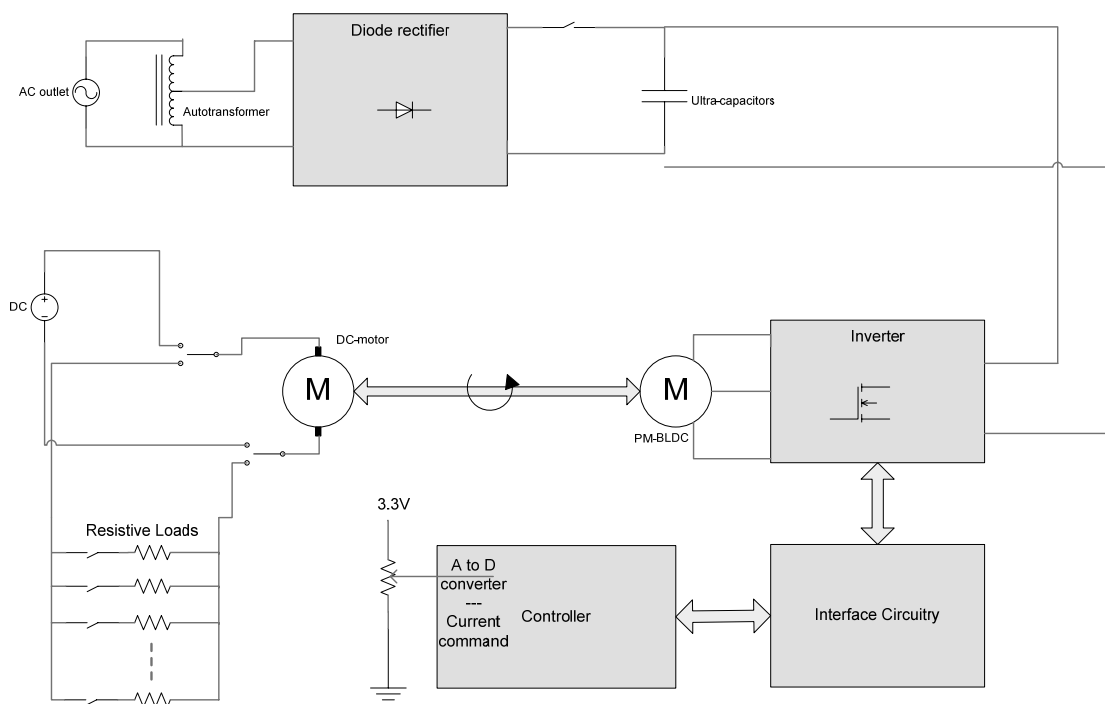


Figure 5-1: DC machine dynamometer test setup

Operations were limited in different ways:

- the maximum power of the DC machine is 5 kW, and its maximum speed is 5000 RPM
- the highest voltage for the DC bus is 190 V (2.5 V per cell), which is limited by the number of ultra-capacitors in the string

- the cable used between the inverter and the motor was only rated to handle up to 80 A
- the current command was not controlled through CAN. One of the A-to-D channels of the DSP was used to read an external command provided through a potentiometer

Motoring and generating operations were performed on the system.

Generation Mode

A back-EMF would appear between the phases of the PM-BLDC machine and its non-accessible neutral point when it will be driven by a DC-motor. Hence, at any point in time, a potential equal to twice the value of the back-EMF is present between two phases. Take for example phases A and B: their back-EMFs are at their maximum absolute value between 30 and 90 electrical degrees. The potential between the switches of phase A and phase B is at twice that value. The diode across the upper switch can become forward biased if the voltage between its anode and its cathode is positive; this is the case when the voltage between the two switches is higher than the value of the DC-bus. When the ultra-capacitors are discharged and the PM-BLDC machine is spun by another source, such as the DC-motor in this case, the inverter will be in uncontrolled regeneration mode. This will recharge the DC-bus and also apply a load on the DC-motor. In order to avoid large in-rush currents, the DC-motor had its speed slowly increased starting from standstill: the DC-bus would charge until its value reaches the potential across the two phases. Once the DC-bus reached the desired value, the speed of the DC-motor would be reduced in order to start the controlled generation.

Motoring Mode

In the motoring mode, the DC-machine operated as a generator with a resistor bank was used as a load for the PM-BLDC machine. The armature of the DC-machine was connected to the resistor bank, which could be set at different loads. Also, the field excitation of the DC-machine was controlled and could be adjusted to vary the load torques.

5.1.2 Testing with the Diesel engine

In the second phase, the PM-BLDC starter/generator system was coupled to the Diesel engine in the laboratory and tested. The setup included the following elements, as shown in Figure 5-2:

- PM-BLDC starter/generator with its inverter and controller
- ICE on a stand, belt-coupled to the starter/generator
- a basic version of a supervisory controller, implemented under LabView with a PXI box, interfacing with the ICE and the DSP of the starter/generator controller. The torque command was an analog value sent by the supervisory controller and read by the DSP's A-to-D converter; the speed feedback sent to the supervisory controller was coded over 8 bits on digital pins.
- a simplified version of the final exhaust system
- the complete string of 160 ultra-capacitors
- a combination of resistor banks in parallel and series
- a "switch-box" to safely connect high voltage devices; relays controlled each line connected to the DC-bus

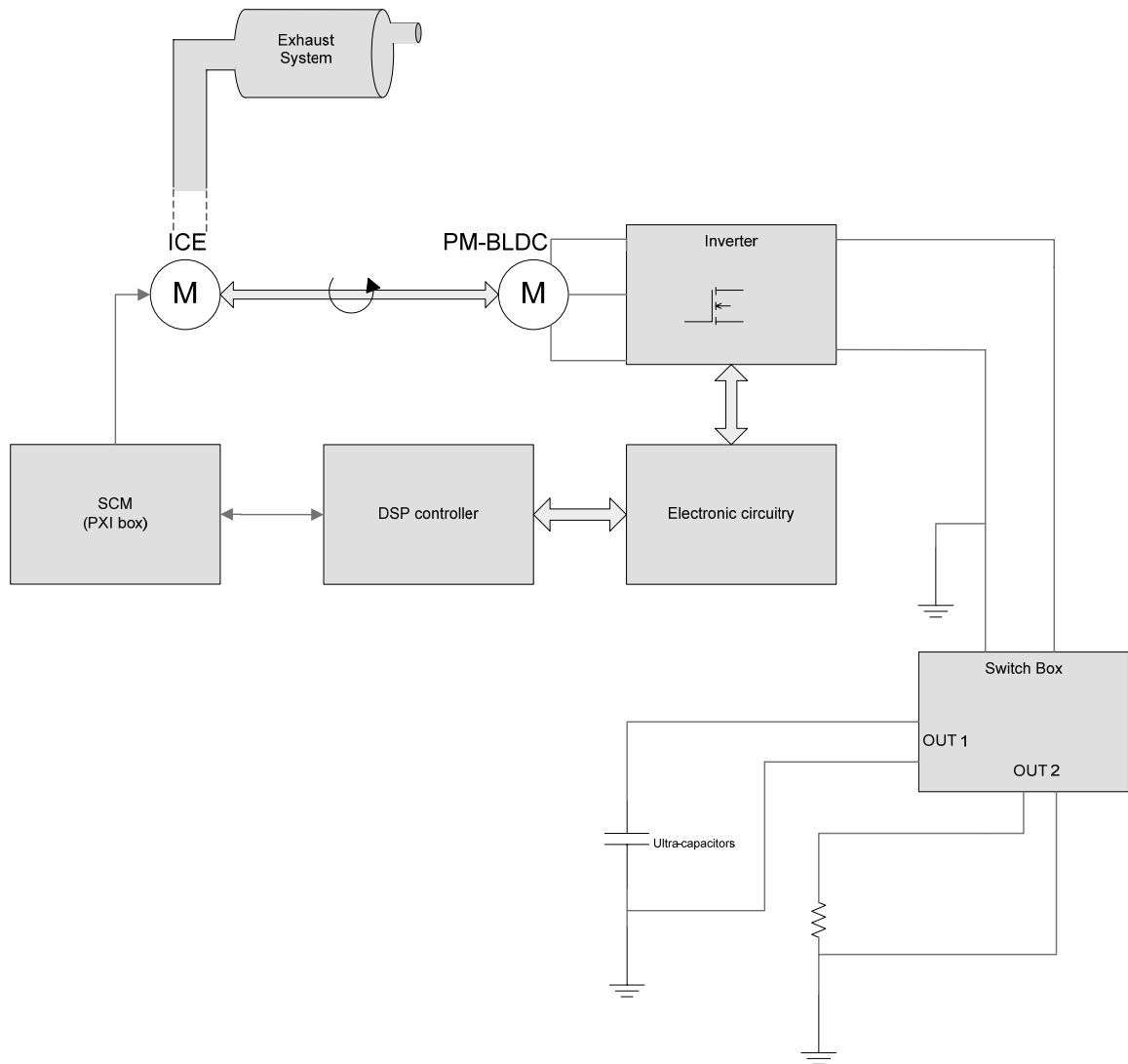


Figure 5-2: Test setup with Diesel Engine

For this set of tests, the limitations of the experiment are as follows:

- the wiring between the inverter and the motor could only handle up to 80 A
- the fuel used was regular diesel in order to get referral values for emissions and fuel consumption evaluations

Certain restrictions and modes of operation were applied during testing which will be described along with the specific tests.

Generating Mode

The limitations in the current ratings led to restricting the testing power to a maximum of 10 HP. For emissions, tests needed to be performed for a certain duration, for which resistor banks had to be used to “dump” the surplus of energy in order not to overcharge the ultra-capacitors. This was controlled manually through the “switch-box.”

Motoring Mode

The only control the supervisory controller has over the ICE is the flow of fuel sent to the engine. The rate of fuel flow corresponds roughly to the ICE torque. The source and load power must match for steady state balanced operation (losses are not accounted for in this approximation). In the motoring case, the ICE would need to act as a load, which means applying a negative torque to the starter/generator. The load for the motor for its intended application is the inertia of the car and the friction of the wheels on the pavement. It can be simulated by using a dynamometer, but this was not available on the test stand. Hence motoring testing was not possible, with the exception of the starter mode; in this case, the PM-BLDC machine has to overcome the compression stages of the engine before it starts.

In the later experiments with the diesel engine, the fuel was replaced with Bio-Diesel (B20) and the wiring between the inverter and the PM-BLDC machine was made compatible with the nominal ratings of the final system.

5.2 Results at Low Power

A first batch of tests was run at low power. The results of those tests are presented and analyzed next.

5.2.1 Motoring test

Tests were conducted with different torque/current references, as well as with various loads, which led to different speeds.

Figure 5-3 shows the current in phase A and the line-to-line voltage between phase A and B, V_{ab} , at 1083 RPM, with a phase current reference value of 40 A. The current scale is 25 A per division. The current is regulated around 40 A. Using the relationships $P = T \times \omega$ and $T = K_t \times I$, the output power is determined to be 712 W.

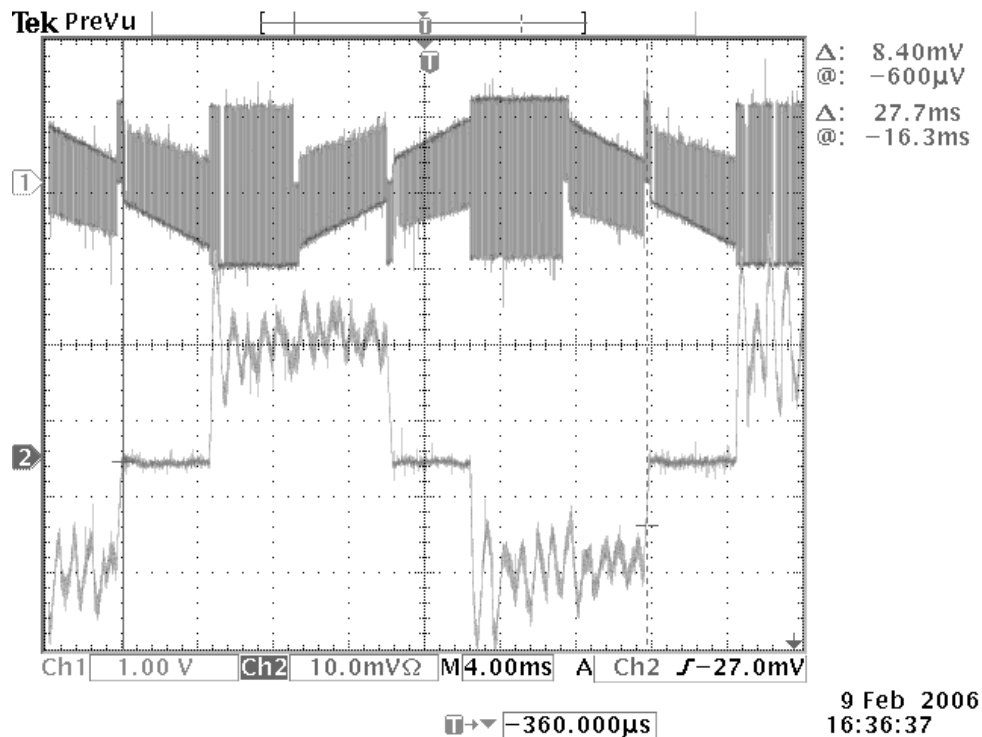


Figure 5-3: V_{ab} and I_a at 1083 rpm, 712 W

The same quantities are shown in Figure 5-4 for an ICE speed of 743 RPM for a reference of 75 A. The output power is 1466 W. The current scale is 50 A per division. The current is regulated at its reference value with an overshoot of about 40% of the final value. It can be seen by comparing Figure 5-3 and Figure 5-4 that the phase current follows the current command better at higher levels of reference current.

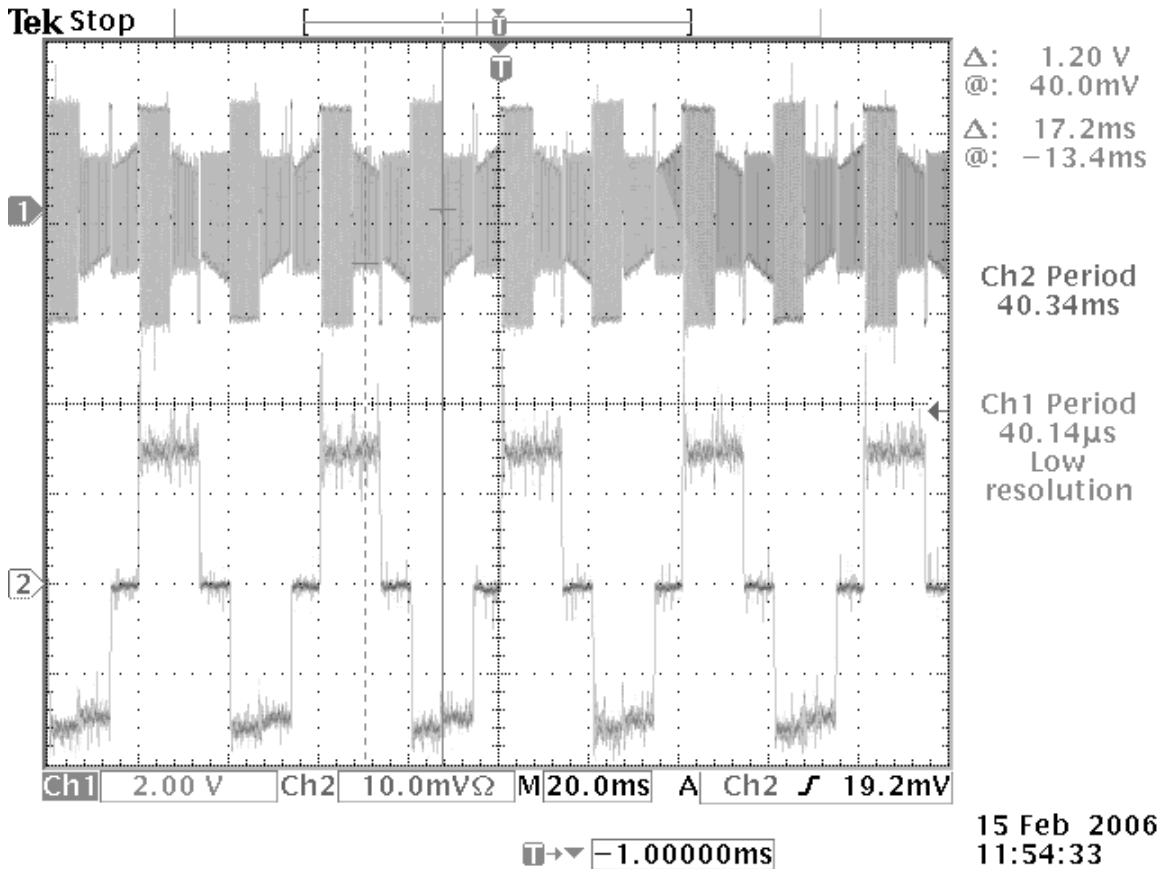


Figure 5-4: V_{ab} and I_a at 743 rpm, 1466 W

The voltage waveform V_{ab} shown in Figure 5-3 and Figure 5-4 reflects the implementation of the hard-switching strategy, where the voltage applied across the two phases in series is alternatively $+V_{DC}$ and $-V_{DC}$ during the phase A conduction period. At a current of 75 A, a ripple of about 5 to 10% of the regulated value can be seen. It can also be seen that there is an overshoot when the phase conduction begins. The overshoot

is due to the gains of the controller. Also, as discussed in Chapter III, these overshoots are due to the fact that the current in a phase cannot be discontinuous, hence resulting in the addition of the remainder of the current in the “remaining phase” to the one that just started flowing in the “newly-energized phase”.

During the tests, the voltage across the ultra-capacitors slowly decayed. The time constant for decay is much longer than the period of the current flowing in one phase, and hence this drooping characteristic is imperceptible in the different oscilloscope screen captures. The voltage decay had no effect on the current control. In a different situation where the variations in the DC bus voltage might occur on a shorter time scale, i.e., close to the switching frequency, these variations would have to be taken into account in the design of the current control.

For the ease of implementation of the controller, the DC bus voltage was assumed constant in determining the duty cycle. Note that the output of the PI controller is the voltage command; but the final command is a duty cycle, which is a percentage of the DC-bus voltage. If the duty cycle had been calculated in proportion to the input voltage, since it varies with time, it would have been equivalent to adding a variable gain after the PI-controller. This would have changed the response of the controller, most likely affecting the transient response. However, it would have involved a large computation time, due to the division that it would require.

5.2.2 Generating tests

Tests were conducted with different torque/current references, as well as with various loads, which led to different speeds.

Figure 5-5 shows the current in phase A and the line-to-line voltage between phase A and B, V_{ab} , for the current reference of 25 A at a speed of 236 RPM. The power was hence 155 W. The current scale is 25 A per division. Comparing this result with the results obtained in Figure 5-3, the overshoot and ripple are the same in both motoring and generating situations, although the speed was about 5 times higher in Figure 5-3.

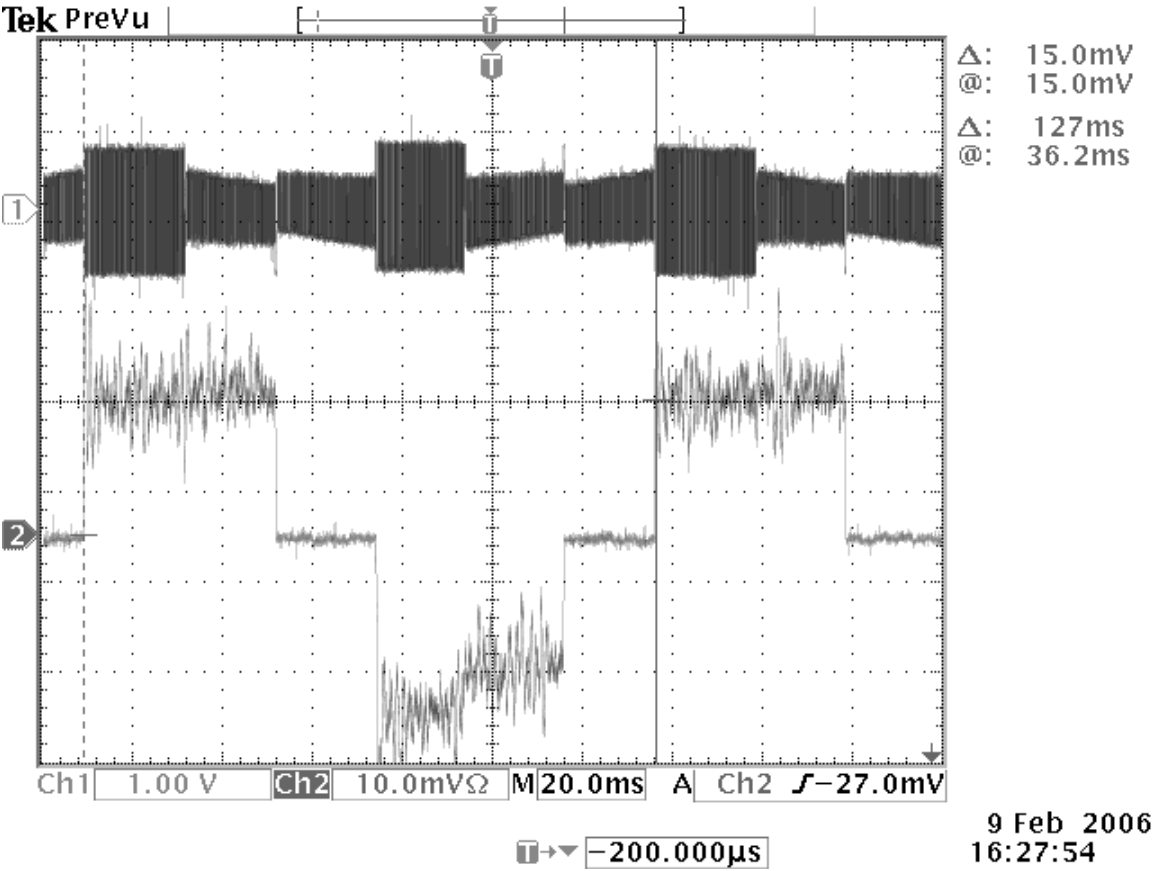


Figure 5-5: V_{ab} and I_a at 236 rpm, 155 W

The same quantities are shown in Figure 5-6 for a current reference of 75A at a speed of 1162 RPM. The power was hence 2281 W. The current scale is 50 A per division. As in Figure 5-5, regulation is reached with similar overshoot and ripple.

Also, Figure 5-6 must be compared with the results obtained in Figure 5-4, which showed the results in motoring mode for a similar current reference, however at a slightly lower speed. The same performances with respect to overshoot and ripple have been reached.

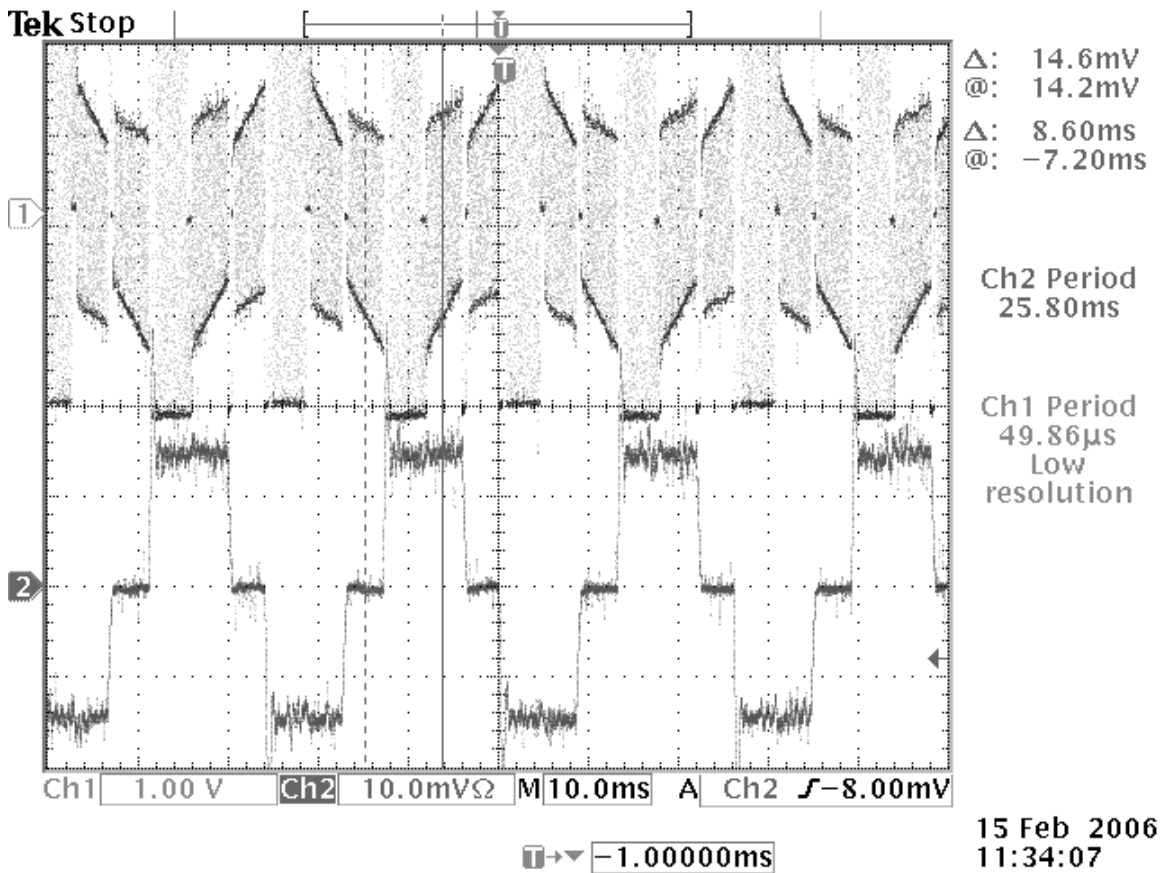


Figure 5-6: V_{ab} and I_a at 1162 rpm, 2281 W

5.3 Medium Power Tests with Diesel Engine

The first set of tests on the diesel engine at a lower power level was a step towards the validation of the concept of the starter/generator application. The setup was

also used to do emissions tests with diesel fuel. The machines were run for a long period of time in order to get meaningful data. This allowed for a durability test, pushing the motor further than it would be in a regular driving cycle.

The results for the current reference of 67 A at a speed of 4290 RPM is shown in Figure 5-7. Figure 5-7 shows the current in phase A as well as the line-to-line voltage between phase A and B, V_{ab} . The power level was 7524 W, i.e. almost 10.1 HP. The scale for the current is 50 A per division.

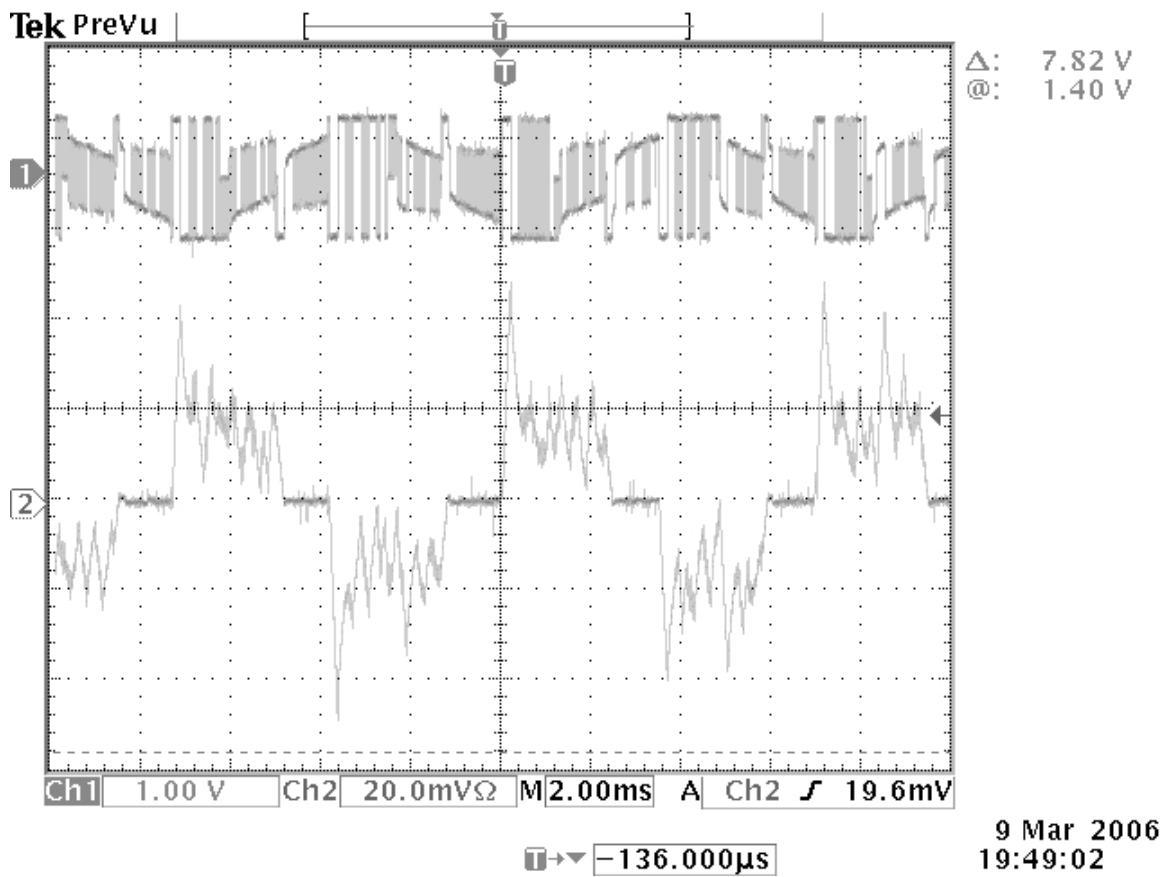


Figure 5-7: V_{ab} and I_a at 4290 rpm, 7524 W

The current regulation was achieved on the average, but the ripple is high as can be seen in Figure 5-7. It can be compared with Figure 5-6 where the current reference was 75 A. The main difference is in the speed, which has almost quadrupled. The

overshoot in current at the transition has the same amplitude, but the ripple is much higher.

The major difference in setup between the results in Sections 5.2 and 5.3 is of course the prime mover. As mentioned in [9], torque jolts on the engine shaft are expected. Also, the mechanical properties of the belt used to couple the ICE and the PM-BLDC machine can amplify those perturbations.

The results presented show that the controller is able to regulate after the initial in-rush of current in the phase. The in-rush lasts about 3 ms.

5.4 Full Power Testing with Diesel Engine

The final phase of laboratory starting and generation testing was at the full power level with suitable power cables installed and using Bio-diesel B20 fuel for the engine.

5.4.1 Startup

A few successful startups of the engine with the PM-BLDC machine were accomplished. Unfortunately, it was not possible to capture any transient of the current. It must be noted that the concept was proven.

The engine was started with a torque (hence current) command applied for a short time (around a second) and then reset to zero. The current reference of 200 A resulted in the successful start of the engine.

5.4.2 Generation testing

The second and most important part of the full power testing was generation testing. The results of those tests are presented and analyzed next.

5.4.2.1 Moderate ICE speed tests

Tests at medium speeds (between 1500 and 2000 rpm on the ICE side) were first attempted.

The phase current for the current reference of 150 A at a speed of 4290 RPM on the PM-BLDC machine side are shown in Figure 5-8. The power level was 16.84 kW, i.e. almost 22.6 HP. The current scale was of 50 A per division. The current overshoots to 200 A and is regulated around 125 A. The current reference could not be reached according to the measurements. However, the probe used to measure the current had a limit of 100 A, and hence saturation is expected, leading to incorrect readings above 100 A. The ratio of the overshoot over the average values is about the same as presented in the Section 5.2; the ripple is comparable. However, the ratio of the settling time to the period is now larger, which leads to higher torque ripple on the machine shaft.

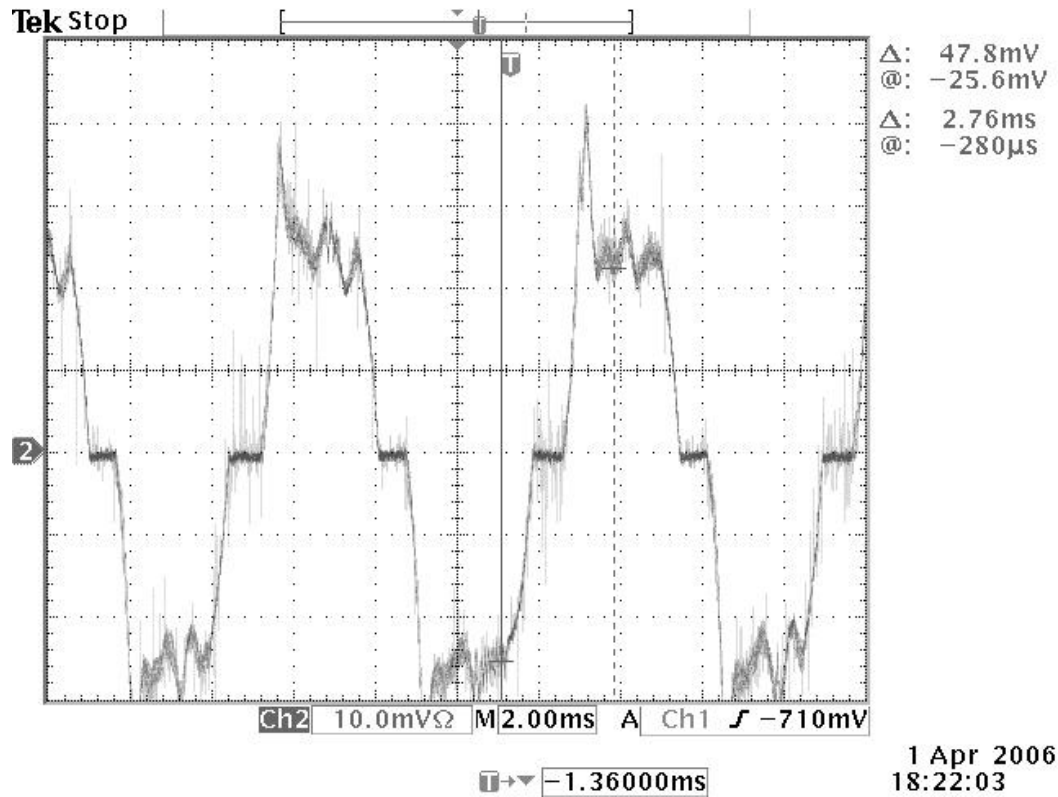


Figure 5-8: I_a at 4290 rpm, 16840 W

The phase current for the current reference 102 A at a speed of 4290 RPM on the PM-BLDC machine side is shown in Figure 5-9. The power level is 11.45 kW, i.e. almost 15.35 HP. The current scale was 50 A per division. The current overshoots to 150 A and regulates roughly just above 100 A. The current regulation is better than the one observed on Figure 5-8, which is due to lower levels of saturation in the current probe.

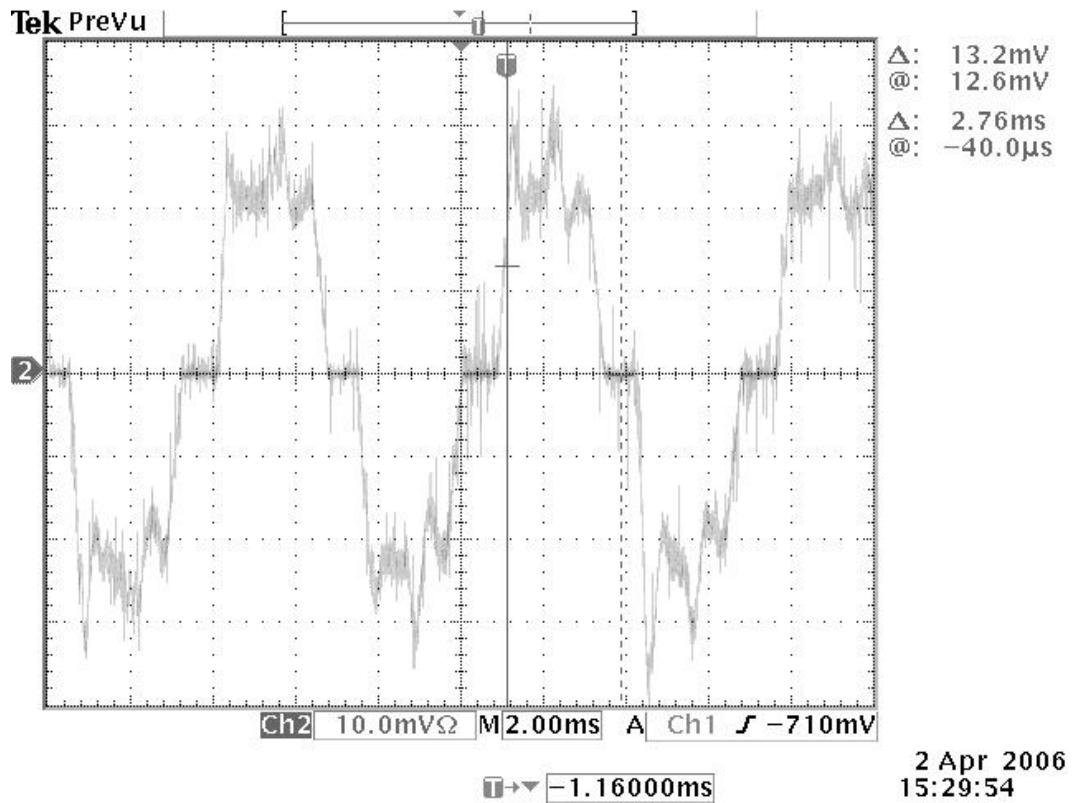


Figure 5-9: I_a at 4290 rpm, 11450 W

The phase current for the current reference 100.5 A at a speed of 5720 RPM on the PM-BLDC machine side is shown in Figure 5-10. The power level is 15.05kW, i.e. almost 20.2 HP. The current scale is 50 A per division. The speed is 33% greater than the experimental result shown in Figure 5-9, but the regulation has approximately the same shape. As seen in Section 5.2, moderate speeds do not affect the regulation too much.

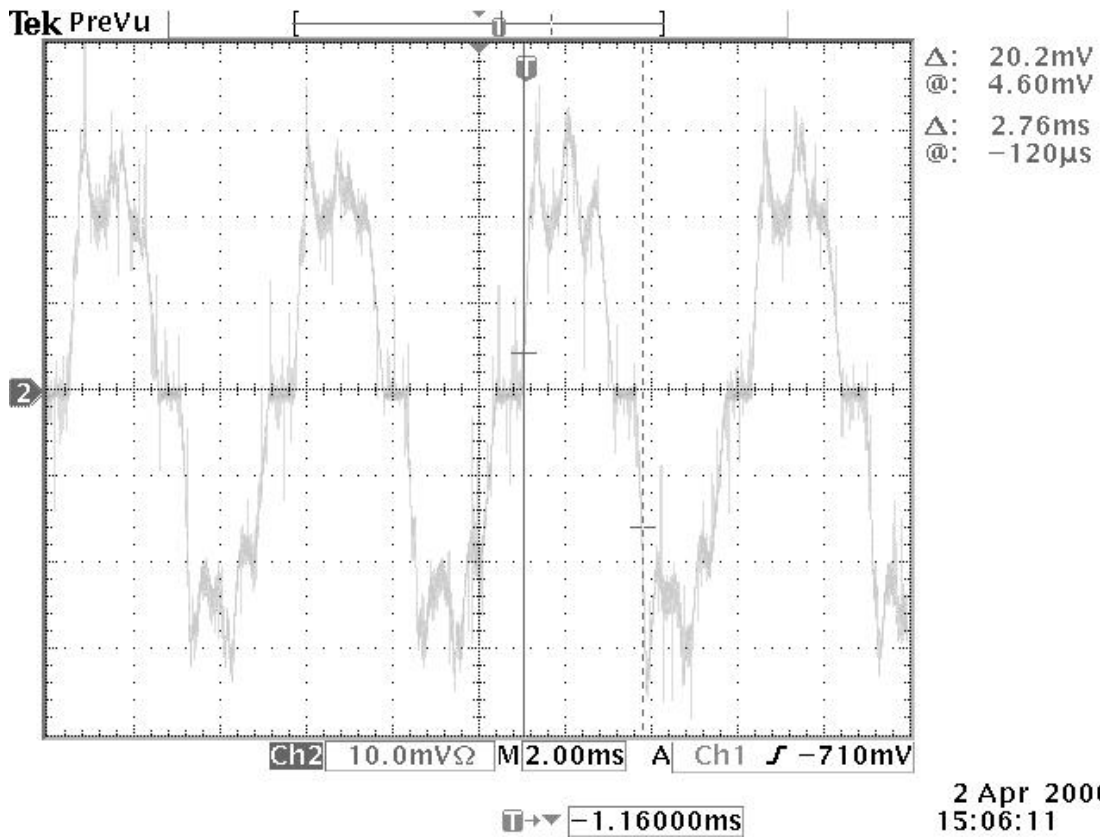


Figure 5-10: I_a at 5720 rpm, 15050 W

Figure 5-8, Figure 5-9 and Figure 5-10 show big overshoots in current each time a phase starts conducting. Also, for a current reference higher than 100 A, the DC value of the current is not reached.

As mentioned previously, the probe used to display the current on the oscilloscope screen was limited to 100 A. It is likely that the probe saturated, hence the scale for the measured current waveforms was non-linear and the current levels shown in the screen captures are lower than the actual levels.

5.4.2.2 Higher speeds and protection

In order to improve the results, empirical modifications to the PI gains of the controller as well as to the inputs of the PI controller algorithm were implemented. Those gains, however, were only modified when certain conditions were met, as mentioned in 4.2.1.2.

To reduce the overshoot for current references above 110 A, the value of the duty-cycle from the previous calculation used by the integrator was divided by two. Hence, the PI controller would start reducing the duty cycle value sooner because the current would appear to get closer to the reference earlier than in reality. This method, however, has the disadvantage of slowing down the response. It is necessary to mention that this operation moves the pole of the controller from $z = 1$ to $z = 0.5$. Theoretical analysis had previously shown that this would lead to a stable loop with a lower DC gain. Also, to further reduce overshoot, the integral gain was reduced for current references over 110 A.

The following figures show the improvements.

The phase current for the current reference of 150 A at a speed of 4290 RPM is shown in Figure 5-11. The power level is 16.8 kW, i.e. almost 22.6 HP. The current scale is of 50 A per division.

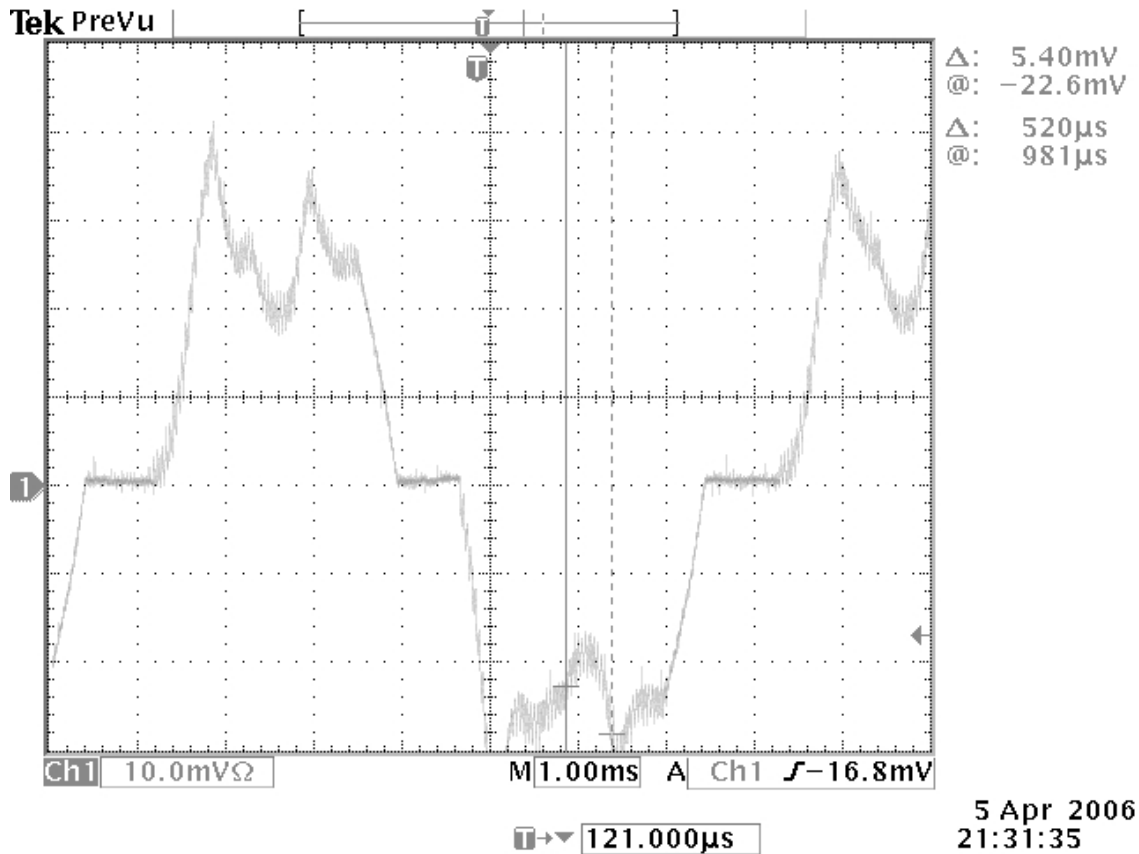


Figure 5-11: I_a at 4290 rpm, 16800 W

Compared to Figure 5-8, the shape is more balanced. Also, the rise time is slower. The value for the current over 100 A cannot be accepted to represent what is actually flowing in the phase due to the limitation of the measurement probe.

The phase current for the current reference of 150 A at a speed of 4862 RPM are shown in Figure 5-12. The power level is hence 19.03 kW, i.e. almost 25.6 HP. The current scale is 50 A per division.

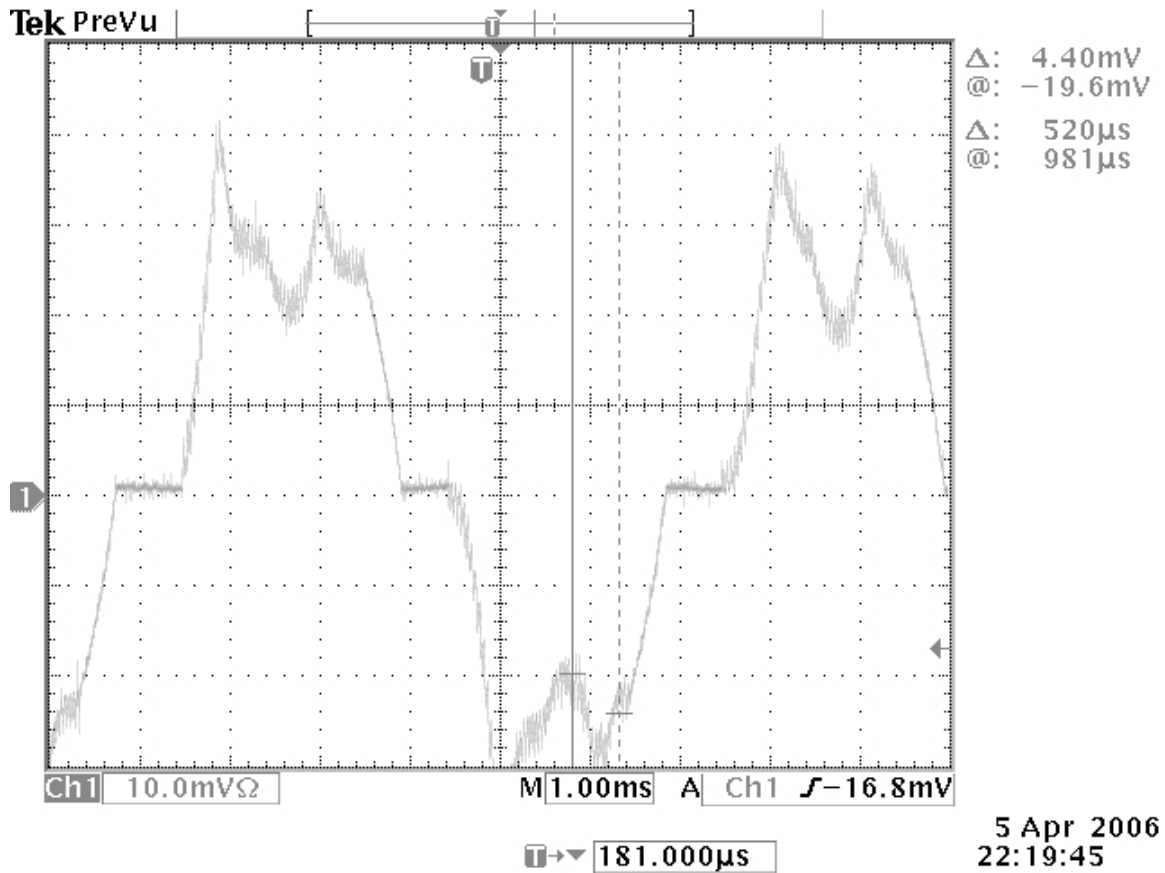


Figure 5-12: I_a at 4862 rpm, 19030 W

The phase current for the current reference of 140 A at a speed of 5720 RPM are shown in Figure 5-13. The power level is hence 20.9 kW, i.e. almost 28.1 HP. The current scale is 50 A per division.

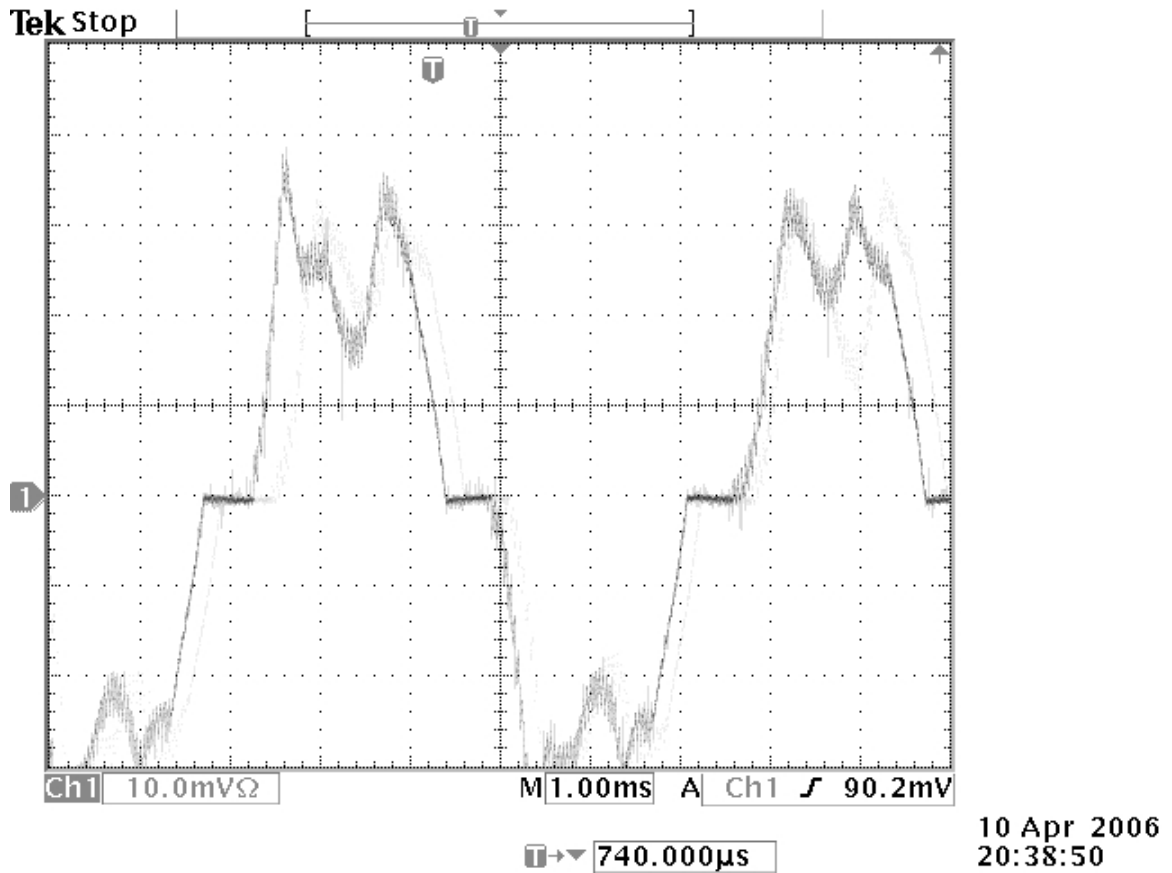


Figure 5-13: I_a at 5720 rpm, 20900 W

The phase current in Figure 5-11, Figure 5-12 and Figure 5-13 show that the current regulation is not significantly affected when the machine is operated at medium speeds. However, it shows that the modifications on the gains (refer to 4.2.1.2) in the code of the DSP played a role on the extent of the overshoots.

The phase current for the current reference of 34 A at a speed of 8580 RPM are shown in Figure 5-14. The power level is 7.6 kW, i.e. almost 10.2 HP. The scale for the current is 20 A per division. The current is on average regulated around the set-point but with relatively high ripple.

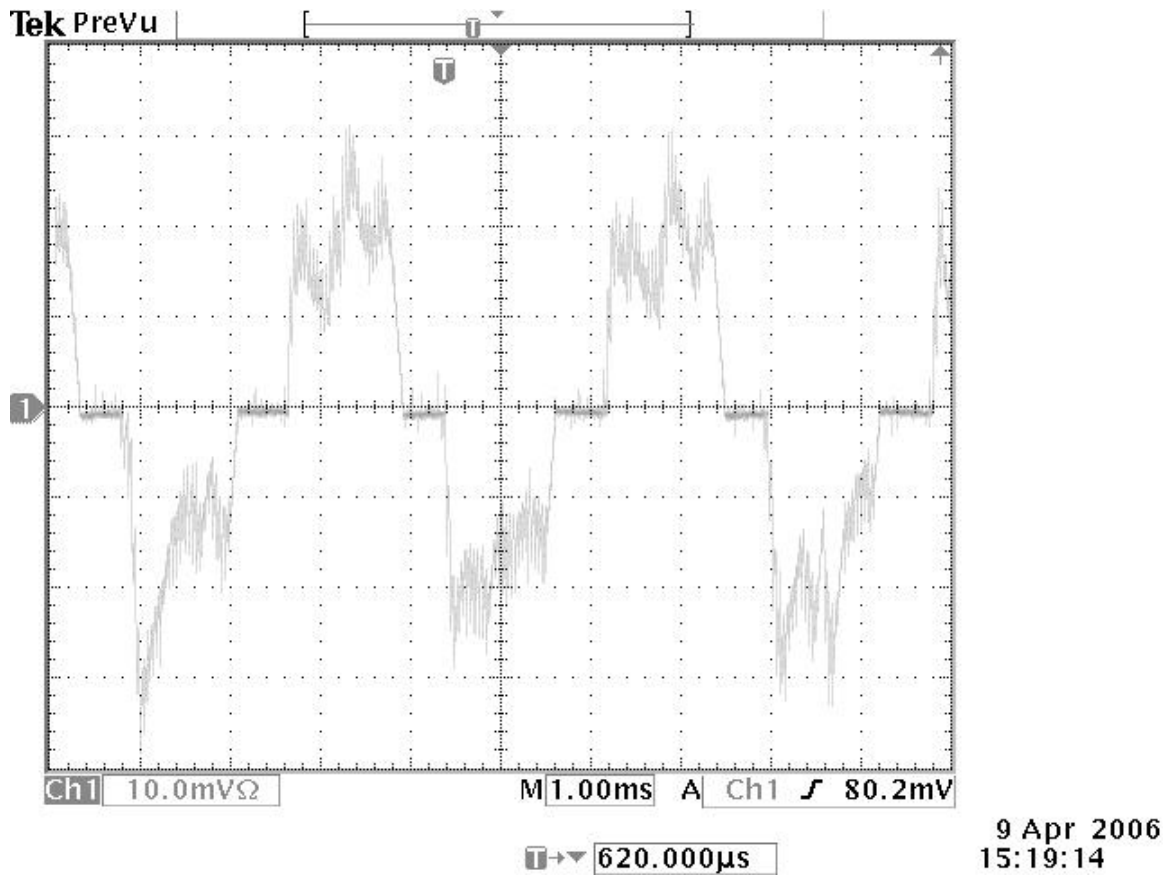


Figure 5-14: I_a at 8580 rpm, 7600 W

In Figure 5-15 the current reference was 68 A, at a speed of 8580 RPM. The power level is hence 15.3 kW, i.e. almost 20.5 HP. The scale for the currents is 50 A per division.

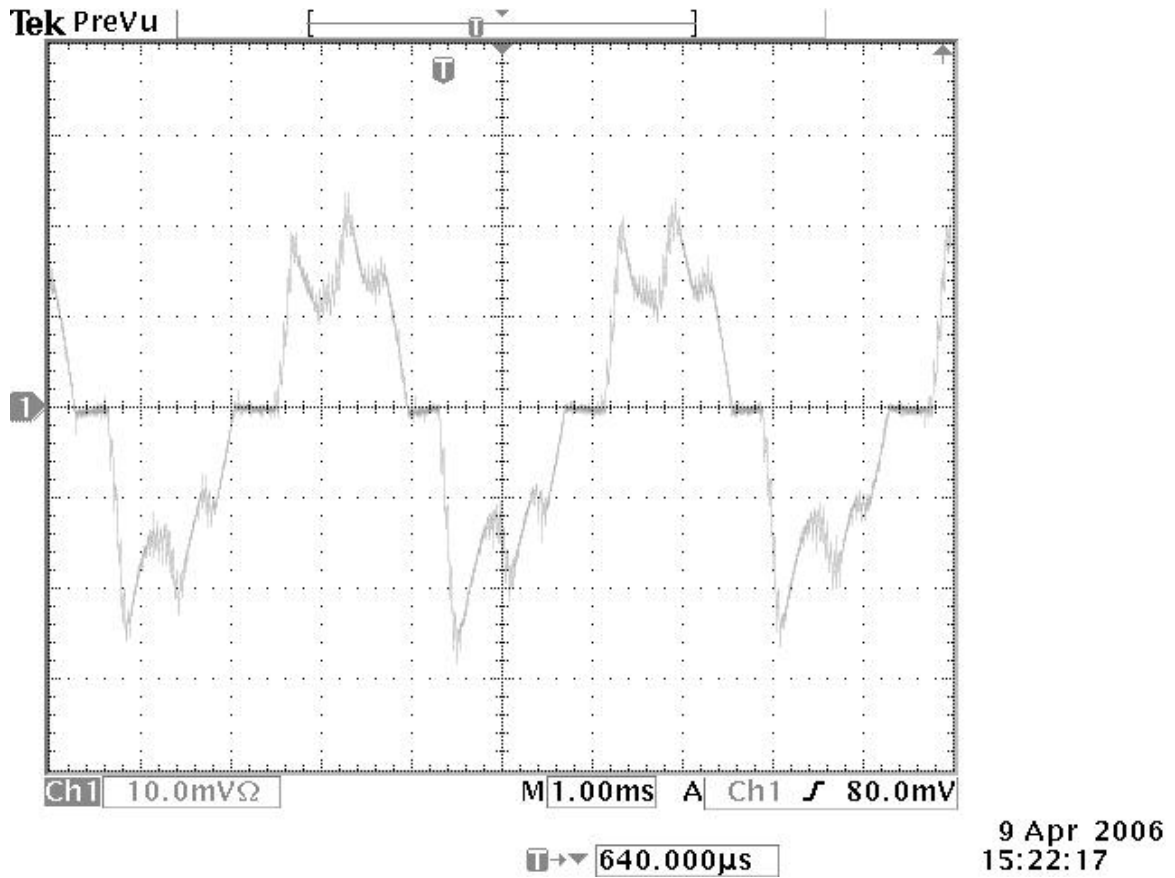


Figure 5-15: I_a at 8580 rpm, 15300 W

The current gets regulated around its reference value with a relatively low overshoot. The limitations implemented in the DSP (as shown in Section 4.2.1.2) for high speeds prevented large overshoots when the phases start to conduct.

Table 5-1 summarizes the different tests ran by the motor in the generating mode. It must be noted that the current and hence torque levels included are the commands; actual phase torque measurement was not possible in the setup. However, average current and hence torque can be graphically determined from the oscilloscope screen captures. Those values are hence merely approximations of the actual value.

Table 5-1: Summary of generation testing

Motor Speed (rpm)	Torque reference (N.m)	Current reference (A)	Estimated Current	Estimated Torque (N.m)
236	6.27	24.97	50	12.56
1162	18.75	74.62	75	18.84
4290	16.75	66.67	45	11.30
4290	25.49	101.45	120	30.15
4290	37.40	148.86	140	35.17
4290	37.48	149.21	135	33.91
4862	37.38	148.78	140	35.17
5720	25.13	100.01	115	28.89
5720	34.89	138.89	130	32.66
8580	8.46	33.67	45	11.30
8580	17.03	67.78	72	18.09

5.5 Changes in the Simulation

Using the theoretical PI gains obtained from simulation in the DSP did not lead to the expected simulation results. Gains had to be tuned in real time, as has been mentioned earlier. Reasons for those problems are multiple: induced noise in the signal wires due to switching frequency, mechanical vibrations affecting the back-EMFs, etc.

Several parameters were idealized and noise in measured signals were neglected in the simulations. The actual shape of the back-EMFs, the noise on the current feedback and the noise on the engine speed due to the diesel four-stroke cycle, and the non-linearities of the inverter were not taken into account in the Simulink simulation program. Hence, it was found interesting to re-run the simulations with some of those non-idealities taken into account, mainly the noise on the current feedback and the speed.

The noise on the current feedback was simulated as a random noise with a maximum amplitude of 15 A. This level of noise was observed on the DSP ADC inputs when the inverter was not switching; one can suppose the noise to be higher with the inverter active.

The noise on the speed was quantified according to the cycle of the engine as described in [3] and [9]; the noise was set to be of sinusoidal shape, at the frequency of the four stroke cycles and with an amplitude of 5% of the speed value. The simulation results obtained with the non-idealities incorporated are given below.

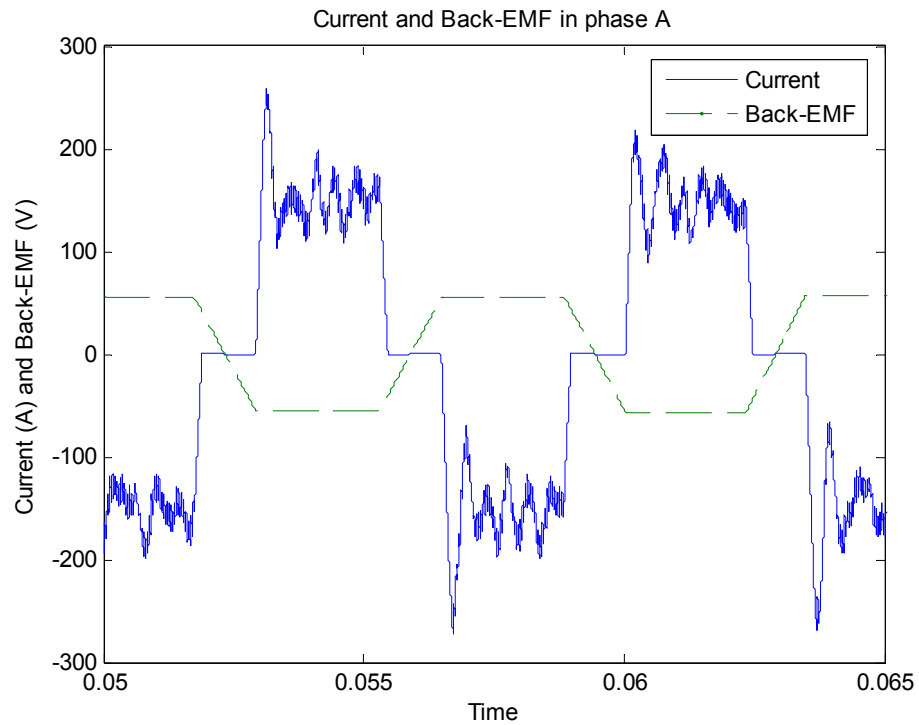


Figure 5-16: E_a and I_a at 4290 rpm, 16846 W, ICE speed = 1500 RPM, phase current command = 150 A

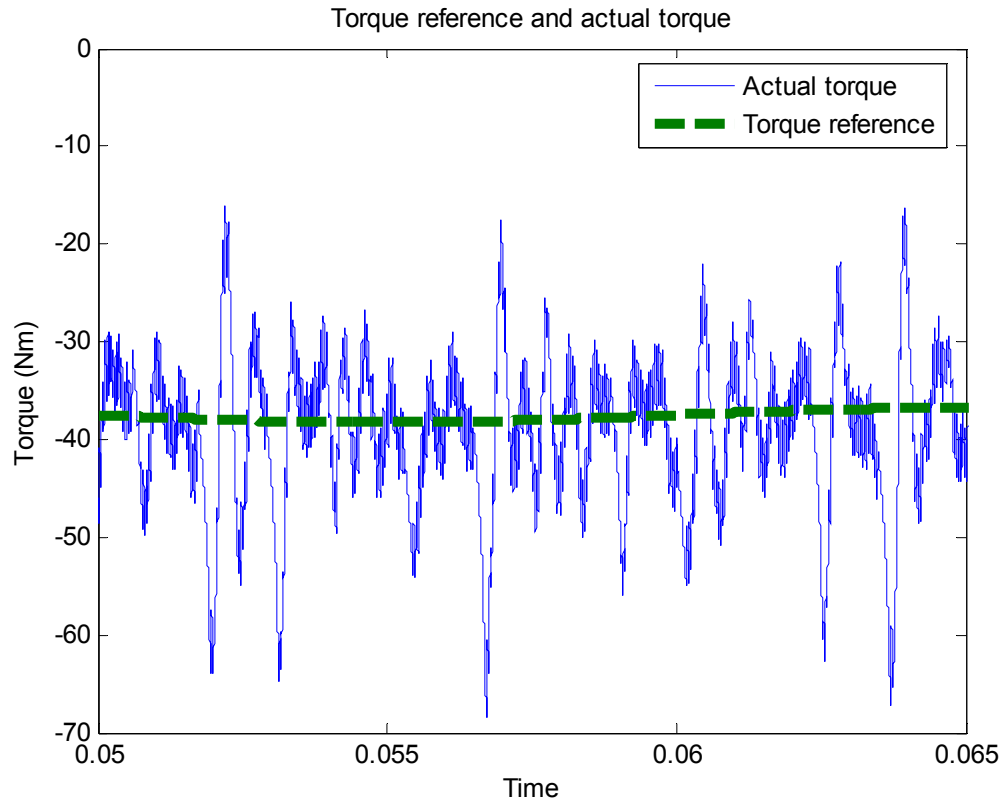


Figure 5-17: T and T_{ref} at 4290 rpm, 16846 W

In Figure 5-16, it can be seen that the phase current overshoots to a value of about 250 A, while in steady state, there is a ripple between 50 and 90 A. The overshoot reflects on the torque as can be seen in Figure 5-17. This result resembles to what was observed during testing as shown previously in Figure 5-11.

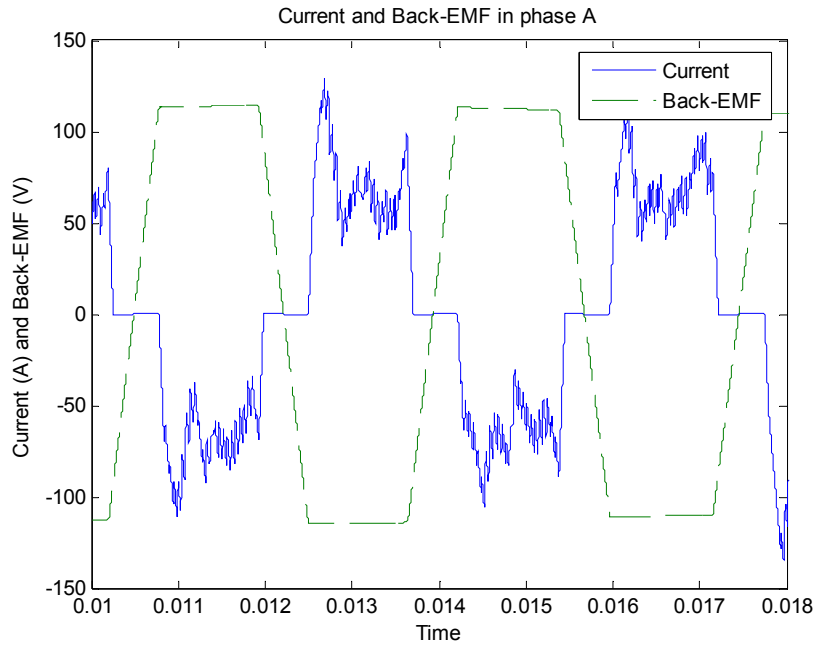


Figure 5-18: E_a and I_a at 8580 rpm, 15274 W, ICE speed = 3000 RPM, phase current command = 68 A

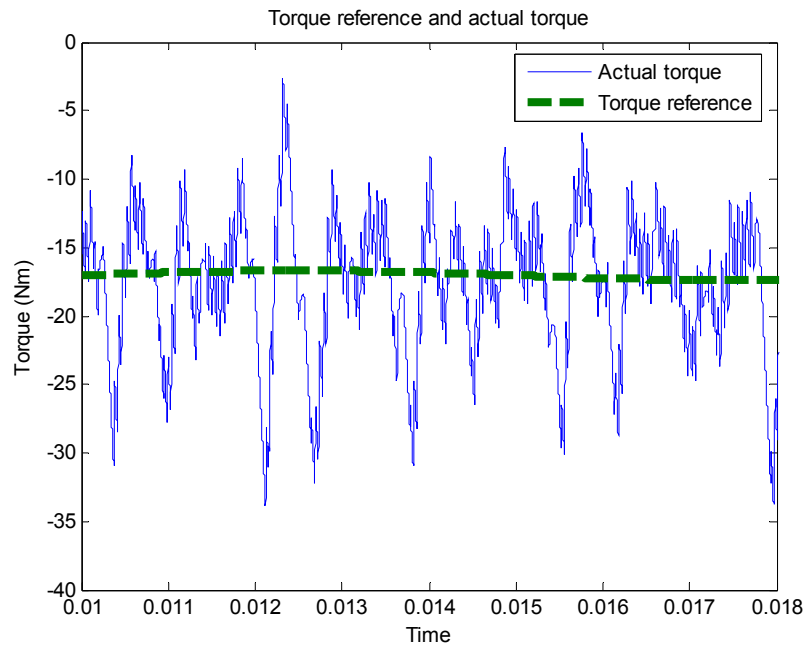


Figure 5-19 T and T_{ref} at 8580 rpm, 15274 W

The simulation results in Figure 5-18 and Figure 5-19 match pretty closely to what was observed during tests (Figure 5-15).

The experience gained during experiments lead the way for future improvements of the system through a more accurate simulation.

5.6 Summary

The torque controller for the PM-BLDC machine for the starter/generator application has been implemented. The levels of power and speed targeted for the starter/generator application in the hybrid electric vehicle were attained.

The shapes of the phase currents and the torque delivered by the PM-BLDC machine were not as smooth as expected. Some characteristics had been idealized in the simulations but proved to be non-negligible with the real implementation. A finer tuning of the controller's gains while simulating noise and adjusting the different approximations should be undertaken to develop a better controller for the PM-BLDC machine.

CHAPTER VI

SUMMARY AND CONCLUSIONS

This final chapter presents the different parts of the work done for this research, the improvements offered in comparison to previous works, and finally describes different directions to improve the torque control of a PM-BLDC machine for a hybrid vehicle application.

6.1 Summary

The objective of this project has been to develop a controller for a PM-BLDC machine which will be used as a starter/generator for a hybrid electric vehicle.

This thesis first presented different methods for torque control of the PM-BLDC machine. In the following chapter, the theory of the PM-BLDC machine and its controller chosen for the application were reviewed in detail. The simulation of the system and its results were presented. This was followed in another chapter by the description of the integration of the system. Finally, the results of the tests run were presented and analyzed.

Several things were accomplished during this project. First, a simulation of the motor in the generating mode was run in order to verify the concept of operation and to tune the controller. Operation in the speed and power ranges required in the final

application was obtained. Notably, the simulation showed an almost constant current ripple at 25A for various power and speed levels. Then a controller has been developed and successfully tested in the laboratory.

6.2 Contributions

The success of this research advanced the development and integration of a PM-BLDC machine torque controller for a hybrid vehicle.

For the particular motor used, this thesis proved that operation at low and high speed was possible with satisfactory performance, allowing this motor drive to be considered for a variety of applications that would require a wide speed range. Furthermore, the thesis proved the system to be adequate for the level of speed and power required for the University of Akron's particular hybrid vehicle application.

The main contribution of this work has been to develop a system integrated in the vehicle, as a first step towards a more complete and compact solution. On the software point of view, the system had an elaborate fault detection management developed, which contributed to its ruggedness. The torque controller developed was an industry approved and documented one. Also, the implemented communication protocol followed the automotive industry standard (CAN). On the mechanical side, the components used for the application were not automotive ready, let-alone fitted for the particular car used, and it hence required specific arrangements and designs.

6.3 Suggestions for Future Work

The results obtained throughout the testing of the system, problems and/or limitations appeared. The following paragraphs discuss possible ways of improvement.

6.3.1 Improvements in simulation

Due to time constraints in the feasibility of the project, a more extensive simulation could not be run. A more detailed version would help in predicting the experimental results. The controller could be easily improved from a more in-depth approach, as further presented.

Back-EMFs

First of all, the shapes of the back-EMFs in the PM-BLDC machine have been approximated to be perfect trapezoidal shaped waveforms, which is only achievable theoretically. A measurement of the actual back-EMFs showed that this assumption is true only to a certain extent, as can be seen on Figure 3-3. Using measurements of the three line-to-line back-EMFs to create a look-up table in Matlab should lead to a good representation of those back-EMFs.

ICE model and Hybrid Vehicle Strategy

One of the limitations of the simulation was the absence of a model for the ICE. Its response was assumed perfect and instantaneous; a better representation of the engine could also have provided the opportunity to test the motoring mode in more details. It could as well model the noise induced by the drive cycle as described in [9]. Also,

coupling the torque command with the different road strategies implemented in the complete hybrid vehicle simulation, as presented in [10], would provide a more precise evaluation of the global performances of the hybrid vehicle, and would help in fine-tuning the controller for the starter/generator.

6.3.2 Design of a feed-forward compensator

Adding a feed-forward block before the proportional-integral controller would immunize the system from possible perturbations due to analog signals corruption such as noise on the current measurements. Since the machine model in continuous-time is known (given in Chapter III), one needs to discretize this model in order to implement the feed-forward compensator in the DSP. The structure would be as described in Figure 6-1 and found in [8].

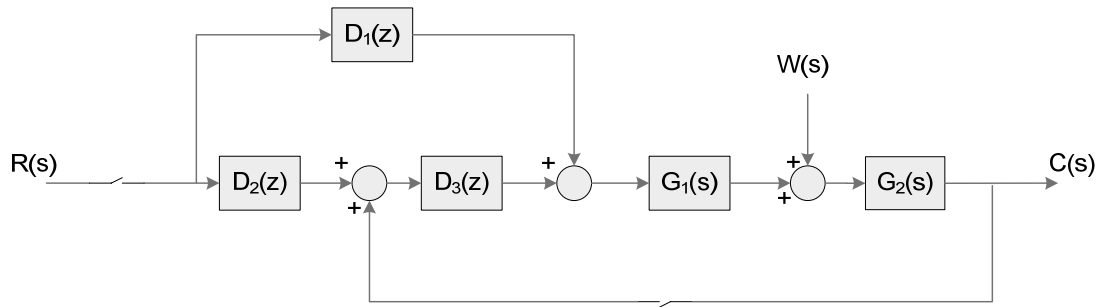


Figure 6-1: Feed-forward model

$D_1(z)$ has to be designed as an open-loop controller so that $[G_2G_1](z)D_1(z)$ is the desired system transfer function. Then, $D_2(z)$ will also be equal to $[G_2G_1](z)D_1(z)$. $D_3(z)$ is the current PI controller.

6.3.3 Additional experiments

The setup, the instruments and the time available for the experiments did not allow power and efficiency measurements of the ensemble constituted of the inverter and the PM-BLDC machine. The current sensing probe by Tektronics was limited to 100A. The results obtained for such a level of current have error, due to the non-linear magnetics in the sensor. A more reliable way to measure the current would be to use a shunt resistor, using additional conditioning electronics. The DSP or the LabView environment through the NI-box (analog and digital interface for LabView) could measure the current as well as the voltage on the DC-bus and compute the power used or generated. The power flowing through the PM-BLDC machine could be calculated with the measurements already available. Hence the efficiency of the system comprised of the inverter and the PM-BLDC machine could be determined.

6.3.4 Noise immunity and controller ruggedness

The electronics used to scale the different analog and digital measurements needed by the controller were proved to be sensitive to noise. The grounding scheme of the sensing board needs to be improved. It would be an important improvement to use and design surface mount PC boards.

In order to ensure the durability of the project, the controller should be made vibration resistant and packaged to minimize electromagnetic interference. Also, automotive-grade connectors should be used in order to ensure good connection between the controller and the different components of the system.

6.3.5 Single-current sensor control

The fact that the current sensors are expensive and cumbersome becomes an issue in the automotive industry. One alternative is to do the torque control of the PM-BLDC machine with only one sensor.

In the PM-BLDC machine drive with the present switching strategy (hard switching), the current is alternatively positive and negative on the DC bus of the inverter, depending on whether the IGBTs or the diodes are carrying the current. Hence, knowing the position with the help of the Hall-effect position sensors and synchronizing the measured current value in the DSP with the switching of the IGBTs, the controller can perform torque control. In the project, the design of the purchased inverter did not allow torque control with only one current sensor. The filtering capacitors are on the DC bus side of the inverter and there was no room to install the current sensor between them and the arms of the inverter. If put on the DC bus but on the other side of the filtering capacitors, the current only reflects the power required or generated by the machine and not the instantaneous values of the phase currents.

6.3.6. Current overshoot control

Simulation and experiments showed that the uncontrolled decay of current in the phase that is turned-off (a change that happens every $\frac{1}{12}$ th of a revolution) could be one of the reasons leading to the overshoots observed. A strategy to reduce this effect would be to have a controller, such as a simple integrator, to act on the phase remaining ON. The controller would take the current in the phase that is turned OFF into account, and would compensate the duty cycle of the phase that has just been turned-ON.

REFERENCES

- [1] Pragasen Pillay, Ramu Krishnan, "Modeling, Simulation, and Analysis of Permanent-Magnet Motor Drives, Part II: The Brushless DC Motor Drive," *IEEE Transactions on Industry Applications*, Volume 25, Issue 2, Mar-Apr 1989 Page(s): 274-279
- [2] Feng Chai, Shumei Cui, Shukang Cheng, "Performance analysis of double-stator starter generator for the hybrid electric vehicle," *IEEE Transactions on Magnetics*, Volume 41, Issue 1, Part 2, Jan. 2005 Page(s):484 - 487
- [3] Shaotang Chen, B. Lequesne, R.R. Henry, Yanhong Xue, J.J. Ronning, "Design and testing of a belt-driven induction starter-generator," *IEEE Transactions on Industry Applications*, Volume 38, Issue 6, Nov.-Dec. 2002 Page(s):1525 - 1533
- [4] Fang Lin Luo, Hock Guan Yeo, "Advanced PM brushless DC motor control and system for electric vehicles," *Conference Record of the 2000 IEEE Industry Applications*, Volume 2, 8-12 Oct. 2000 Page(s):1336 - 1343 vol.2
- [5] L.F. Teng, K.J. Tseng, F.L. Luo, "A VSS torque control strategy for multiphase PM brushless DC motor drive," *Proceedings of the 1998 International Conference on Power Electronic Drives and Energy Systems for Industrial Growth*, Volume 1, 1-3 Dec. 1998 Page(s):409 - 414 Vol.1
- [6] C.C. Chan, K.T. Chau, "An advanced permanent magnet motor drive system for battery-powered electric vehicles," *IEEE Transactions on Vehicular Technology*, Volume 45, Issue 1, Feb. 1996 Page(s):180 - 188
- [7] Fang Lin Luo, Hock Guan Yeo, "Advanced PM brushless DC motor control and system for electric vehicles," *Conference Record of the 2000 IEEE Industry Applications Conference*, Volume 2, 8-12 Oct. 2000 Page(s):1336 - 1343 vol.2
- [8] B.C. Kuo, "Digital Control Systems," 2nd edition, Saunder, 1992
- [9] Hyeoun-Dong Lee, Seung-Ki Sul, "Diesel engine ripple torque minimization for parallel type hybrid electric Vehicle," *IEEE Industry Applications Society Annual Meeting*, October 5-9, 1997 Page(s): 942-946 vol.2

- [10] Raymond B. Sepe Jr., Chris M. Morrison, John M. Miller, Allan R. Gale, "High Efficiency Operation Of A Hybrid Electric Vehicle Starter/Generator Over Road Profiles," *Industry Applications Conference, 2001. Thirty-Sixth IAS Annual Meeting. Conference Record of the 2001 IEEE*, Volume 2, 30 Sept.-4 Oct. 2001
Page(s):921 - 925 vol.2

APPENDICES

APPENDIX A: PM-BLDC MACHINE SYSTEM SIMULATION BLOCKS

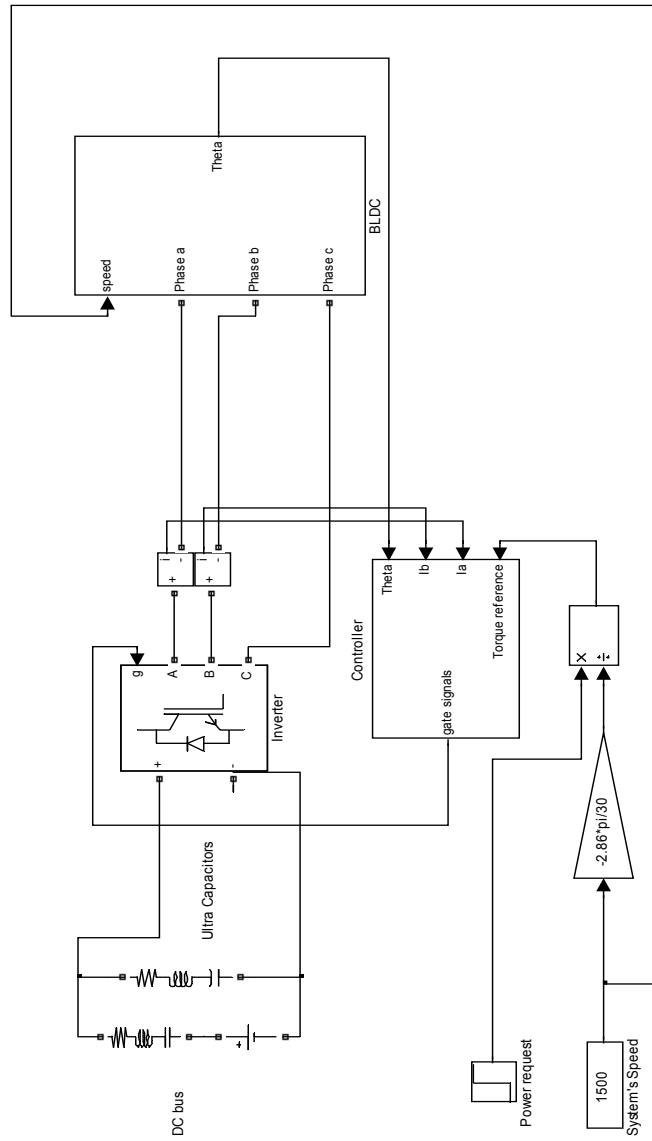


Figure A1: Main simulation window

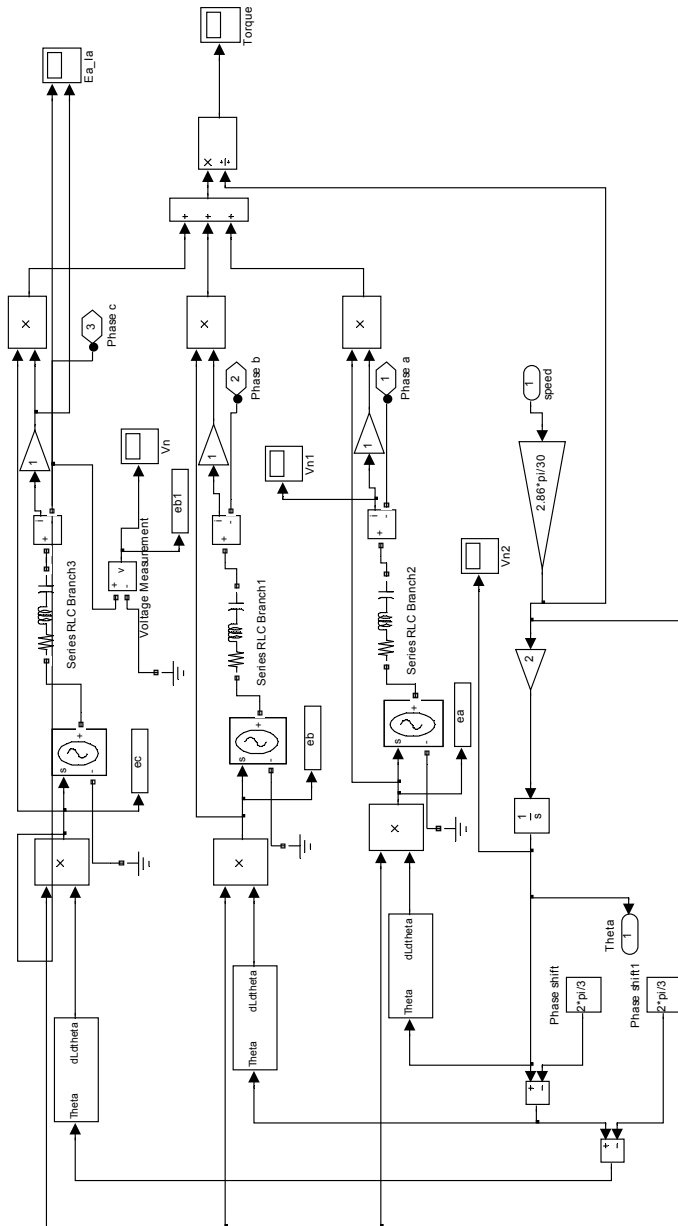


Figure A2: “BLDC” block

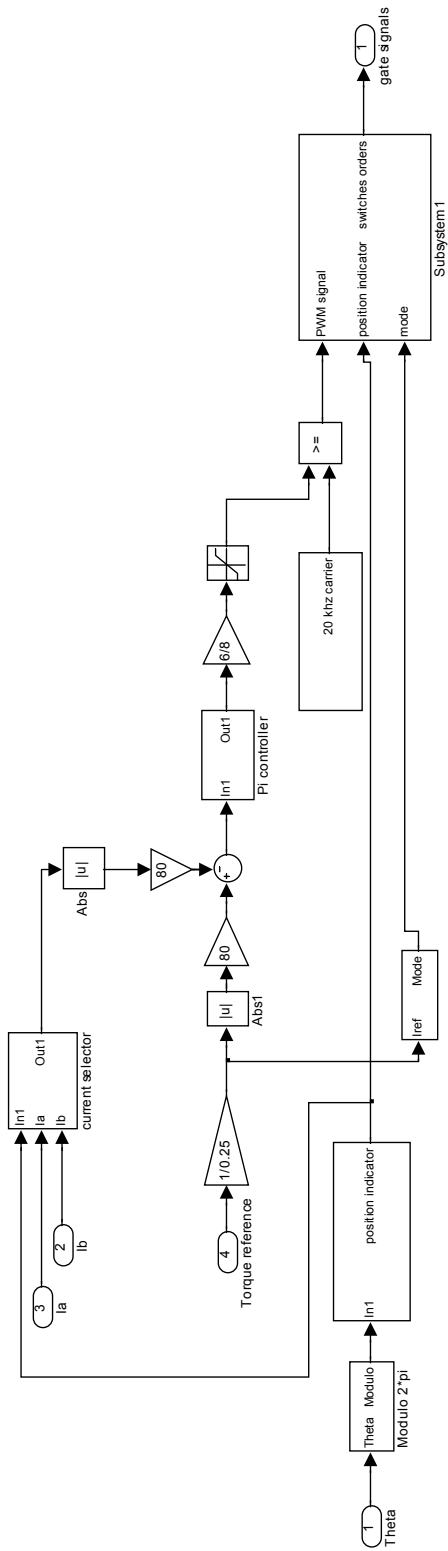


Figure A3: “Controller” block

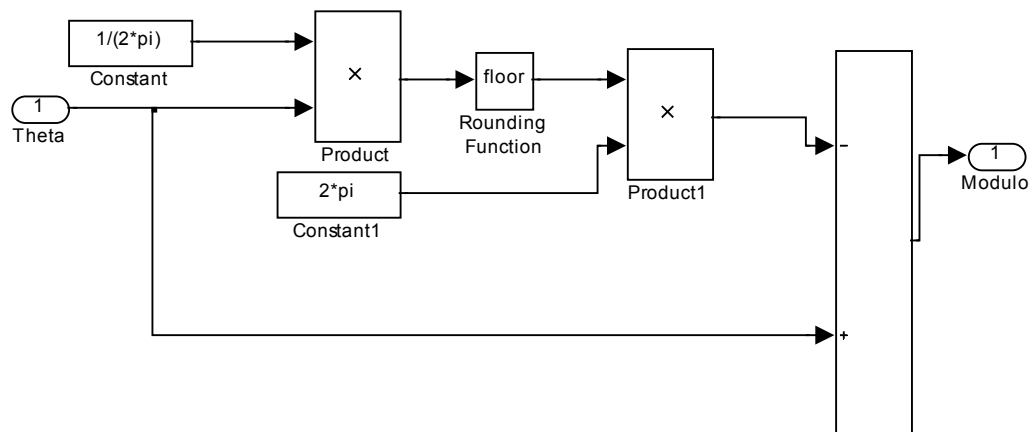


Figure A4: “Modulo 2*pi” block

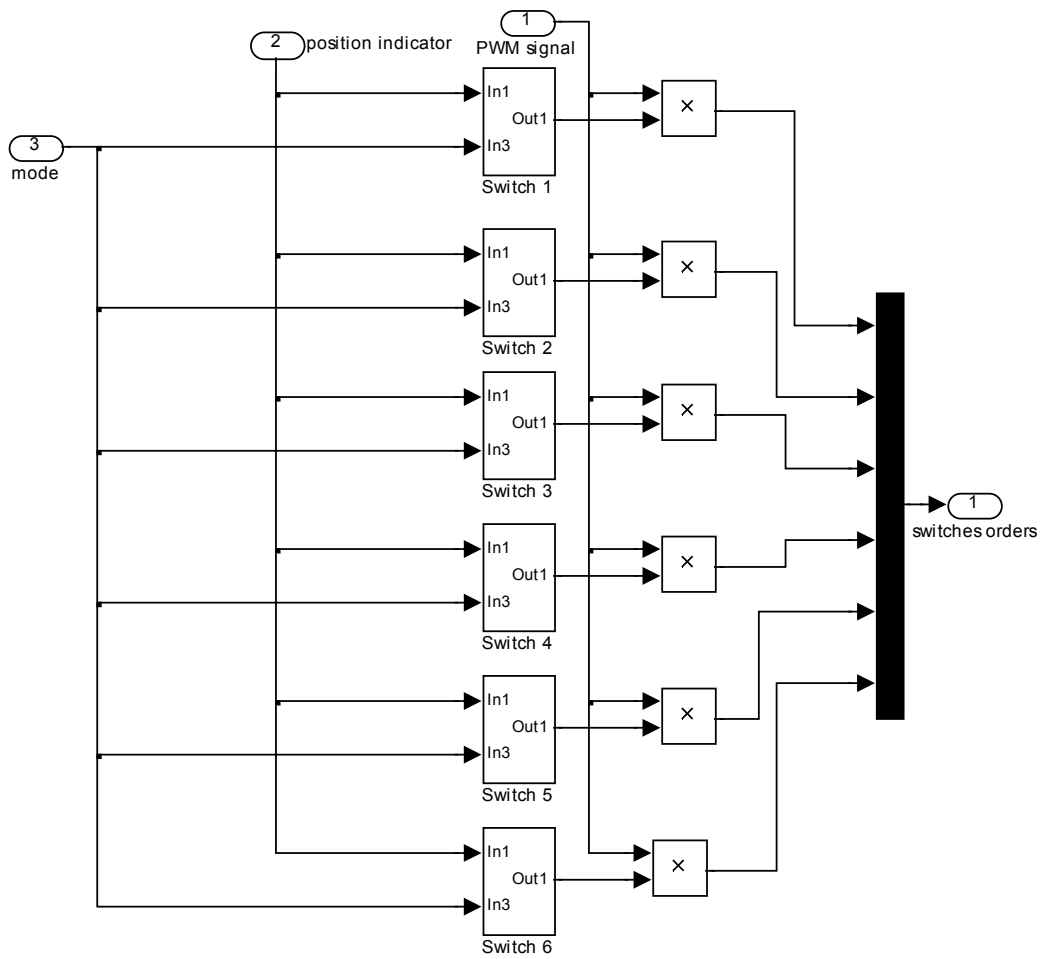


Figure A5: "Subsystem 1" block

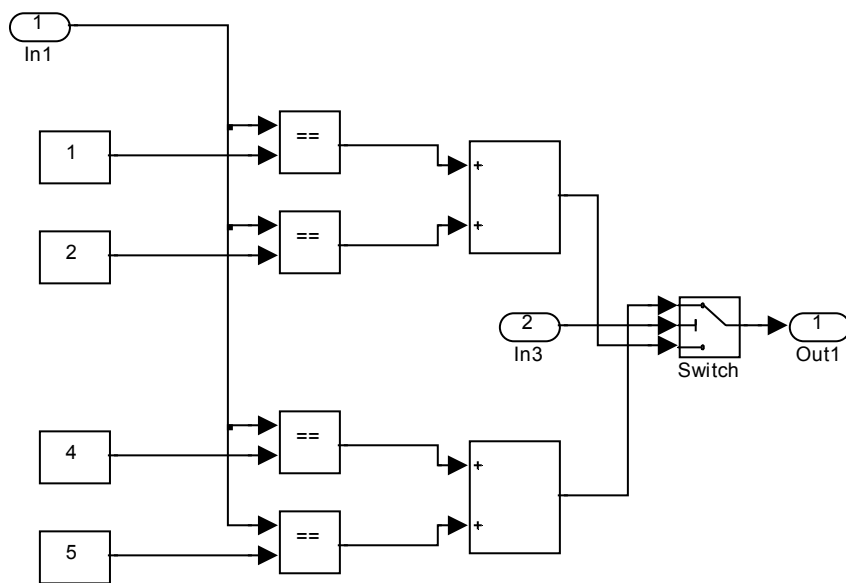


Figure A6: "Switch 1" block

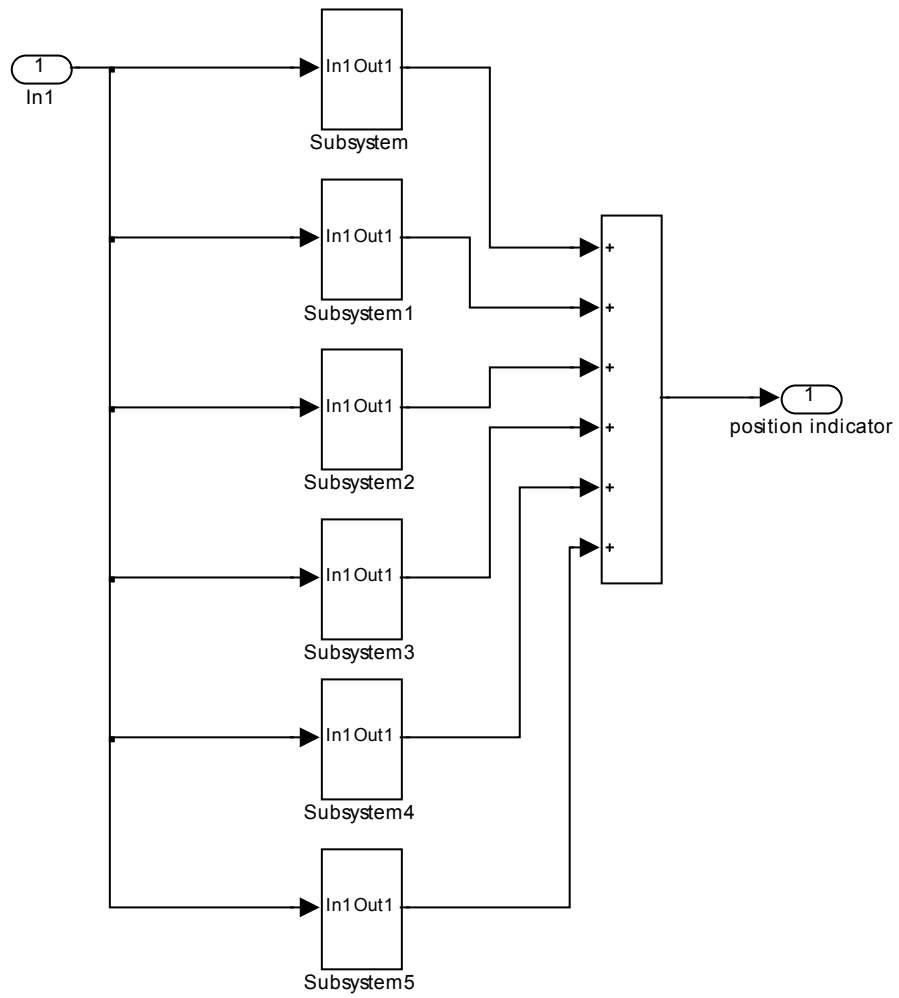


Figure A7: “In1 – Position indicator” block in “Controller” block

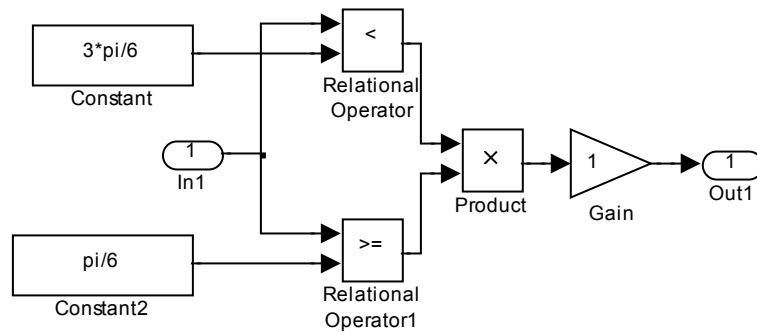


Figure A8: "Subsystem" block

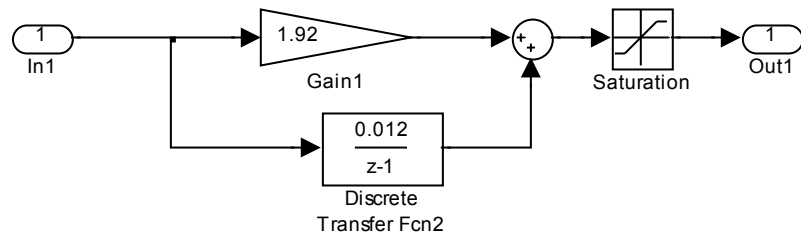


Figure A9: "PI controller" block

APPENDIX B: ELECTRONIC BOARD CIRCUITS

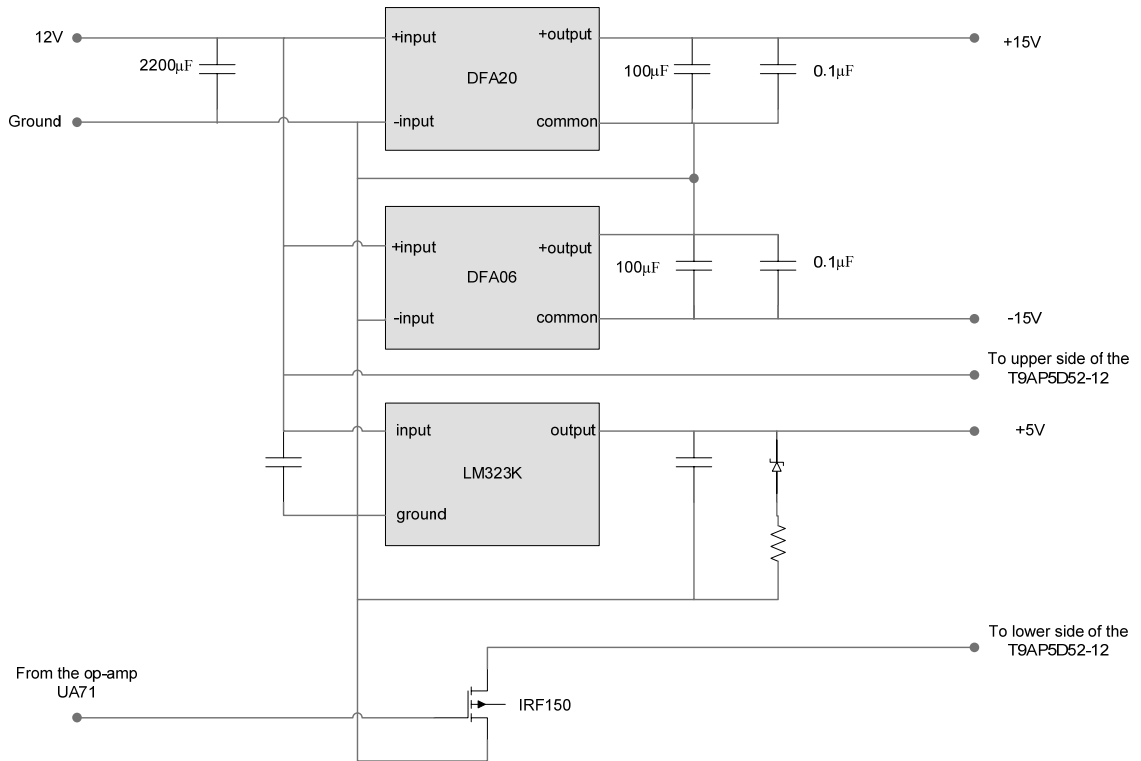


Figure B1: Power Supply board schematic

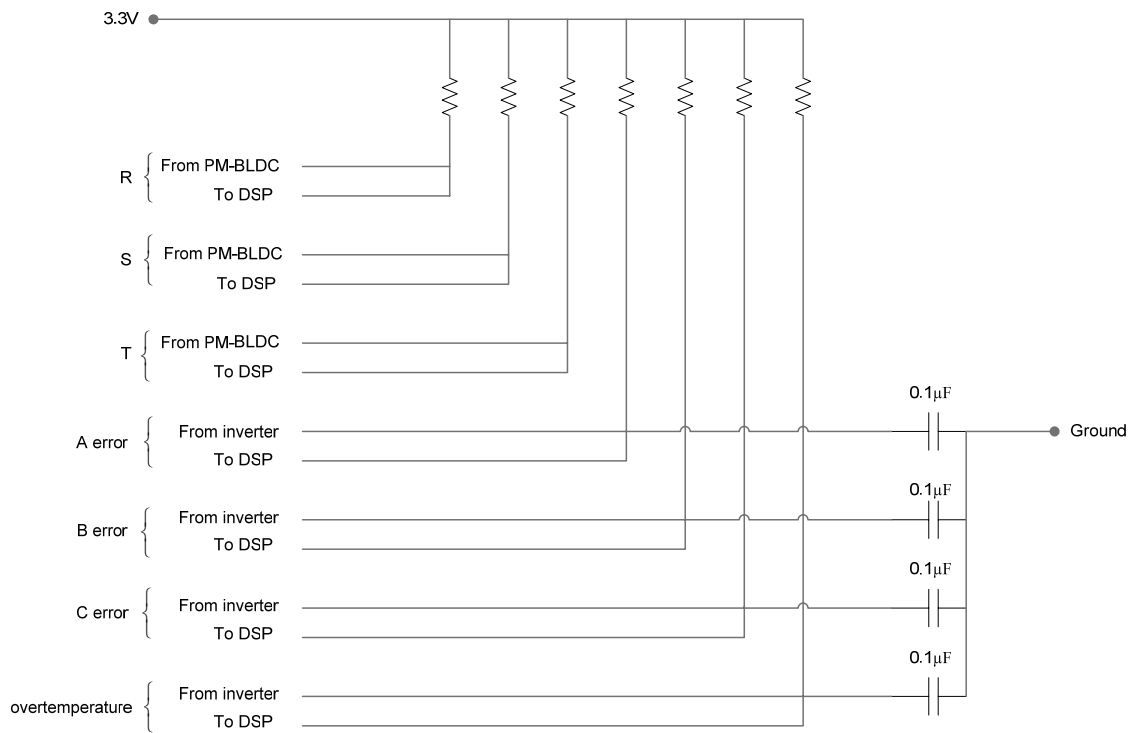


Figure B2: Circuitry for information through Pull-up signals

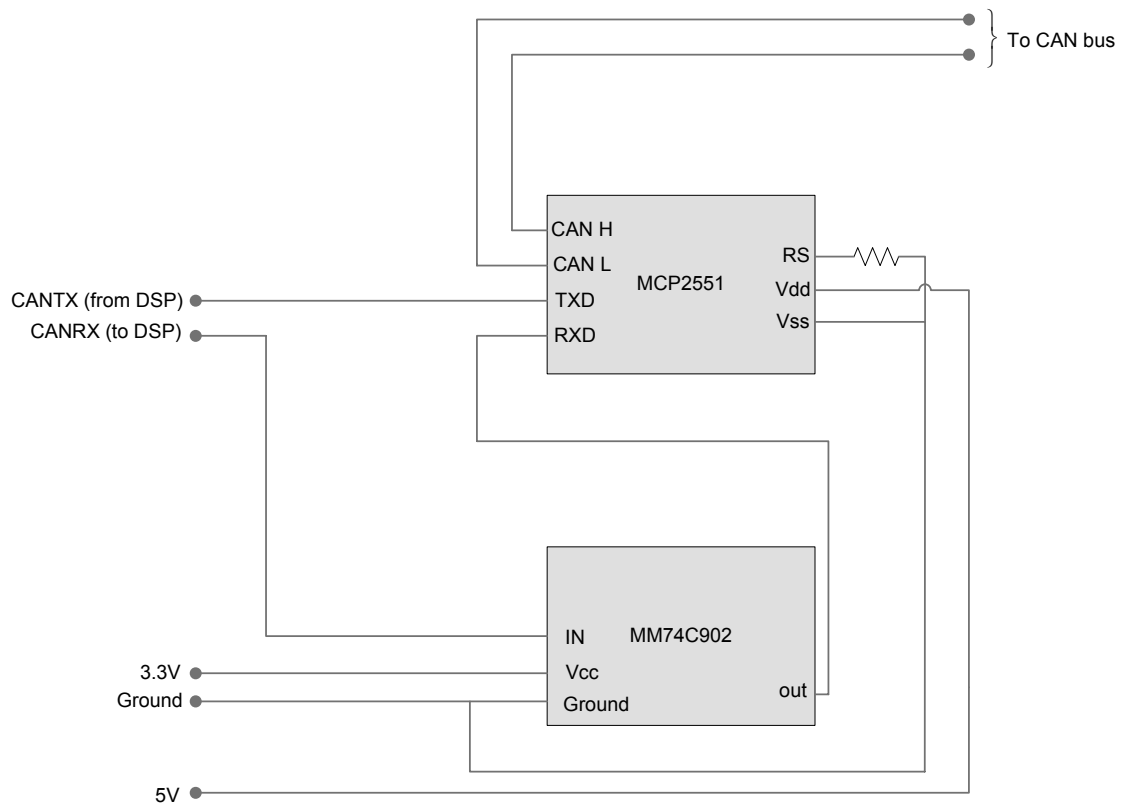


Figure B3: CAN communication hardware

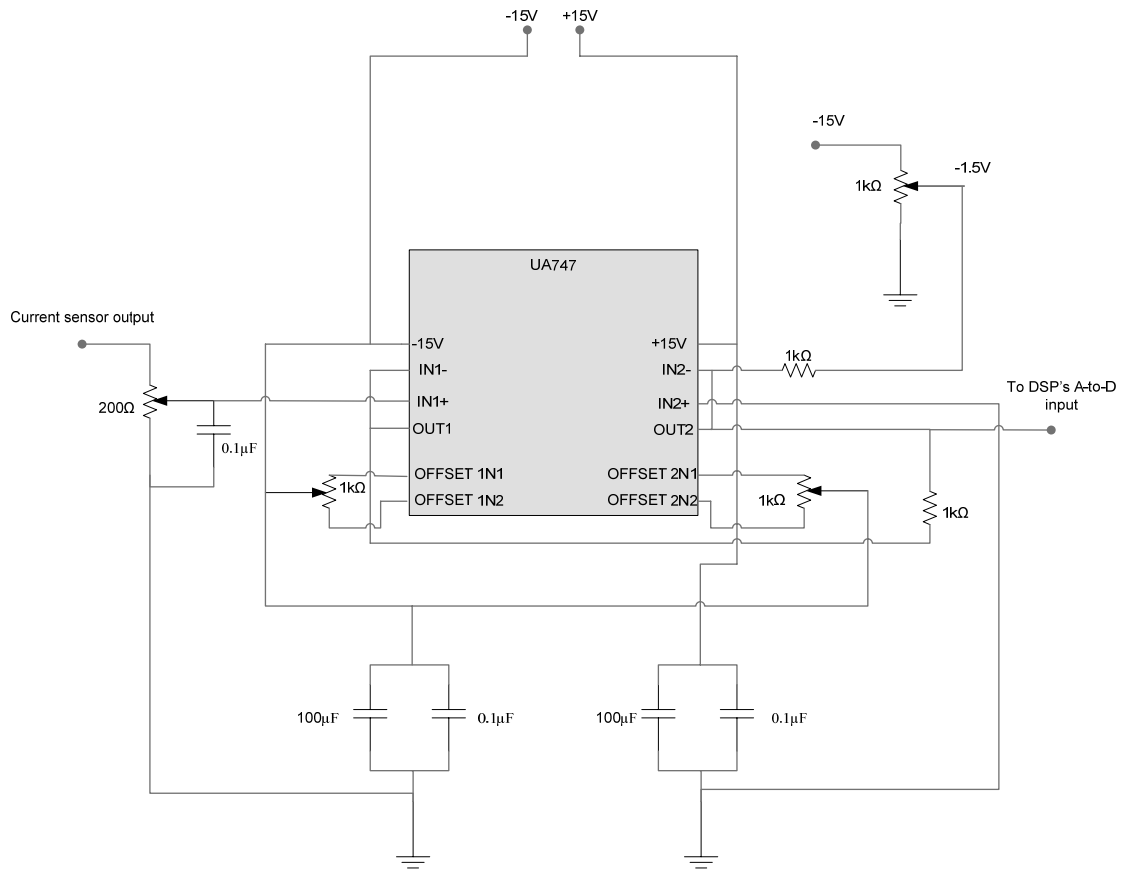


Figure B4: Current sensing circuitry

APPENDIX C: PICTURES OF THE ACTUAL HARDWARE

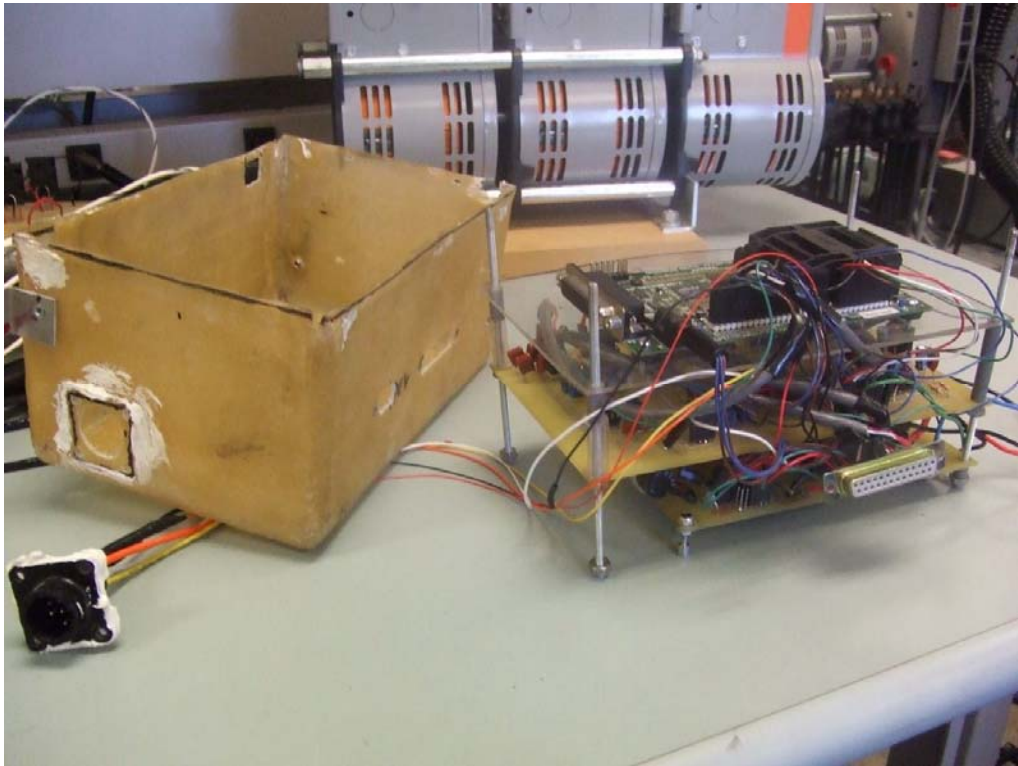


Figure C1: Power Supply and Instrumentation Boards



Figure C2: Inverter



Figure C3: PM-BLDC Machine

APPENDIX D: CAN MESSAGES DESCRIPTION

Messages sent by the DSP																		
Identifier	Periodicity	Description	Length (bits)	Bit Number								Byte number	Format	Range				
				b7	b6	b5	b4	b3	b2	b1	b0							
0x148	aperiodic	Generator Critical Emergency	Not Used	7									0					
			Generator Emergency Shutdown	1								X	0	Bit		0x00 = False 0x01 = True		
0x440	10 ms	Generator Status	Not Used	6									0					
			Generator Speed Actual	10	X	X	X	X	X	X	MSB	X	LSB	0	10-bit unsigned	0 to 12000 rpm	E=N/32; resolution is to nearest 32 rpm	
			Not Used	7											2			
			Generator Current Actual	9									MSB		2	9-bit signed integer	256 to 255 A	E = N
						X	X	X	X	X	X	X	LSB	3				
		HV Bus Voltage	8	X	X	X	X	X	X	X	X	4	8-bit unsigned integer	0V to 511V	E = 2*N; resolution to nearest 2V			
0x448	500 ms	Generator Limp-Home Emergency	generator critical fault	1								X	0	bit		0x00 = False 0x01 = True		
			generator fault	1							X	0	bit		0x00 = False 0x01 = True			
			Inverter too hot	1					X				0	bit		0x00 = False 0x01 = True		
			phase A overcurrent	1				X					0	bit		0x00 = False 0x01 = True		
			phase B overcurrent	1			X						0	bit		0x00 = False 0x01 = True		
			phase C overcurrent	1		X							0	bit		0x00 = False 0x01 = True		
			any phase or leg shorts	1		X							0	bit		0x00 = False 0x01 = True		
			over 5 errors in a row'signal	1	X								0	bit		0x00 = False 0x01 = True		
			position error (faulty hall effect sensors)	1								X	1	bit		0x00 = False 0x01 = True		
			error on the measured currents (possibly because of a failure of the power supplies)	6							X		1	bit		0x00 = False 0x01 = True		

Messages received by the DSP																	
Identifier	Periodicity	Description	Length (bits)	Bit Number								Byte number	Format	Range			
				b7	b6	b5	b4	b3	b2	b1	b0						
0x240	aperiodic	Generator Three-Phase Motor Relay Disconnect	Not Used	7									0				
			Disconnect Relay	1								X	0	Bit		0x00 = False 0x01 = True. We may not need this message, if SCM controls hardware disconnect to this relay.	
0x340	10 ms	Generator Command	Not Used	6									0				
			Generator Speed Actual, Redundant from SCM	10	X	X	X	X	X	X	MSB	X	LSB	0	10-bit unsigned	0 to 12000 rpm	E=N/32; resolution is to nearest 32 rpm
			Not Used	7											2		
			Generator Current Commanded	9		X	X	X	X	X	X	MSB	X	LSB	2	9-bit signed integer	256 to 255 A
0x4F0	500 ms	Rear Electrical Systems Data	Not Used	8										0			
			Not Used	8											1		
			Ballard Outlet Temperature	8	MSB	X	X	X	X	X	X	X	LSB	2	8-bit unsigned integer	-40..110 degrees C	See Delphi Thermistor mapping
			DC/DC Converter Temperature	8	MSB	X	X	X	X	X	X	X	LSB	3	8-bit unsigned integer	-40..110 degrees C	See Delphi Thermistor mapping
			Not Used	8											4		
			HV Bus Voltage	8	MSB	X	X	X	X	X	X	X	LSB	5	8-bit unsigned integer	0..400V	E=(400/255)*N (resolution is to nearest 1.6V)
			HV Bus Voltage (duplicate copy)	8	MSB	X	X	X	X	X	X	X	LSB	6	8-bit unsigned integer	0..400V	E=(400/255)*N (resolution is to nearest 1.6V)
			Not Used	8											7		

APPENDIX E: FAULTS DESCRIPTION

Fault number	Fault flag present in the CAN message 0x448	Severity	Definition	Action in the PM-BLDC controller or Supervisory controller	Recovery
1	Generator critical fault	critical	reflects that Fault #7,9 or 10 is detected	PM-BLDC controller: opens the phase relay Supervisory controller: opens the phase relay	The DSP needs to be rebooted; hence, the car needs to be restarted
2	Generator fault	non-critical	reflects that Fault #3,4, 5 or 8 is detected	PM-BLDC controller: opens the phase relay	PM-BLDC controller: reboots the inverter to clear the error. If any critical faults active, this will not resume generating or motoring mode
3	Inverter too hot	non-critical	temperature over the limit of the inverter, detected by the inverter that goes in an automatic shutdown mode	PM-BLDC controller: opens the phase relay	PM-BLDC controller: reboots the inverter to clear the error. If any critical faults active, this will not resume generating or motoring mode
4	Phase A overcurrent	non-critical	current over the limit of the inverter, detected by the inverter that goes in an automatic shutdown mode	PM-BLDC controller: opens the phase relay	PM-BLDC controller: reboots the inverter to clear the error. If any critical faults active, this will not resume generating or motoring mode
5	Phase B overcurrent	non-critical	current over the limit of the inverter, detected by the inverter that goes in an automatic shutdown mode	PM-BLDC controller: opens the phase relay	PM-BLDC controller: reboots the inverter to clear the error. If any critical faults active, this will not resume generating or motoring mode
6	Phase C overcurrent	non-critical	current over the limit of the inverter, detected by the inverter that goes in an automatic shutdown mode	PM-BLDC controller: opens the phase relay	PM-BLDC controller: reboots the inverter to clear the error. If any critical faults active, this will not resume generating or motoring mode
7	Any phase or leg shorts	critical	Current present in either phase when the phase is supposed to be turned off, current of maximum possible reference and reference asked is zero	PM-BLDC controller: opens the phase relay Supervisory controller: opens the phase relay	The DSP needs to be rebooted; hence, the car needs to be restarted
8	"Over 5 errors in a row" signal	non-critical	flag raised once 5 errors have happened in a row	PM-BLDC controller: opens the phase relay	The DSP needs to be rebooted; hence, the car needs to be restarted
9	Position error	critical	faulty hall effect sensors	PM-BLDC controller: opens the phase relay Supervisory controller: opens the phase relay	The DSP needs to be rebooted; hence, the car needs to be restarted
10	Error on the measured currents	critical	both phase A and B are shorted or failure on in the instrumentation board	PM-BLDC controller: opens the phase relay	The DSP needs to be rebooted; hence, the car needs to be restarted